Derivations of Spin Alignment Rules and Their Applications to Organic Ferromagnetic Crystals

Takashi Kawakami

Department of Chemistry
Graduate School of Science
Osaka University
1999

Derivations of Spin Alignment Rules and Their Applications to Organic Ferromagnetic Crystals

Takashi Kawakami

Department of Chemistry
Graduate School of Science
Osaka University
1999

Acknowledgement

This doctorate thesis has been completed under the guidance and supervision of Professor Kizashi Yamaguchi. The author would like to express sincere gratitude for his support, valuable suggestions and encouragement. Sincerely acknowledgement is also made to Professor Wasuke Mori (Kanagawa University, at present) for his continuous encouragement and helpful advice.

The author is grateful to Dr. Mitsutaka Okumura (Osaka National Research Institute, at present) and Dr. Hidemi Nagao for his advice of computational methods and quantum statistical approach to this thesis, respectively. The author would also like to acknowledge Associate Professor Sadamu Takeda (Gunma University, at present), Dr. Masayoshi Nakano and Associate Professor Yasunori Yoshioka for many valuable discussions.

The author gratefully acknowledges Professor Mikiharu Kamachi, Professor Kazuhiro Nakasuji and Associate Professor Atsushi Kajiwara for his helpful advice about symmetry rules for spin alignments (Chapter 3, 4 and 5).

The author is indebted to Professor Hiizu Iwamura (Kyushu University) and Associate Professor Katsuya Inoue (Institute for Molecular Science) for his valuable comments from experiments and offers of the X-ray crystal structure data for *p*-NNBA$^-$ crystal. The author would also like to thank Professor Olivier Kahn for offers of the data for 1, 2, 4-triazole NN crystals (Chapter 4).

The author gratefully acknowledges Professor Takashi Nogami (The University of Electro-Communications), Professor Fujiko Iwasaki, Associate Professor Takayuki Ishida and Associate Professor Masanori Yasui for his sincere collaboration and offers of the crystal structure data for TEMPO derivative crystals (Chapter 5).

The author would like to thank Professor André Rassat for offers of the data for TMAO crystals (Chapter 6).

Sincerely acknowledgement is made to Professor Minoru Kinoshita (Science University of Tokyo, at present) and Professor Kunio Awaga (The University of Tokyo) for offers of their experimental measurements for β-*p*-NPNN. The author is also grateful to Professor

Kazuyoshi Takeda (Kyushu University) and Dr. Masaki Mito for the discussion about crystal structure and changes under pressure (Chapter 7).

The author is very grateful to Professor Toyonari Sugimoto (Osaka Prefecture University) and Dr. Kazumasa Ueda for indispensable support in his studies on TCNQ crystal (Section 8.2).

The author would like to thank Professor Kiyoshi Nishikawa (Kanazawa University) and Hiroyuki Kawabe (Kinjo Junior College) (Chapter 1 in Part II).

For related discussions on magnetic crystals, the author gratefully acknowledges Professor Tadashi Sugawara (The University of Tokyo), Dr. Masashi Tamura (Toho University), Dr. Akira Izuoka (The University of Tokyo), Dr. Michio M. Matsushita (Tokyo Metro University) and Dr. Yuko Hosokoshi (Institute for Molecular Science).

Many thanks are given to all the members and secretaries of the laboratory of Professor Kizashi Yamaguchi, especially to Dr. Shusuke Yamanaka, Dr. Goro Maruta, Mr. Akifumi Oda, Mr. Yasuteru Shigeta and Mr. Yu Takano for many valuable discussions. The author thanks Mr. Shinji Kiribayashi and Mr. Yasutaka Kitagawa for helping of his system engineering of computar systems in the laboratory. The author had a specially pleasant time with Mr. Daisuke Yamaki, Dr. Satoru Yamada, Dr. Takao Kobayashi and Mr. Kenji Ueda as the same grade in the laboratory.

The author would like to thank all the members of the same class of chemistry and all his friends, especially Dr. Koichi Takamiya, Mr. Masahiro Okita, Mr. Hiroyuki Komiyama, Mr. Yasuji Ozaki, Mr. Shigenobu Nakamura, Mr. Kazuya Yamashiro and Mr. Seiji Takuma, for enjoying his schooldays together.

The author has been assisted by the Research Fellowship of the Japan Society for the Promotion of Science for Young Scientists (Apr. 1996 – Mar. 1999). The numerical calculations were carried out on the IBM RS/6000, SGI-Cray Origin and DEC Alpha Server systems in the Yamaguchi laboratory.

Abbreviations

(General)

J_{ab}	effective exchange integral
KE	kinetic exchange term
PE	potential exchange term
SP	spin polarization term/effect
SD	spin delocalization effect
SOMO	singly occupied molecular orbital

(Calculation methods)

INDO	intermediate-neglect-of-differential overlap method
ab initio MO	ab initio molecular orbital method
HF	Hartree-Fock method (R- restricted, U- unrestricted)
MP	Moller-Plesset perturbation method
CC	coupled cluster method
CASCI	complete active space; configuration interaction
CASSCF	complete active space; self consistent field
UNO	natural orbital analysis (of UHF orbital)
DFT	density functional theory
BLYP	Becke (for exchange functional); Lee-Yang-Parr (for correlation functional)
B3LYP	(Becke's three parameter hybrid method)

(Magnetic species)

NN	nitronyl nitroxide
NO	nitroxide
β-*p*-NPNN	β-phase *p*-nitrophenyl nitronyl nitroxide
p-NNBA$^-$	*p*-carboxylate phenyl nitronyl nitroxide
m-MPYNN$^+$	*m*-N-methylpyridinium nitronyl nitroxide
triazole NN	1,2,4-triazole nitronyl nitroxide
HQNN	2',5'-dihydroxyphenyl nitronyl nitroxide
TMAO	1,3,5,7-tetramethyl-2,6-diazaadamantane-N,N'-dioxyl
TEMPO	2,2,6,6-tetramethylpiperidinyloxy
TCNQ	tetracyanoquinodimethane
TANOL suberate	4,4'-[1,8-dioxoctane-1,8-diyl)bis(oxy)]bis(2,2,6,6-tetramethylpiperidin-1-yloxyl)
galvinoxyl	2,6-di-*tert*-butyl-4-(3,5-di-*tert*-butyl-4-oxocyclohexa-2,5-di-enylidenemethyl)phenoxyl
p-CDTV	3-(4-chlorophenyl)-1,5-dimethyl-6-thioxoverdazyl

Contents

PART II

Part I

Chapter 1.

General Introduction

Section 1.1

Scope of present thesis

There is currently rapid development in the field of molecule-based magnetic materials involving pure organic crystals, organic/organometallic polymers, metal-organic radical systems and transition-metal complexes. The research of genuine organic ferromagnets, consisting exclusively of light elements has its long history, and various experimental and theoretical studies have been reported by many researchers. In 1991 it was found that *p*-NPNN in β-phase undergoes a ferromagnetic transition at 0.6 K, though it had been generally believed that almost all of radical crystals would be magnetically inactive or antiferromagnetic. Following this, various organic ferromagnets have been reported. These findings have initiated investigations into the magnetic properties of molecular crystals. These researches have become one of the main subjects of "molecular magnetism" which is a relatively new field involving materials science and cooperative phenomena played in molecular spin systems.

However, the detailed mechanism of the ferromagnetic intermolecular interactions in these crystals is still open to research. Understanding the origin of the ferromagnetic interactions would help to improve the rational design of molecular magnets in terms of molecular and crystal structures, which are not fully available yet. In order to elucidate the physics behind the magnetism of molecular crystals, knowledge of the relation between the molecular packing and the intermolecular magnetic interactions is primary important.

Not only many experimental but also theoretical studies have been carried out to elucidate the mechanism of the magnetic interaction. These theoretical treatment based on molecular orbital calculations have been performed in several groups for various molecular systems in cooperation with experimental studies. It was shown that the magnetic interaction between organic radicals can be characterized quantitatively by the effective exchange integral (J_{ab}). In addition, treatment of quantum spin model also carried out by quantum spin diagonalization method and quantum Monte Carlo method, etc. The author thinks that cooperation of both theoretical point of view and experiment one is very

important. The analytical and numerical investigations in theoretical quantum studies may lead to experimental studies, and vice versa.

The purposes of the present thesis are theoretical interpretation of the magnetic couplings with *ab initio* MO theory and DFT depend on quantum mechanics, and quantum statistical mechanics. In this study both simple model of nitroxide radicals and real crystalline organic systems are employed to discover intrinsic features of organic magnetism. These stable organic radicals are suitable for investigation of origins and propagation of magnetic interaction. On the other hand, *ab initio* MO and DFT methods are feasible for detail analyses and designing of unique magnetic materials.

The author starts this study as the following policy.

(1) Computational schemes [Part I]
(2) Spin alignment rules (through-space, through-hydrogen bond)
(3) Application to real crystals
(4) Statistical approach [Part II]

About (1), the formulation of effective exchange integrals were derived and quantitative evaluation were enabled. Recent development of *ab initio* MO and DFT methods expands the new science field, i.e. "computational chemistry". In this study the author made full use of these advanced approach. About (2), essential and simple spin alignment rules to ferromagnetic interactions in organic crystals are established. Decomposition of effective exchange integral were carried out and selection rules could be extracted. Theoretical calculations with model systems are useful for evaluating the classification principle of the mechanisms for ferromagnetic interactions. About (3), recent many experimental studies by many scientists reveal novel organic crystals, for example TMAO crystal with remarkable high T_c temperature, β-*p*-NPNN crystal with ferro- to antiferro-transition under pressure, etc. Numerical analysis of ferromagnetic interaction in "real" crystalline organic ferromagnets become feasible because of recent remarkable progress of computer technology. The author have been carrying out these analysis successfully. About (4), the author challenges another way to magnetic behavior. The quantum statistical approaches with the Monte Carlo method enable to calculate numerical partition function directly. Thus, magnetization with temperature term could be evaluated.

(See Section 1.6 for details of the following chapters)

Section 1.2

Crystalline organic magnetic materials

1.2.1 History and development

The search for a bulk ferromagnetic substance composed only of light elements such as H, C, N, and O has been one of the most challenging problems in this field of material science. Most organic radicals exhibit intermolecular antiferromagnetic interactions. On the basis of the chemical bonding, an antiparallel electron spin alignment is favorable between the unpaired electrons. The spin alignment in the organic compound must be arranged with strong interactions between the spins to be parallel. This appears to work against nature because organic compounds normally have a strong tendency to bond together with antiparallel spin alignment. Thus special control of the spin alignment is needed to develop organomagnetic materials, this is the most difficult aspect in this research field.

In organic radical materials, a ferromagnetic intermolecular coupling is quite rare as compared with an antiferromagnetic one. Although several substances such as galvinoxyl radical and TANOL radical are known to possess a positive paramagnetic Curie temperature, they do not fall into a ferromagnetically ordered state. The intermolecular ferromagnetic interactions can be observed only in special cases.

Eventually, it took over twenty years until a historic discovery of the first organic bulk-ferromagnet of the β-phase *p*-NPNN by Kinoshita, Awaga and co-worker in 1991[1], although its transition temperature (T_c = 0.61 K) is fairly low for practical use. The detailed magnetism has been investigated by the heat capacity, ac-susceptibility, magnetization, zero-field muon spin rotation (μSR), neutron diffraction and electron spin resonance (ESR).

Following the first example of organic bulk ferromagnet, several examples have been reported within a few years. It seems that the discovery of the first organic ferromagnet

lead to the successive rapid development and discoveries of other organic ferromagnets during the past few years, with almost twenty being known by the present time. It is also noteworthy that a large number of them are nitroxide radicals.

Nitroxide radicals are well known, constituting one of the rare classes of radicals capable of being handled under ordinary conditions on the laboratory bench. These radicals have been central to the development of molecular-based magnetic materials, i.e. Phenyl-NN, TMAO, TEMPO and etc. Many nitroxide radicals have been prepared and isolated as stable substances. Therefore, model study with these are suitable for this purpose and we have carried out detailed theoretical calculations. Of course, other stable organic radicals, i.e. carbene radical (CH_2) polymer etc., can be executive and several group carried out their investigation vigorously.

1.2.2 Several crystals

Some organic ferromagnets are summarized below and molecular structures (**1-16**) are shown in **Fig. 1.1**. Of course, many other species are available now.

p-NPNN

The *p*-NPNN (**1**), is a unique organic radical in the sense that all of the four metamorphic phases (α, β, β_h, and γ) are supposed to possess a ferromagnetic intermolecular coupling. The β phase was found to transform into a long-range ferromagnetic state at 0.60 K, as the first discover of ferromagnetic materials. For the γ phase it is found that the intra-plane exchange interactions are ferromagnetic, whereas the inter-plane one is antiferromagnetic. A systematic theoretical explanation was already carried out for the magnetic long-range ordering in the β- and γ-phase crystals of *p*-NPNN. (Refs. [1,2,3,4,5,6])

Phenyl-NN (aromatic-, heteroaromatic-substitutes)

The series of phenyl α-nitronyl nitroxides, which is an aromatic substitutes at the α-position, afford satisfactory crystallinity and stability. These characteristics are suitable for the purpose of surveying the interrelations between the molecular form, crystal structure and the magnetism in organic radical crystals. By classifying the molecular packing of these compounds in the crystals, useful information can be found for the control of molecular magnetism. Many derivatives of this series can be readily obtained. Inoue and co-worker reported synthesis of *p*-$NNBA^-$ salts (**2**). They performed the magnetic measurements and manifested that dimers have a short intermolecular contact between the oxygen atom in NN group and the alpha carbon atom in the nearest-neighbor NN group with T-shape

conformation. These salts provided not only the first example of ferromagnetic dimers of radical anions but also the largest J_{ab} value ever reported for exchange couplings between PNNO derivatives. Hosokoshi and co-workers reported the crystal **3** and it was said that the magnetic properties are explained by the formation of a triplet state within the dimer and additional inter-dimer ferromagnetic interactions. (Refs. [7])

In addition, the development of heteroaromatic systems carrying nitroxide radicals is also an attractive way to obtain new organomagnetic materials. For example, Awaga et al. developed *m*-MPYNN$^+$ (**4**) and reported that in its molecular crystal it is manifested as dimers with short intermolecular contact between the NO group and the pyridinuim ring and have ferromagnetic intermolecular interactions. As another example, a triazole nitronyl nitroxide radical (**5**) was prepared by Kahn and co-workers. (Refs. [8,9,10,11,12])

Hydrogen bonding has been extensively demonstrated to be a powerful tool for the design of crystalline architectures. The wide variety of crystalline architectures with different packing structures suggested to us that hydrogen bonds could be used to study magnetic exchange coupling mechanisms. Not only to control the crystal packing but also to propagate ferromagnetic interactions are important. There are many reports concerning the ability of hydrogen bonds to propagate weak magnetic exchange coupling. Sugawara and co-workers prepared the phenol derivatives of nitronyl nitroxides (**6**) to control the arrangement of spin sources through the phenolic hydrogen bond and found that they are really ferromagnets. (Refs. [13])

TMAO

Rassat and co-workers synthesized and studied the TMAO crystal (**7**), namely. This compound was expected to possess intra-molecular ferromagnetic interactions from the orthogonality of the two NO groups of the biradical, and owing to the favourable three-dimensional network of NO chains for inter-molecular ferromagnetic interactions. It shows a ferromagnetic transition at 1.48 K, which is the highest T_c value among the organoferromagnets of radical crystals. (Refs. [14,15,16,17])

TEMPO derivative

The use of *ph*-CH=N-TEMPO radical and related derivatives (**8**) has been recognized in recent years. These extensive studies were carried out by Nogami and co-workers. They investigated over 165 radicals and 52 radicals were found with ferromagnetic interactions, and 9 radicals with ferromagnetic transitions at very low temperatures were found. (Refs. [18,19,20,21,22,23])

TCNQ

Sugimoto and co-workers have recently reported ferromagnetic behavior at room temperature in some organic crystals consisting of light elements, but a too small saturation moment and poor reproducibility left the problem unsettled. One of these species is the tetramethylammonium (NMe_4^+) salts (**9**) of TCNQ and its radical anion ($TCNQ^{-\bullet}$) in a molecular ratio of 1:2. The saturation magnetizations and coercive forces are 0.79 emu/mol and *ca.* 300 Oe for ($NMe_4^+ \cdot TCNQ^{-\bullet}$) $\cdot$ 1/2 TCNQ, respectively.

The others

Some other organic radical crystals, such as TANOL suberate (**10**), galvinoxyl (**11**), *p*-CDTV (**12**) are known to possess dominant ferromagnetic intermolecular interactions as suggested by the positive Weiss constants. Various nitroxide radicals (**13**, **14**, **15**, **16**) developed recently in order to investigate magnetic interactions. Many experimental and theoretical efforts for organic magnetic materials make progress.

Such as above many synthesized materials, there are many organic ferromagnets observed until now. However, the transition temperature to the bulk-ferromagnetic state is generally lower than 1 K, and the characterization of their magnetism is mostly unrevealed from a physical point of view. From both theoretical and experimental points of view several useful methods are proposed and the author mentions these briefly as following.

To carry out research projects on organomagnetic materials, because of the possibility of collaborating with physicists or physical chemists who could measure magnetic properties of organic compounds such as magnetic susceptibility, heat capacity and so on. Moreover, it is no longer unusual for organic chemists themselves to measure magnetic susceptibility using a SQUID susceptometer, which was almost inconceivable ten years ago. The rapid progress in this field of science is therefore surely owed to such developments in research circumstances. In addition to experimental facilities, technology of computers have remarkably progresses and comes to reveal new science. Recent development of *ab initio* MO and DFT methods also extend possibility of quantum mechanics. Cooperation of these enable us calculate several properties without experiments. Thus, since evaluations of very weak magnetic interactions become to feasible, the author practices theoretical studies for magnetic interactions

1.2.3 Radical spins

Nitroxide (NO) and nitronylnitroxide (NN) radicals have been central to the development of molecular-based magnetic materials, though triplet carbene and so on are

important components for polymer ferromagnetic species. The phenyl-NN radicals, TEMPO radicals, TMAO radicals and so on, are classified into several types of common structures and these classifications have been widely used and studied for this purpose. From the theoretical point of view, it is recognized that the unpaired electrons of nitroxides in the SOMO are essential. Induced spin densities are delocalized between the nitrogen and the oxygen atoms in the TEMPO and TMAO series, and those in the NN series are evenly distributed between two N-O groups making a node at the α-carbon atom. Without these electronic features the magnetic properties of these radicals would be difficult to understand. Their derivatives could offer a wide variety of magnetic materials with interesting three-dimensional structures, solid-state properties and so on.

1.2.4 Spatial networks and molecular packing

From both theoretical consideration and experimental verification, it is now generally recognized that the route to the preparation of organomagnetic materials with efficient intermolecular ferromagnetic interactions. Although the desirable condition of the ferromagnetic intermolecular interaction is clear, the interpretation of the magnetic interactions in terms of molecular arrangement for the actual system is still open. Assignment of the magnetic couplings to the specific molecular arrangement is not so easy. The study of the magnetic properties of organic radicals is still at the beginning.

The molecular packing that leads to one, two and three dimensional ferromagnetic interactions in the crystal is crucial to bulk ferromagnetism. To clarify and to understand the structure-magnetism relationship are important. A very serious point for development is control of the molecular arrangement in three dimensions, because the magnetic properties of materials depend subtly on the packing mode of molecules.

In addition to interest of ferromagnetic crystals with higher T_c, active control of electronic, magnetic and optical properties by external conditions is challenges in molecule-based materials. Packing modes and local orientations of molecules can vary under external conditions because of the nature of crystalline materials. The flexibility is one of interesting points of magnetic crystals. For example, ferro- to antiferro-magnetic transition under pressure occurs in *p*-NPNN crystals and more detailed experimental and theoretical studies are desired. In this point, computational studies can simulate crystalline property and magnetic behavior in valuable situations.

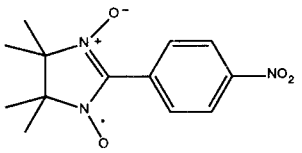

β-*p*-NPNN (T_c = 0.65 K, 1991)

1

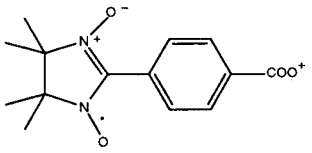

p-NNBA$^-$ (T_c = 0.45 K, 1993)

2

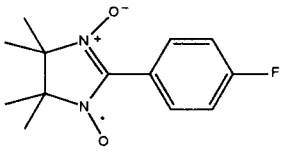

p-FPNN (1994)

3

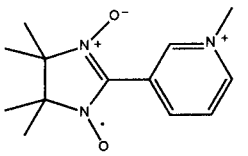

m-MPYNN$^+$ (1992)

4

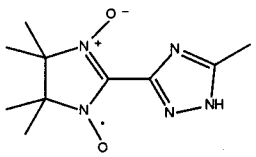

1,2,4-triazole NN (T_c = 0.60 K, 1994)

5

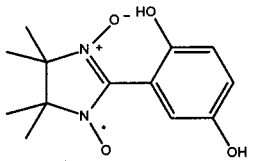

HQNN (T_c = 0.5 K, 1994)

6

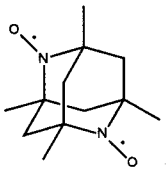

TMAO (T_c = 1.48 K, 1993)

7

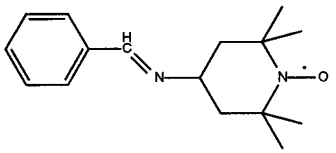

ph-CH=N-TEMPO (T_c = 0.18 K, 1994)

8

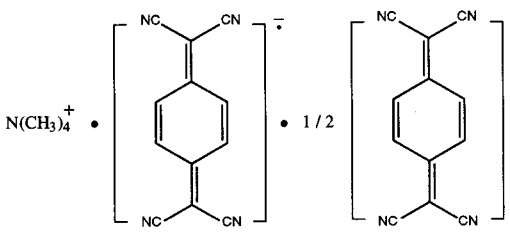

$(N(CH_3)_4^+ \cdot TCNQ^{-\bullet}) \cdot 1/2TCNQ$ (1995)

9

Figure 1.1 Various molecular-based ferromagnetic materials and nitroxide radicals.

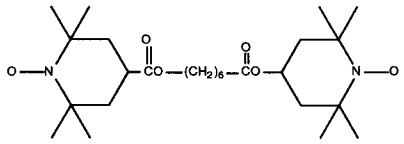

TANOL suberate

10

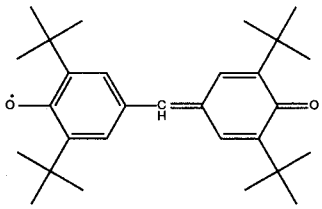

galvinoxyl

11

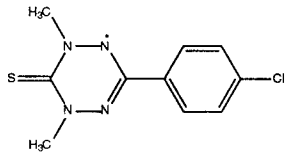

p-CDTV

12

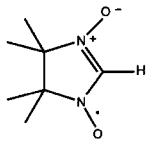

HNN

13

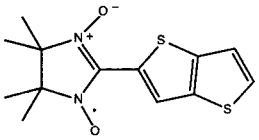

14

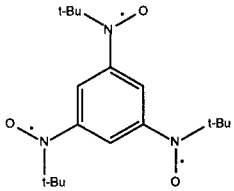

15

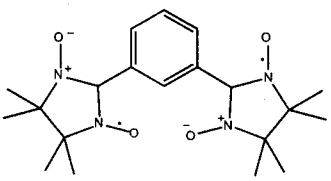

16

(Continued)

Section 1.3

Types of ferro- and antiferro-magnetic interactions

1.3.1 McConnell rules

In 1963 McConnell suggested that the through-space exchange interaction between two aromatic radicals could be considered in approximation with Heisenberg model, i.e. the effect of spin polarization (SP) within a molecule[24,25,26,27]. This basic concept for the stabilization of the parallel spin alignment is considered as exchange interactions between the positive spin density of one molecule and the negative spin density of another

$$H_{ab} = -S^A \cdot S^B \sum 2J_{ij}^{AB} \rho_i^A \rho_j^B \qquad (1.1)$$

where J_{ij}^{AB} is an exchange integral between atom i of molecule A and atom j of molecule B, and ρ_i^A (ρ_j^B) is a spin density on atom i(j) of molecule A(B), respectively. This Hamiltonian mentions that the effective exchange interaction between two radicals can be ferromagnetic if the spin-density product $\rho_i^A \cdot \rho_j^B$ ($i \neq j$) is negative, since J_{ij}^{AB} is usually negative.

In addition, another a stabilization mechanism for realizing parallel spin alignment between radical molecules is introducing the concept of the charge transfer (CT) between molecular orbitals (MO's)[28]. This CT model is based on the spin-unrestricted picture, where α (up) spin and β (down) spin occupy different orbitals by the effect of spin polarization and we guess that admixture of the virtual triplet excited states with the ground state. For example, the charge transfer from the SOMO to the LUMO and/or the doubly occupied NHOMO to the SOMO occur.

Yamaguchi et al. extended this McConnell's model to more generalized magnetic system. Generally the orbital overlap of singly occupied molecular orbitals (SOMO's) between free radicals is predominant in the decision of the effective exchange integrals J_{ab}, and that contribution brings about the negative (antiferromagnetic) J_{ab}. On the other hand, the computational experiment suggests that the spin polarization (SP) effect induces the possibility to bring about the positive (ferromagnetic) J_{ab}. In this extended McConnell's model (EMM), therefore, the nearest neighbor effective exchange integral J_{ab}(EMM) for radical clusters is given as follows:

$$J_{ab}(EMM) = J_{ab}(OO) + J_{ab}(SDP) = J_{ab}(OO) + J(SDP)\sum \rho_i(A)\rho_j(B) \qquad (1.2)$$

where J_{ab}(OO) is the orbital interaction term depends on the SOMO-SOMO overlap, and J_{ab}(SDP) is the spin density term. The sign of J_{ab}(OO) is generally negative and J_{ab}(SDP) may have a positive value if a value of $\Sigma\rho_i(A)\rho_j(B)$ is negative. That is to say, according to this EMM, the ferromagnetic exchange integral (positive J_{ab}(EMM)) can be brought about, when a magnitude of positive J_{ab}(SDP) overcomes that of negative J_{ab}(OO). It is necessary for positive J_{ab}(EMM) to minimize the SOMO-SOMO overlap and, furthermore, make the product of the spin density negative.

1.3.2 Twelve types of magnetic interaction

Previously, Yamaguchi, Okumura and co-workers have carried out the spin-projected UHF calculations of diradicals and polyradicals in the past decades. These computational results have revealed that there are two different intermolecular approaches: one is a perpendicular approach which exhibits a ferromagnetic interaction and the other is a parallel one with antiferromanetic interaction. The high-spin or low-spin clusters are formed by the through-space couplings of intrinsic spin in the SOMO (NBMO), induced spin by the spin polarization (SP) mechanism, or induced spin by the spin delocalization (SD) mechanism. The magnitudes of the intermolecular effective exchange couplings (J_{ab}) between these spins are classified into three cases as summarized in **Table 1.1**. The computational results for these three cases are generally explained by the spin alignment rules based on the SP and SD mechanisms as summarized in **Table 1.2**. **Figure 1.2** illustrates schematically typical types of through-space exchange couplings between spins.

Since the overlap integral disappears in the case of perpendicular approach, the potential exchange (PE) interaction between the spins in the SOMO(A) and SOMO(B) of the composite systems (A+B) plays an important role for the spin alignment as illustrated in Type I of **Fig. 1.3**, leading to the high-spin (HS) ground state. On the other hand, the intermolecular SOMO(A)-SOMO(B) overlap term (namely kinetic exchange (KE)) usually overweighs the PE term in the case of the parallel approach, giving rise to the negative J.

Therefore the ground state becomes the low-spin (LS) in this case as shown in Type II of **Fig. 1.3**.

The classification of the perpendicular and parallel approaches is also essential for other cases (Types III-XII) in **Fig. 1.2**. For example, Type III expresses the PE interaction between the SOMO(A)-spin and the induced negative spin (B) by the SP effect. Therefore the through-space interaction gives rise to the antiparallel spin alignment of the SOMO-spins as illustrated in **Fig. 1.2**, leading to the LS ground state. On the other hand, Type IV expresses the KE interaction between SOMO(A)-spin and induced negative spin (B) by the SP effect. The SOMO-spins align parallel because of this interaction as illustrated in **Fig. 1.2**, showing the HS ground state. The so-called McConnell model corresponds to this case. The spin alignment rules are reversed when the SOMO(A)-spin interacts with the induced positive spins by the SD or SP effects as shown in Types V and VI. Types VII-XII show both PE and KE interactions between induced spins by SP or SD. Type X denotes the McConnell-type spin alignment rule.

Thus, our intermolecular spin alignment rules are applicable to all of the parallel and perpendicular orientations of radical components. However, conformations of radicals and their packing modes are usually complex in real organic magnetic crystals. This in turn indicates that effective exchange interactions between the radicals are given be superpositions of the twelve different type interactions in general. Therefore, reliable molecular orbital calculations are necessary to elucidate contributions of these terms in many cases.

Table 1.1 The through-space exchange couplings (J_{ab}) between spins (X, Y)

case	X	Y	|Jab|
I	intrinsic spin in SOMO(or NBMO)	intrisic spin in SOMO(or NBMO)	large
II	intrinsic spin in SOMO(or NBMO)	induced spin by SP(or SD)	medium
III	induced spin by SP(or SD)	induced spin by SP(or SD)	small

a) notations : SP(spin polarization), SD(spin delocalization).

Table 1.2 Intramolecular spin alignment rules

Type	X	A.M.	Y	G.S.
I	SOMO(NBMO)	per.	SOMO(NBMO)	HS
II	SOMO(NBMO)	par.	SOMO(NBMO)	LS
III	SOMO(NBMO)	per.	negative IS by SP	LS
IV	SOMO(NBMO)	par.	negative IS by SP	HS
V	SOMO(NBMO)	per.	positive IS by SD or SP	HS
VI	SOMO(NBMO)	par.	positive IS by SD or SP	LS
VII	negative IS by SP	per.	negative IS by SP	HS
VIII	negative IS by SP	par.	negative IS by SP	LS
IX	negative IS by SP	per.	positive IS by SD or SP	LS
X	negative IS by SP	par.	positive IS by SD or SP	HS
XI	positive IS by SD or SP	per.	positive IS by SD or SP	HS
XII	positive IS by SD or SP	par.	negative IS by SD	LS

a) notations : A.M.: approach models, per. : perpendicular approach, par.: parallel approach ; IS: induced spin, SP : spin polarization, SD: spin delocalization, HS: high spin, LS: low spin, G.S.: ground spin state.

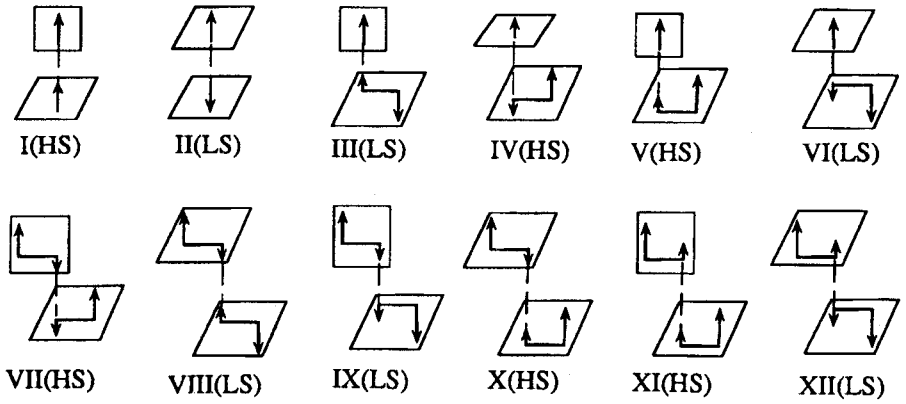

Figure 1.2 Schematic illustration of spin alignment rules based on the APUMP calculations. Small arrows denote the induced spin by SD or SP effects.

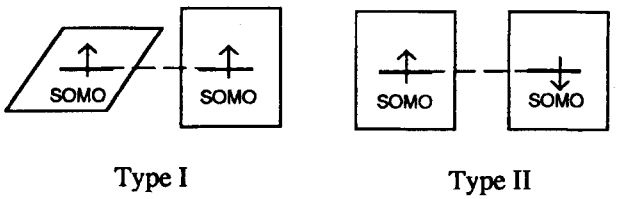

Figure 1.3 Potential (PE) and kinetic (KE) exchange interactions between spins in the SOMO(A) and SOMO(B)

Section 1.4

Recent development of *ab initio* MO and DFT theories

1.4.1 Theoretical background of HF and post-HF methods

HF (Hartree-Fock) method

The Hartree-Fock (HF) approximation, which is equivalent to the molecular orbital approximation, is central to quantum chemistry. This approximation is important not only for its own sake but as a starting point for more accurate approximations, which include the effects of electron correlation. Most of the computational methods of quantum chemistry depend on the Hartree-Fock approximation. Separated α and β orbitals will be computed in unrestricted HF (UHF) method, though α and β electrons occupied same orbitals in restricted HF (RHF) method.

CI (Configuration Interaction) method

Configuration interaction (CI) is a systematic procedure for going beyond the Hartree-Fock approximation. It has the important advantage that it is variational (i.e., at each level it gives an upper bound to the exact energy), but it has the disadvantage that it is only size consistent when all possible excitations are incorporated into the trial function (i.e., full CI).

MP (Møller-Plesset perturbation) method

A different systematic procedure for finding the correlation energy, which is not variational but is size consistent at each level, is perturbation theory (PT). In this approach the total Hamiltonian of the system is divided or partitioned into two pieces: a zeroth-order part and a perturbation. The exact energy is then expressed as an infinite sum of contributions of increasing complexity. If we have chosen the zeroth-order part wisely, then the perturbation is small and the perturbation expansion (i.e., the sum of the 1st, 2nd, ..., *n*th-order energies) converges quickly. Since we are interested in obtaining a perturbation expansion for the correlation energy, we choose the Hartree-Fock Hamiltonian as our zeroth-order Hamiltonian. The form of perturbation theory by Rayleigh and Schrodinger (RSPT) was applied to *N*-electron systems by C. Møller and M. Plesset. Hence it is sometimes called Møller-Plesset perturbation theory (MPPT). Alternatively, this approach is called many-body perturbation theory (MBPT).

CC (Coupled-Cluster) method

The coupled-cluster (CC) method is an attempt to introduce interactions among electrons within clusters (predominantly pairs) as well as coupling among these clusters of electrons and to permit the wavefunction to contain all possible disjoint clusters. For example, we know that electron pair interactions are of utmost importance and that contributions of quadruply excited configurations to |0> arise predominantly as products of doubly excited configurations. CC wavefunctions in which such electron pair interactions (clusters) are assumed to dominate still contain terms that describe disjoint products of electron pair clusters would suggest. The mechanism for introducing these cluster interactions is to write the wave-function |0> in terms of a so-called cluster operator T acting on a reference function describing noninteracting or noncoupled electrons $|0^0\rangle$:

$$|0\rangle = \exp(T)|0^0\rangle \tag{1.3}$$

CASSCF (Complete Active Space; Self Consistent Field) method

An multi-configuration SCF (MC-SCF) calculation is a combination of an SCF computation with a full CI involving a subset of the orbitals; this subset is known as the complete active space (CAS). A CASSCF method with the number of electrons *n* and the number of orbitals *m* in the active space is specified CASSCF[n, m].

In this study the author mainly used (AP)UHF, (AP)UMPn (n = 2, 4), (AP)UCC, UNO CASSCF[n, m] methods (indicated as italic-face in **Fig. 1.4**). The abbreviation AP indicates approximate spin projection which eliminates higher-order spin contamination from evaluated energy. Natural orbital analysis of UHF orbital (UNO) can improve and optimize its CAS space.

Unrestricted Hartree-Fock (UHF) molecular orbital calculations have been carried out for elucidation of effective exchange interactions between organic radicals. The UHF Møller-Plesset (MP) type (UHF MP = UMP) calculations have been carried out for their clusters in order to elucidate the correlation corrections for the through-space interaction modes. In addition UCC (concretely, APUCCSD(T), etc.) methods have been carried out, though these methods are very expensive for CPU time. On the other hand, UNO CASSCF methods are employed in order to include nondynamical correlation correction effect.

1.4.2 Theoretical background of DFT method

The treatment of the many-fermion systems, such as electrons, are characterized by a non-relativistic time-independent Hamiltonias have been developed with the Hohenberg-Kohn theorem. Thus, the total energy in the density functional theory (DFT)[29,30] is given by

$$E_{el} = -\frac{1}{2}\sum_i \int \phi_i(r_1)\nabla^2\phi_i(r_1)dr_1 + \sum_A \int \frac{Z_A}{|R_A - r_1|}\rho(r_1)dr_1 + \frac{1}{2}\sum_i \int \frac{\rho(r_1)\rho(r_2)}{|r_1 - r_2|}dr_1dr_2 + E_{xc} \qquad (1.4)$$

$$\rho(r_1) = \sum_i \phi_i(r_1)\phi_i(r_1) \quad (density) \qquad (1.5)$$

$$E = T(r) + V(r) + G(r) + E_{XC}(r) \qquad (1.6)$$

where T(r), V(r), G(r) and $E_{XC}(r)$ are the electronic kinetic energy, the electron-nuclear attraction energy, the Coulombic repulsion energy between electrons and the exchange-correlation energy, respectively. The total density ρ is given by the spin-unrestricted approximation as

$$\rho = \rho^\alpha + \rho^\beta \qquad (1.7)$$

where the densities of the up- and down-spins are given by their orthogonal orbitals

$$\rho^\alpha = \sum|\phi_i^\alpha|^2, \quad \rho^\beta = \sum|\phi_i^\beta|^2 \qquad (1.8)$$

The spin orbitals ϕ_i^{γ} ($\gamma = \alpha, \beta$) can be determined by the spin-unrestricted Kohn-Sham (UKS) equation obtained by the minimization of the total energy in Eq. (1.6)

$$\left[-\frac{1}{2}\nabla^2 + \sum_A \frac{Z_A}{|R_A - r_1|} + \int \frac{\rho(r_2)}{|r_1 - r_2|} dr_2 + V_{XC}\right]\phi_i(r_1) = h_{KS}\phi_i(r_1) = \varepsilon_i\phi_i(r_1) \tag{1.9}$$

$$V_{XC}[\rho] = \delta E_{XC}[\rho]/\delta\rho \quad (exchange-correlation\ \ potential) \tag{1.10}$$

$$\hat{H}(UKS)\phi_i^{\gamma} = \varepsilon_i\phi_i^{\gamma} \tag{1.11}$$

The explicit form of H(UKS) is identical to the UHF equation except for the exchange-correlation part.

There are several approximate formulas for the exchange-correlation energy $E_{XC}(r)$ in the UKS-based DFT methods. The local density approximation (LDA) is given by

$$E_{XC}^{LDA} = E_X^{LDA} + E_C^{LDA} \tag{1.12}$$

where exchange and correlation parts are given[29,30,31,32,33,34], respectively, as

$$E_X^{LDA} = -\frac{9}{4}\alpha_{ex}\left(\frac{3}{4\pi}\right)^{\frac{1}{3}} \times \sum_r \int \left\{\left[\rho_1^{\alpha}(r_1)\right]^{\frac{4}{3}} + \left[\rho_1^{\beta}(r_1)\right]^{\frac{4}{3}}\right\} dr_1 \tag{1.13}$$

$$E_C^{LDA} = \int dr_1 \rho_1^{\gamma}(r_1)\varepsilon_i\left[\rho_1^{\alpha}(r_1), \rho_1^{\beta}(r_1)\right] \quad (\gamma = \alpha, \beta) \tag{1.14}$$

The α_{ex}-value in Eq. (1.13) is 2/3 in the case of Slater's (S) functional[35], whereas it is assumed to be 0.7 for the X_{α} functional. Becke's 1988 (B) functional[36] includes Slater's (S) functional plus nonlocal gradient correction.

In Eq. (1.14), E_c^{LDA} represents the correlation energy per electron with spin densities for the up- and down-spins:

$$\varepsilon_i\left[\rho_1^{\alpha}(r_1), \rho_1^{\beta}(r_1)\right] \tag{1.15}$$

The analytical form of this functional is not known yet, but several approximations have been developed. The LDA approximation originated from the theory of homogeneous

electron gas, and therefore the non-local (NL) correlation correction was required in order to represent the inhomogeneity of electron density in molecular systems.

$$\tilde{E}_X = E_X^{LDA} + E_X^{NL} \tag{1.16}$$

$$E_X^{NL} = \sum_{\gamma} \int dr_1 g\left[\frac{\left|\nabla \rho_1^{\gamma}(r_1)\right|}{\left|\rho_1^{\gamma}(r_1)\right|}\right]\left[\rho_1^{\gamma}(r_1)\right]^{\frac{4}{3}} \tag{1.17}$$

The approximate correlation-correction functionals were proposed as follows: (1) Vosko-Wilk-Nusair (VWN)[37] and (2) Perdew's 1981 (PL) functionals[38], which are the LDA correlation functionals, (3) Perdew's 1986 (P86)[39] and (4) Lee-Yang-Parr functional (LYP)[40], which are gradient-corrected correlation functionals. For example, the following equation is LYP functional:

$$\begin{aligned} E_C = & -a\int \frac{4}{1+d\rho^{-1/3}} \frac{\rho_\alpha \rho_\beta}{\rho} - ab\int \omega \Bigg\{ \rho_\alpha \rho_\beta \Bigg[2^{11/3} C_F \left(\rho_\alpha^{8/3} + \rho_\beta^{8/3}\right) + \left(\frac{47}{18} - \frac{7}{18}\delta\right)|\nabla\rho|^2 \\ & - \left(\frac{5}{2} - \frac{1}{18}\delta\right)|\nabla\rho|^2 - \left(\frac{5}{2} - \frac{1}{18}\delta\right)\left(|\nabla\rho_\alpha|^2 + |\nabla\rho_\beta|^2\right) - \frac{\delta - 11}{9}\left(\frac{\rho_\alpha}{\rho}|\nabla\rho_\alpha|^2 + \frac{\rho_\beta}{\rho}|\nabla\rho_\beta|^2\right)\Bigg] \\ & - \frac{2}{3}\rho^2|\nabla\rho|^2 + \left(\frac{2}{3}\rho^2 - \rho_\alpha^2\right)|\nabla\rho_\beta|^2 + \left(\frac{2}{3}\rho^2 - \rho_\beta^2\right)|\nabla\rho_\alpha|^2 \Bigg\} dr \end{aligned} \tag{1.18}$$

$$\omega = \frac{\exp\left(-c\rho^{-1/3}\right)}{1+d\rho^{-1/3}} \rho^{-11/3}$$

$$\delta = c\rho^{-1/3} + \frac{d\rho^{-1/3}}{1+d\rho^{-1/3}}$$

$$C_F = \frac{2}{10}\left(3\pi^2\right)^{2/3}$$

In addition to these correlation corrections, the self-energy correction is required in several cases such as transition states for free radical reactions.

1.4.3 Evaluation of spin densities by *ab initio* MO and DFT theories

The distribution of the spin densities on some atoms within a molecule is important. The spin distribution propagates the intermolecular magnetic interactions and yields complicated relation between the magnetic interactions and the molecular packing. It must be mentioned that the spin density becomes an important parameter because it can affect the sign of intermolecular interactions and so on.

Recent development of semi-empirical, *ab initio* MO and DFT method enable us evaluate these spin densities and computational discussion for them become important. Thus, the author employed these quantum calculation methods for studying spin densities and successfully obtained detailed numerical results. For experimental studies Schweizer and his collaborators have made extensive neutron-diffraction experiments for several nitroxides such as TANOL suberate and phenyl nitronylnitroxide (PNNO) in order to elucidate spin density populations.

For the remarkable example studied by the author and his co-worker, spin densities for *p*-NPNN in the β-phase crystal were calculated by UHF, APUHF and UKS B(S)-LYP methods. **Figure 1.5** indicates the atoms numbering in a β-*p*-NPNN molecule and **Table 1.3** summarized the obtained results. *Ab initio* UHF overestimated a negative spin density induced on the α-carbon atom of nitronylnitroxide group by spin polarization effect, whereas the approximately spin-projected UHF(APUHF)/6-31G* method provided a reasonable negative spin density on the α-carbon atom and almost equal distributions of spin density on nitrogen and oxygen atoms in *p*-NPNN, in accord with the recent experiments. The spin populations on the benzene ring in these species by APUHF/6-31G* and APUHF/INDO and UKS B-LYP/6-31G* methods were similar to the experimental values, indicating the important role of the spin polarization effect.

1.4.4 Magnetic dipole-dipole interactions

Since the recent discovery of bulk ferromagnetism, much interest has been aroused in molecular magnetism and many organic molecular crystals have been found to show long range magnetic ordering. In the sense that the molecular magnets can be described in terms of Heisenberg Hamiltonian of S=1/2 spins, their magnetic properties are essentially the same as those of transition-metal compounds. However, Kawamoto and Suzuki expect some peculiar features to the molecular organic magnets[41]. One is the origin of anisotropy. The anisotropy of the exchange coupling in molecular magnets is expected to be small compared with that in transition-metal compounds because of smallness of the spin-orbit interaction. Then, it is naturally expected that the dipole-dipole interaction will dominantly contribute to the anisotropy energy in molecular magnets.

Table 1.3 Spin densities of *p*-NPNN in the β-phase crystal by the UHF- and UKS-based methods

Atoms	UHF[a)]	APUHF[a)]	UHF[b)]	APUHF[b)]	B-LYP[a)]	Exp[c)]
N_1	0.484	0.251	0.287	0.199	0.223	0.278
N_2	0.484	0.251	0.287	0.199	0.223	0.258
O_1	0.443	0.282	0.526	0.378	0.322	0.283
O_2	0.443	0.282	0.526	0.378	0.322	0.283
C_1	-0.868	-0.090	-0.572	-0.150	-0.111	-0.090
C_2	0.777	0.032	0.077	0.000	0.014	-0.000
C_3	-0.717	-0.013	-0.072	-0.007	-0.010	-0.001
C_4	0.678	0.004	0.040	0.000	0.004	-0.011
C_5	-0.649	-0.022	-0.054	-0.004	-0.009	-0.008
C_6	0.678	0.004	0.040	0.000	0.004	-0.011
C_7	-0.717	-0.013	-0.072	0.007	-0.010	-0.001
N	0.098	-0.000	0.007	-0.000	0.000	0.021

a) The 6-31G* basis set is used.
b) The INDO parameter is used.
c) J. Schweizer, private communacation.

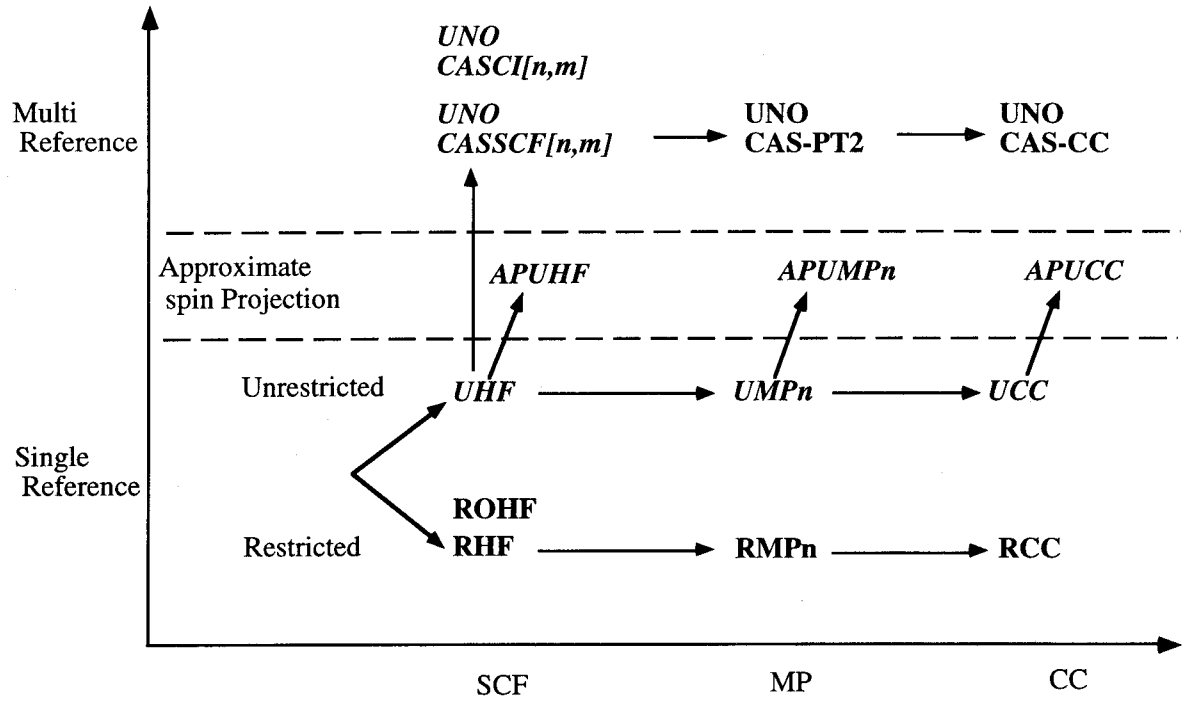

Figure 1.4 Several methods in *ab initio* MO theory are summarized. Italic-face indicates the methods which were employed in this study.

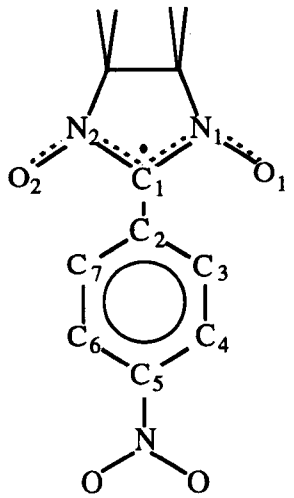

Figure 1.5 Geometries of *p*-NPNN in the β-phase crystal and atoms numbering.

Section 1.5

Formulation of effective exchange integral (J_{ab})

1.5.1 UHF solution and regions I, II and III

The theoretical background which is necessary for systematic investigations of molecular magnetism is briefly considered. Supposing that the composed atoms are equidistant each other in the linear (one-dimension) clusters, the potential energy curves with variation of the interatomic distance are schematically illustrated in **Fig. 1.6** for several calculation procedures. They are divided into three characteristic regions. The region I is a nonmagnetic or weak correlation region which is characterized by strong orbital interactions and formations of strong covalent bonds. On the other hand, the region III is regarded as a magnetic region where component radicals exhibit weak intermolecular interactions. The region II is characterized as a transition region from the nonmagnetic region I to the magnetic region III. The *ab initio* restricted Hartree-Fock (RHF) molecular orbital (MO) and closed-shell DFT methods have been utilized for elucidation of electronic structures of closed-shell one-dimension clusters in the region I. However, the intrinsic deficiency of the RHF MO and closed-shell DFT methods is that they can not describe dissociation process of a covalent bond from the region I to III even in qualitative sense. An approach to this problem within the Hartree-Fock (HF) MO and DFT frameworks leads to use of the unrestricted HF (UHF) and spin-polarized DFT theories.

1.5.2 Computational scheme of effective exchange integrals

The experimental results for molecular magnetic materials have been reasonably explained by the spin Hamiltonian models. In fact, the linear atomic clusters in the region III are well described by valence-bond (VB) picture such as Heisenberg model Hamiltonian:

$$H = -\sum 2J_{ab}S_a \cdot S_b \tag{1.19}$$

J_{ab} presents the effective exchange integral between the spins of S_a and S_b at sites a and b as shown in **Fig. 1.7**. The negative sign of J_{ab} leads the antiferromagnetic coupling of spins in the system, while positive sign results in ferromagnetic coupling.

Since the total energies of the highest-spin (HS) and lowest-spin (LS) UHF (or SP DFT) solutions correspond to those of the HB models, respectively, the energy gap can be used to estimate effective exchange integrals (J_{ab}) as

$$J_{ab}(Z) = \left[{}^{HS}E(Z) - {}^{LS}E(Z)\right] / \Delta(ZI) \tag{1.20}$$

where,

$$\Delta(ZI) = 4(N-1)S_a \cdot S_b \tag{1.21}$$

and Z = UHF or SP DFT and N is number of spin site under consideration. The S_a and S_b are the sizes of spins at sites a and b. If the electron correlation is taken into account under the UHF approximation, the effective exchange integrals by UHF in Eq. (1.20) is replaced by that of UHF-X (X= UMP, UCC or DFT).

$$J_{ab}(UHF-X) = \left[{}^{HS}E(UHF-X) - {}^{LS}E(UHF-X)\right] / \Delta(ZI) \tag{1.22}$$

On the other hand, the spin projection of the UHF-X wavefunctions in region II is a difficult task, since the orbital overlaps between radical orbitals are significantly large. The Löwdin-type spin-projection scheme is utilized for this purpose. However, it often provides incorrect J_{ab} values because, of the introduced approximations. Alternately, approximate spin projections are feasible for UHF-based and spin-polarized DFT methods to calculate potential curves for dissociations from region I to region III. To this end, we have considered an approximate but size-consistent spin-projection procedure, where the denominator in Eq. (1.20) is modified so as to reproduce the extreme values of the total spin angular momentum in regions I and III as

$$\Delta(ZII)={}^{HS}\langle S^2\rangle(Z)-{}^{LS}\langle S^2\rangle(Z)-S_a g(N)\left[{}^{LS}\langle S^2\rangle(Z)-S_r(S_r+1)\right] \tag{1.23}$$

where

$$\begin{aligned} g(N)&=(N-2)^2/N \quad (N>2 \ \textit{and even numbers}) \\ &=(N-3) \qquad (N>3 \ \textit{and odd numbers}) \end{aligned} \tag{1.24}$$

and Z = UMP, UCC or DFT, and S_r denotes the exact spin angular momentum for the clusters under discussion:

$$\begin{aligned} S_r&=n(S_a-S_b) \qquad (N=2n) \\ &=n(S_a-S_b)+S_a \quad (N=2n+1) \end{aligned} \tag{1.25}$$

The effective exchange integral by the approximate spin-projected (AP-) UMP, UCC and DFT methods are, therefore, given by

$$J(AP-Z)=\left[{}^{HS}E(Z)-{}^{LS}E(Z)\right]/\Delta(ZII) \tag{1.26}$$

The J_{ab}(AP-Z) value almost reduces to that of Eq. (1.20) in magnetic region III, whereas it becomes a theoretical parameter for the spin projection in the intermediate (II) and strong overlap (I) regions, where the spin-contamination effects in UHF and spin-polarized DFT wavefunctions are more or less decreased.

The potential curves by the UMP method often show humps arising from the spin contaminations. The J_{ab}(AP-Z) values in Eq. (1.26) can be used to improve the shapes of the potential curves by Z, as illustrated in **Fig. 1.8**. The total energies by AP-Z are given by

$${}^{LS}E(AP-Z)={}^{LS}E(Z)+J_{ab}(AP-Z)\left[{}^{LS}\langle S^2\rangle(Z)-S_r(S_r+1)\right]\left[1-h(N)\right] \tag{1.27}$$

where

$$\begin{aligned} h(N)&=(N-2)^2/N^2 \quad (N>2 \ \textit{and even numbers}) \\ &=(N-3)/(N+1) \ (N>3 \ \textit{and odd numbers}) \end{aligned} \tag{1.28}$$

The AP-Z energy reduces to that of RHF-X or ORHF-X (X=MP, CC) in region I, since the second term in Eq. (1.27) disappears, whereas it becomes equivalent to the projected UHF-X energy by Eq. (1.20) in region III. As previously, the AP-Z potential curves are good approximations to those of UNO CASSCF PT2 (CASPT2) in the case of small hydrogen

clusters. The energy correction by spin projection should be normalized by the size of the cluster (N) in order to appropriately estimate the projection effect for large N.

$$\Delta E(AP-Z)=\left[{}^{LS}E(AP-Z)-{}^{LS}E(Z)\right]/N \tag{1.29}$$

$$=J_{ab}(AP-Z)\left[{}^{LS}\left\langle S^2\right\rangle(Z)-S_r(S_r+1)\right]\left[1-h(N)\right]/N \tag{1.30}$$

Since $^{LS}\langle S^2\rangle(Z)$ is approximately proportional to N, the projection effect of Eq. (1.30) approaches zero if N becomes larger. In fact, for large N,

$$\Delta E(AP-Z)\approx 4J_{ab}(AP-Z)/N \tag{1.31}$$

Therefore, the spin-projection correction for the LS state decreases along with an increase in the cluster size (N) and the energy correction by the spin projection is negligible if the site number N exceeds a certain limit.

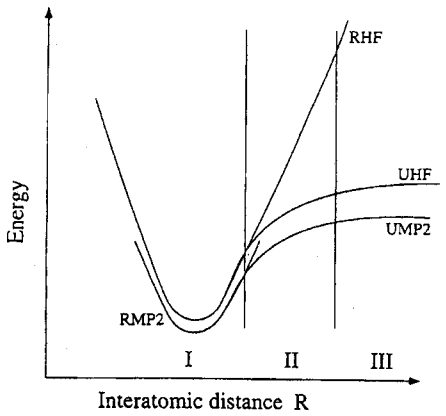

Figure 1.6 Schematic illustrations of potential curves for the lowest-spin (LS) ground state of one-dimension cluster, where the composed atoms are equidistant each other, with variation of interatomic distance at levels of RHF, UHF, MP2. Region I is a nonmagnetic region, III is a magnetic region, and II is a intermediate region from I to III.

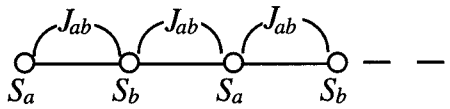

Figure 1.7 One-dimension magnetic cluster with sizes of spins, S_a and S_b, at sites a and b, and also a uniform effective exchange integral (J_{ab}) between sites a and b.

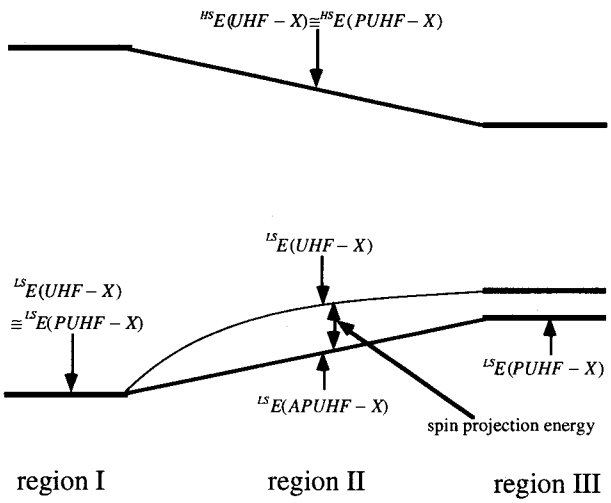

Figure 1.8 Schematic illustrations of the potential curves of spin-unprojected and -projected post UHF solutions (UHF-X) for mesoscopic clusters with N-magnetic sited.

Section 1.6

Details of the following chapters

To the purpose of fulfillment this doctorate thesis, step by step studies are carried out and summarized systematic. The contents will be mainly divided into the following subjects:

(1) to examine the J_{ab} formulation, since the author has already developed the formulation of effective exchange integral in the section 1.5. The numerical investigation with the quantum *ab initio* molecular orbital theory in several cases, i.e. liner clusters composed of triplet methylenes and quartet nitrogen atoms within the face-to-face stacking and the perpendicular stacking. (Chapter 2)

(2) to carry out basic discussion of interaction modes between two radicals. The decomposition of effective exchange interaction leads to essential and important solutions. Next, the classification of magnetic interaction is derived for simple approach models. (Chapter 3)

(3) to verify and extend no-overlap and orientation principles for ferromagnetic exchange interactions between organic radicals in several cases. In order to accomplish ferromagnetic interactions between organic radicals, the KE-term should disappear, leading to the no-overlap between SOMOs. (Chapter 4)

(4) to investigate possibilities of the ferromagnetic interaction through bridge hydrogen atoms under adequate intermolecular stacking conditions and orientations. It has been suggested that hydrogen-atom bridges are effective for weak intermolecular ferromagnetic exchange interactions between nitroxides. Such weak interactions via hydrogen bridges attract current interest in relation to the ferromagnetic phase transitions in several crystalline organic ferromagnets discovered recently. (Chapter 5)

(5) to take into account not only inter- but also intra-molecular magnetic interaction and discuss coupling among these interactions. For this purpose, the biradical species, i.e TMAO which was reported by Rassat and co-workers, are very important. (Chapter 6)

(6) to investigate active control of magnetic interaction by external conditions such as the high pressure is challenges in molecule-based materials. For this purpose, the pressure effect on the intermolecular effective exchange interactions in the β-phase of *p*-NPNN was investigated. (Chapter 7)

(7) to apply the quantum statistical method to the theoretical studies of the magnetic properties. We have been progressing the numerical treatment of it. In our treatments the numerical partition function can be calculated directly. Numerical calculations were performed with the Monte Carlo (MC) method. (Chapter 1 in Part II)

Chapter 2.

Computational Methods of Effective Exchange Integrals (Methylene and Nitrogen Radical Clusters)

Section 2.1

Introduction

Molecule-based magnetic materials have received continuous experimental and theoretical interest. The author has already developed the formulation of effective exchange integral in the section 1.5. As is well known, the electronic structures and thermodynamic properties of low-dimensional magnetic clusters, chains and sheets are fundamental problems.

In this chapter, the verification of formalism are ensured. The numerical investigation with quantum *ab initio* molecular orbital theory in several cases, i.e. liner clusters composed of triplet methylenes and quartet nitrogen atoms within the face-to-face stacking and the perpendicular stacking. We discuss the electronic structures of linear magnetic clusters comprising eleven methylenes, eleven nitrogen atoms, and five methylenes plus six nitrogen atoms by the unrestricted Hartree-Fock (UHF) and post UHF methods in combination with the Heisenberg model. In addition, spin-polarized density functional (BLYP and B3LYP) calculations followed by a size-consistent spin projection have also been carried out for comparisons with these methods, since the DFT methods are heavily used in the solid state physics.

Section 2.2

ab initio MO calculations for J_{ab} values

Linear clusters of triplet methylenes

Let us first consider the face-to-face (parallel conformation) clusters (N = 2, 3 and 11) of triplet methylenes, as illustrated in **Figs. 2.1**-A(N = 3) and B(N = 11). The effective exchange interactions were calculated from Eqs. (1.20) and (1.26) using the total energies of the lowest-spin (LS) singlet and the highest-spin (HS) states by the 6-31G* basis sets. **Table 2.1** summarizes the calculated results.

About dimer, the calculated J_{ab} values were negative (antiferromagnetic) in sign over the entire intermolecular interaction region. The magnitude of J_{ab}(UHF) by Eq. (1.20) and J_{ab}(APUHF) by Eq. (1.26) are quite similar, showing that the orbital overlaps between the magnetic orbitals are very small in the region. The J_{ab}(APUHF) values are also close to the corresponding J_{ab} values by CASSCF, which utilizes the four active orbitals and four active electrons {4,4}. This indicates that both APUHF and UNO CASSCF involve only the so-called nondynamical correlation within the {4,4} space. It is noteworthy that a larger CAS space than {4,4} is necessary for the latter approach to include dynamical correlation corrections.

Next, about trimer the magnitude of the J_{ab}(UHF) and J_{ab}(APUHF) values are almost the same. The J_{ab} values are also close to the corresponding J_{ab} values for the dimer. This supports the nearest-neighbor approximation used in Eqs. (1.20) and (1.26). The slight difference on the J_{ab} value between the dimer and trimer should be related to the weak delocalization effect.

Finally, about linear cluster (N = 11), the total energies of both the LS triplet and HS 23-th multiplet (S = 11) states were calculated. The difference between J_{ab} (UHF) and J_{ab} (APUHF) is small, even in this cluster, in accord with the small orbital overlaps between the magnetic orbitals in the region III. The magnitude of the J_{ab} value is quite similar to the

corresponding value for the dimer and trimer, showing a non-dependency of the size effect of clusters.

The present numerical results conclude that the sign and magnitude of the J_{ab} values for magnetic clusters comprising triplet methylenes can be estimated on the basis of small cluster models, such as a dimer and trimer.

The calculated J_{ab} values for face-to-face clusters of triplet methylenes are negative in sign. The negative J_{ab} values mean that the spins ($S_a = S_b = 1$) at sites a and b align intermolecularly in the antiparallel manner. The orbital average J_{ab} value for the dimer is given by

$$J_{ab} = (2\times 2)^{-1}\left(J_{p\sigma-p\sigma} + J_{n-n} + 2J_{n-p\sigma}\right) , \qquad (2.1)$$

where $J_{p\sigma\text{-}p\sigma}$, $J_{n\text{-}n}$ and $J_{n\text{-}p\sigma}$ denote, respectively, the effective exchange integrals for the pσ-pσ, n-n (n: lone pair orbital) and n-pσ orbital pairs as illustrated in **Fig. 2.2**A. Although the sign of $J_{p\sigma\text{-}p\sigma}$ and $J_{n\text{-}n}$ should be negative (antiferromagnetic) because of non-zero orbital overlaps, the sign of $J_{n\text{-}p\sigma}$ becomes positive (ferromagnetic) because of the orbital orthogonality. The negative J_{ab} value implies that the pσ-pσ orbital overlap interaction plays a predominant role for the effective exchange interaction in this conformation, in conformity with our orbital overlap and orientation principles for molecular magnetism.

Similarly, the orbital average J_{ab} value for the dimer in the perpendicular stacking illustrated in **Fig. 2.2**B is given by

$$J_{ab} = (2\times 2)^{-1}\left(J_{p\sigma-p\pi} + J_{n-p\pi} + J_{p\sigma-n} + J_{n-n}\right) . \qquad (2.2)$$

It is expected from a consideration of the orbital orthogonality and non-zero orbital overlap interaction that the $J_{p\sigma\text{-}p\pi}$ and $J_{n\text{-}p\pi}$ values should be positive in sign, and $J_{p\sigma\text{-}n}$ and $J_{n\text{-}n}$ are negative. It can be seen from **Table 2.1** that the calculated J_{ab} value for a cluster of eleven triplet methylene in the perpendicular stacking shown in **Fig. 2.1**C are positive in sign in all of the interatomic regions examined here. This indicates that the orbital orthogonality effects of pσ-pπ and n-pπ are more important for the effective exchange integral than the orbital overlap interaction of pσ-n and n-n, in contrast with the case of the face-to-face conformers.

Linear cluster of quartet nitrogen atoms

The ground state of the nitrogen atom is a quartet and the orbital average J_{ab} value for the dimer of the quartet nitrogen atom is given by, as illustrated in **Fig. 2.2**C,

$$J_{ab} = (3\times 3)^{-1}\left(J_{p\sigma-p\sigma} + 2J_{px-px} + 4J_{p\sigma-py} + 2J_{px-py}\right) , \qquad (2.3)$$

where $J_{px\text{-}px}$, $J_{p\sigma\text{-}py}$ and $J_{px\text{-}py}$ denote, respectively, the effective exchange integrals for the px-px, pσ-py and px-py orbital pairs. The sign of $J_{p\sigma\text{-}p\sigma}$ and $J_{px\text{-}px}$ should be negative (antiferromagnetic) because of non-zero orbital overlaps, but the sign of $J_{p\sigma\text{-}py}$ and $J_{px\text{-}py}$ becomes positive (ferromagnetic) because of the orbital orthogonality. Since the pσ-pσ orbital overlap interaction plays a predominant role for the effective exchange interaction, the J_{ab} value should be negative, but its magnitude becomes smaller than that of the triplet methylene dimer, since the latter two terms in Eq. (2.3) are contributable.

In order to confirm the above prediction, a linear cluster comprising eleven nitrogen atoms with equal interatomic distance was examined by the UHF/4-31G method. Both the LS and HS states were constructed, and the total energies of these states were calculated to obtain a J_{ab} value. They are summarized in **Table 2.2**. The J_{ab} values are negative, showing that the antiferromagnetic spin alignment is more stable than other spin alignments, such as the ferromagnetic one. The J_{ab} values by UHF and APUHF were calculated to be quite similar, in conformity with the small orbital overlaps between the magnetic orbitals. The magnitude of the J_{ab} value was reduced to about one-tenth of the J_{ab} value of the methylene cluster, supporting the above orbital interaction arguments based on the model in **Fig. 2.2**.

Linear cluster of six quartet nitrogen atoms plus five triplet methylenes

Figure 2.1D shows a linear cluster comprising five triplet methylenes and six quartet nitrogen atoms. This cluster has a distinct size of spins, such as $S_a = 3/2$ and $S_b = 1$, at sites a and b for nitrogen atoms and methylenes, respectively, being different from those having an equivalent size of spins of $S_a = S_b = 1$ in the case of linear clusters comprising triplet methylenes. The orbital average J_{ab} value for the dimer of the nitrogen atom and methylene, which is illustrated in **Fig. 2.2**D, is given as

$$J_{ab} = (3\times 2)^{-1}\left(J_{px-n} + J_{py-n} + J_{p\sigma-n} + J_{py-p\sigma} + J_{px-p\sigma} + J_{p\sigma-p\sigma}\right) , \qquad (2.4)$$

where $J_{px\text{-}n}$, $J_{p\sigma\text{-}n}$, and $J_{p\sigma\text{-}p\sigma}$ values should be negative in sign because of a non-zero orbital overlap, while the $J_{py\text{-}n}$, $J_{py\text{-}p\sigma}$, and $J_{px\text{-}p\sigma}$ values becomes positive in sign due to the orbital orthogonality. The effective exchange integrals at the levels of UHF/4-31G and APUHF/4-31G are also summarized in **Table 2.2**. The J_{ab} values are negative in sign for both methods, indicating that an antiparallel spin alignment (antiferromagnetic) is more stable than a parallel spin alignment (ferromagnetic). The negativity of the J_{ab} values comes from greater contributions of $J_{px\text{-}n}$, $J_{p\sigma\text{-}n}$ and $J_{p\sigma\text{-}p\sigma}$ rather than $J_{py\text{-}n}$, $J_{py\text{-}p\sigma}$ and $J_{px\text{-}p\sigma}$. $J_{p\sigma\text{-}p\sigma}$

could be expected to be the main factor because of a strong pσ-pσ overlap. It is, furthermore, noted that the APUHF method gives J_{ab} values similar to those of UHF method, even different sizes of spins at sites a and b, compared with the cases of equivalent sizes of spins at sites a and b.

Table 2.1 Effective exchange integrals J_{ab} (cm^{-1}) of clusters composed of triplet methylene, using 6-31G* (4-31G in parenthesis) basis sets for N = 2 and 3, 4-31G basis sets for N = 11.

R	$(CH_2)_2$[‖]					$(CH_2)_3$[‖]			
Å	UHF		APUHF		CASSCF	UHF		APUHF	
3.0	−401.2	(−390.8)	−396.6	(−386.5)	−411.7	−405.7	(−393.3)	−400.7	(−393.3)
3.2	−228.6	(−220.7)	−227.1	(−219.3)	−233.1	−230.2	(−221.4)	−228.7	(−220.0)
3.4	−129.3	(−123.3)	−128.8	(−122.8)	−130.5	−130.1	(−123.4)	−129.6	(−123.0)
3.6	−72.46	(−67.79)	−72.30	(−67.66)	−71.9	−72.64	(−67.80)	−72.49	(−67.67)
3.8	−40.03	(−36.46)	−39.98	(−36.43)	−38.7	−40.23	(−36.46)	−40.19	(−36.42)
4.0	−21.71	(−19.05)	−21.69	(−19.04)	−20.2	−21.95	(−19.05)	−21.94	(−19.04)
4.4	−5.877	(−4.613)	−5.876	(−4.616)	−4.9	−6.507	(−4.617)	−6.507	(−4.616)
4.8	−1.366	(−0.9118)	−1.366	(−0.9118)	−0.96	−1.852	(−0.9118)	−1.852	(−0.9118)
5.5	−0.0604	(−0.0295)	−0.0604	(−0.0295)	−0.03	−0.618	(−0.291)	−0.618	(−0.0291)
6.0	−0.0055	(−0.0014)	−0.0055	(−0.0014)	−0.001	−0.0466	(−0.0013)	−0.0466	(−0.0013)
10.0	0.00	(0.00)	0.00	(0.00)	−0.00	−0.00	(0.00)	−0.00	(0.00)

$(CH_2)_{11}$[‖]		$(CH_2)_{11}$[⊥]	
UHF	APUHF	UHF	APUHF
−395.4	−371.6	141.7	144.5
−222.0	−216.9	85.37	87.54
−123.6	−123.7	50.15	51.58
−67.82	−68.83	28.88	29.76
−36.46	−37.31	16.37	16.89
−19.05	−19.58	9.167	9.461
−4.617	−4.764	2.772	2.863
−0.9120	−0.9420	0.7821	0.8079
−0.0295	−0.0305	0.0617	0.0637
−0.0016	−0.0016	0.0067	0.0069
−0.00	−0.00	0.00	0.00

Table 2.2 Effective exchange integrals J_{ab} (cm^{-1}) of linear clusters of N_{11} and N-$(CH_2$-N$)_5$ using 4-31G basis set.

R	N_{11}		N-$(CH_2$-N$)_5$	
Å	UHF	APUHF	UHF	APUHF
3.0	−31.77	−31.96	−120.0	−117.3
3.2	−15.82	−15.82	−64.31	−64.06
3.4	−7.896	−7.919	−34.17	−34.41
3.6	−3.913	−3.930	−17.90	−18.13
3.8	−1.891	−1.901	−9.152	−9.302
4.0	−0.8737	−0.8786	−4.519	−4.601
4.4	−0.1533	−0.1542	−0.9490	−0.9674
4.8	−0.0195	−0.0197	−0.1547	−0.1577
5.5	−0.0023	−0.0024	−0.0031	−0.0032
6.0	−0.0000	−0.0000	−0.0001	−0.0001
10.0	0.0000	0.0000	0.0000	0.0000

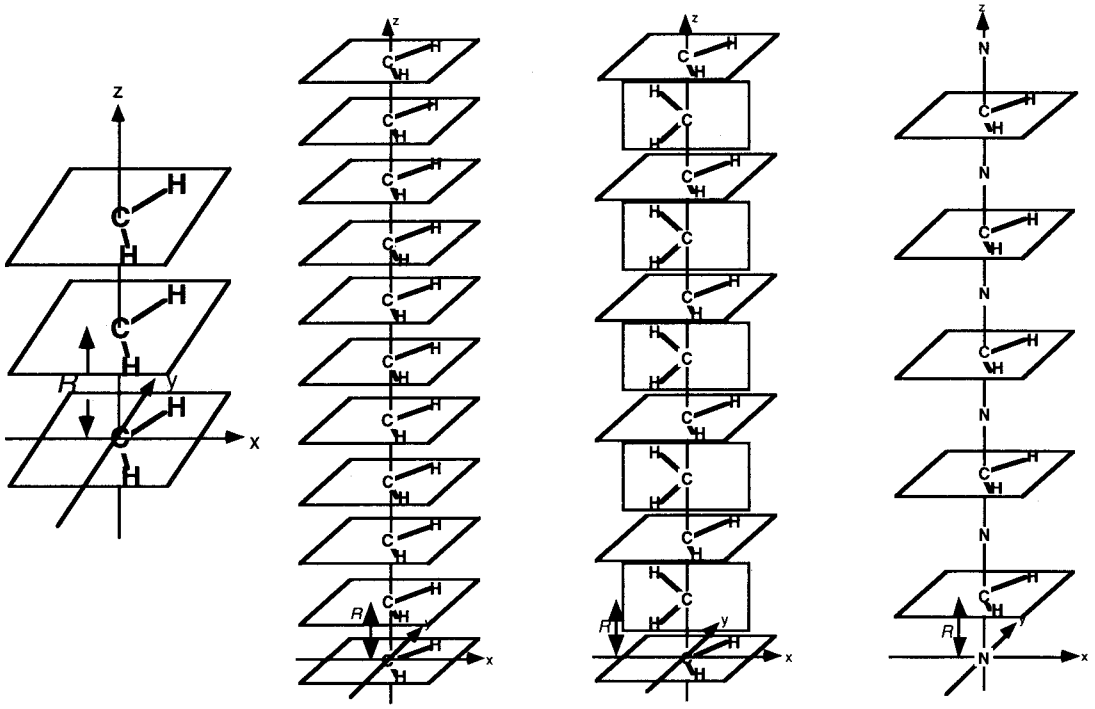

Figure 2.1 Schematic illustrations of liner clusters composed of triplet methylenes and quartet nitrogen atoms; (A) trimer of triplet methylenes in the face-to-face stacking, (B) eleven triplet methylenes in the face-to-face stacking, (C) eleven triplet methylenes in the perpendicular stacking, (D) five triplet methylenes and six quartet nitrogen atoms.

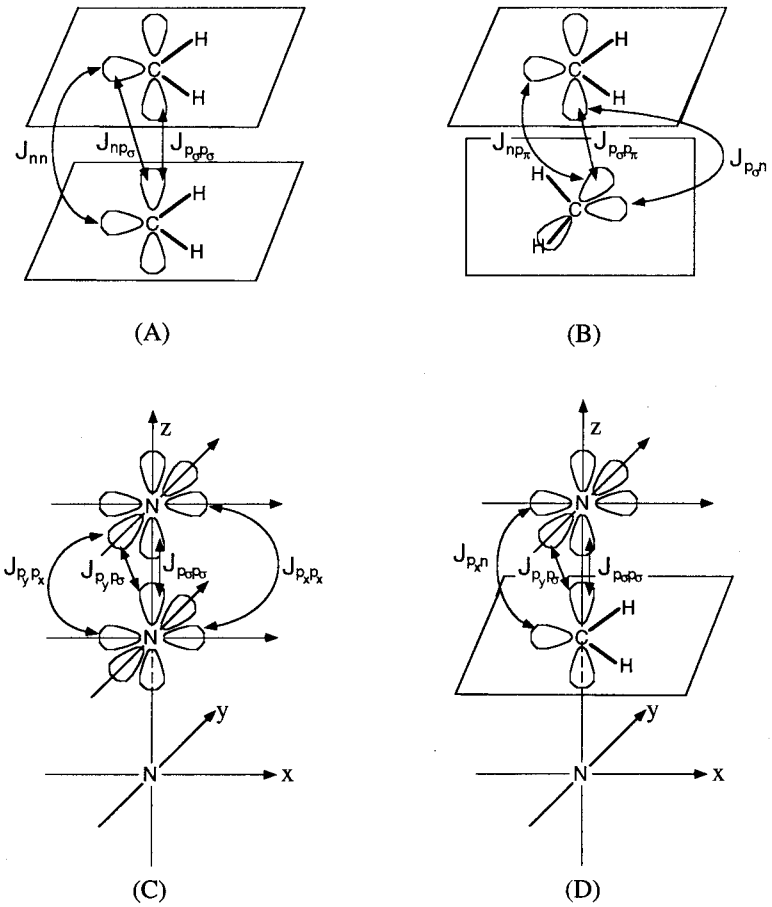

Figure 2.2 Schematic representations of the orbital averaged effective exchange integral J_{ab} composed of exchange integrals between interatomic orbitals. (A) $(CH_2)_2$; face-to-face conformation, (B) $(CH_2)_2$; perpendicular conformation, (C) dimer composed of quartet nitrogen atoms, (D) dimer composed of quartet nitrogen atom and triplet methylene.

Section 2.3

DFT calculations for J_{ab} values

The density functional (DFT) methods have been successfully applied to computations of the potential surfaces for organic reactions. Therefore, it is particularly interesting to examine the applicability of the DFT methods to compute the J_{ab} values.

First, we applied DFT methods to evaluation of J_{ab} values for the triplet methylene dimer. The spin-projection scheme by Eq. (1.20) is equally applicable to the DFT method, since it utilizes the expectation values of the total spin angular momentums. **Table 2.3** summarizes the calculated results. From this table, it is found that the J_{ab} values by BLYP and B3LYP methods are negative over the entire region. The stability of the LS state is relatively overestimated by BYLP. Here, the $|J_{ab}|$ values by B3LYP are smaller than those of BLYP, showing a significant improvement in the overstabilization of the LS state by BLYP.

Next, DFT methods were also investigated for linear radical clusters comprising eleven triplet methylenes, eleven quartet nitrogen atoms, and five triplet methylenes plus six quartet nitrogen atoms at the B3LYP/4-31G level. The calculated J_{ab} values are summarized in **Table 2.4**. From these results, the DFT methods is seen to be applicable for qualitative discussions of the J_{ab} values for organic radical clusters, even with long linear stacking. It is, however, noteworthy that the DFT method often overestimates the stability of the low-spin state and the contribution from the exchange integrals of non-zero orbital overlap for radical clusters. Therefore, it predicted a negative (antiferromagnetic) J_{ab} value for a hydrogen-bridged system, though the experiment showed a positive (ferromagnetic) J_{ab} value.

Table 2.3 Effective exchange integrals J_{ab} (cm^{-1}) of face-to-face dimer of triplet methylene at level of BLYP and B3LYP/6-31G*.

R	BLYP		B3YLP	
Å	BLYP	APBLYP	B3LYP	APB3LYP
3.0	−1060.7	−981.1	−826.1	−790.1
3.2	−655.0	−623.5	−502.1	−488.6
3.4	−404.2	−392.1	−305.5	−300.6
3.6	−247.4	−242.9	−184.6	−182.9
3.8	−149.8	−148.3	−110.7	−110.1
4.0	−88.80	−88.26	−65.02	−64.83
4.4	−28.97	−28.87	−20.95	−20.93
4.8	−8.552	−8.535	−6.144	−6.143
5.5	−0.8049	−0.8049	−0.5765	−0.5765
6.0	−0.1341	−0.1333	−0.0961	−0.0961
10.0	0.0000	−0.0000	0.0001	−0.0000

Table 2.4 Effective exchange integrals J_{ab} (cm^{-1}) of linear clusters estimated at level of B3LYP/4-31G.

R	$(CH_2)_{11}$[‖]		$(CH_2)_{11}$[⊥]		N_{11}		N–$(CH_2$–N$)_5$	
Å	B3LYP	APB3LYP	B3LYP	APB3LYP	B3LYP	APB3LYP	B3LYP	APB3LYP
3.0	−792.7	−590.8	56.35	55.19	−93.93	−89.73	−307.7	−260.0
3.2	−478.7	−396.6	38.95	38.71	−52.38	−51.18	−182.5	−164.7
3.4	−287.6	−256.9	25.52	25.55	−29.23	−28.93	−106.9	−100.8
3.6	−202.3	−189.9	16.37	16.44	−15.89	−15.83	−61.41	−59.58
3.8	−99.25	−96.18	10.45	10.52	−8.471	−8.468	−34.16	−33.71
4.0	−55.98	−55.29	6.699	6.750	−4.342	−4.348	−18.43	−18.36
4.4	−16.09	−16.16	2.718	2.742	−1.107	−1.110	−4.509	−4.528
4.8	−4.143	−4.177	0.9939	1.003	−0.1687	−0.1692	−0.8994	−0.9049
5.5	−0.3106	−0.3134	0.1152	0.1162	−0.0126	−0.0126	−0.0375	−0.0378
6.0	−0.0460	−0.0464	0.0208	0.0210	−0.0001	−0.0001	−0.0074	−0.0074
10.0	−0.0006	−0.0006	0.0000	0.0000	0.0000	0.0000	0.0000	0.0000

Chapter 3.

Derivations of Spin Alignment Rules

Section 3.1

Introduction

The orbital symmetry (OS) rules or Kanamori-Goodenough (KG) rules[42,43] play important roles for qualitative explanation, understanding and prediction of the signs of effective exchange integrals between transition metal ions. Thus, in this study the author extended this rule to organic radicals and establish the classified table. Historically, in the papers[44,45,46] entitled "Heisenberg models for radical reactions", the OS and KG rules have been extended to derive several selection rules for organic radical reactions on the basis of overlap and orientation principles for radical pairs. The extended KG (EKG) rules predicted that favored radical reactions occur so as to maximize kinetic exchange (KE) interactions which give rise to stable covalent pairs of spins. Thus, radical reactions are classified into kinetic exchange (KE)-allowed and -forbidden types. These are also referred to as spin-symmetry allowed and forbidden on the basis of the magnetic group theory.

Recently several research groups have reported ferromagnetic effective exchange interactions between nitroxide derivatives and ferromagnetic phase transitions of pure crystals of some of these species at low temperatures. They pointed out the importance of conformations between nitroxide groups for ferromagnetic interactions. However, the theoretical explanations are not settled yet. In this chapter the author carried out basic discussion of interaction style between two radicals. The decomposition of effective exchange interaction leads to essential and important solutions. Next, the classification of magnetic interaction is derived for simple approach.

Section 3.2

Decomposition of J_{ab} and selection rules

As shown previously[47,48], the effective exchange integral J_{ab} is generally expressed by three different terms under the approximately spin-projected unrestricted Hartree-Fock (APUHF) approximation,

$$J_{ab}(APUHF) = J_{ab}(KE) + J_{ab}(PE) + J_{ab}(SP) \tag{3.1}$$

where the kinetic (KE) and potential (PE) exchange terms are, respectively, given by the SOMO-SOMO overlap S_{ab} and the intermolecular exchange integral K_{ab} between them.

The J_{ab}(SP)-term is given by the product of spin densities ($\rho_{a(b)}$) induced by the SP effect.

$$J_{ab}(KE) = -CS_{ab} < 0 \tag{3.2}$$

$$J_{ab}(PE) = J_{ab}(SDP\ \ I) = K_{ab} > 0 \tag{3.3}$$

$$J_{ab}(SP) = J_{ab}(SDP\ \ II) = -\sum A\rho_a\rho_b \tag{3.4}$$

where the parameters C and A can be determined nonempirically by ab initio computations.

These three terms are useful to explain and design ferromagnetic interactions and organic ferromagnetism. For example, the simple rules to predict the magnetic interactions were derived from these terms, leading to the classifications in **Table 3.1**.

The cases I and II are understood intuitively with the symmetries of SOMOs, and the orbital symmetry rule is resulted in order to predict and explain the strong ferromagnetic interactions between nitroxides. The effective exchange interactions between free radicals are usually antiferromagnetic ($J_{ab} < 0$) since the KE interaction stabilizes the low spin (LS) state (Case I). However, if the orientation of radical components is controlled in order to

reduce the KE term, the ferromagnetic interaction ($J_{ab} > 0$) is expected at a moderate intermolecular distance (Case II) because of the nonzero Coulombic exchange integral (PE = K_{ab}) as shown in the case of nitroxide dimer.

It was well-known that the KE and PE terms stabilize the antiferro- and ferromagnetic spin states, respectively. The effective exchange interactions between free radicals are usually anti-ferromagnetic since the kinetic exchange (KE) interaction stabilizes the low-spin (LS) state. Therefore organic ferromagnetism is KE-forbidden as shown in the case I in **Table 3.1**. It was already emphasized that the suppression of the KE term is essential for ferromagnetic intermolecular interaction, leading to the no-overlap principle. In this regards, perpendicular interplane orientations instead of parallel one are often required. In addition to the no-overlap principle, mutual orientations of organic radicals should be controlled so that the J_{ab}(PE)-term becomes larger than the $|J_{ab}$(KE)|-term. Then ferromagnetic interaction is potential exchange (PE)-allowed as shown in the case II in **Table 3.1**.

On the other hand, when both the KE and PE terms become almost zero, the SP term arising from the indirect through-bond and through-space interactions becomes important (Case III, IV). For example, β-phase crystal of *p*-NPNN corresponds to the case III. If the KE term becomes zero and the PE term is largely positive (Case II), the effective exchange integral is expected to be a larger positive value. Thus ferromagnetic interactions represented by the KE and PE terms can become much stronger than those caused by SP effect (Case III) because the SOMO-SOMO direct interaction is usually about ten times as large as SP effect.

In order to confirm these simple rules, *ab initio* configuration interaction (CI) method by the use of the complete active space (CAS) selected on the basis of the occupation numbers of the UHF natural orbitals (UNO), i.e., UNO CAS CI, is carried out in order to calculate the SOMO-SOMO direct interaction terms, i.e. the KE and PE terms, together with spin polarization (SP) and other electron correlation (EC) terms responsible for the higher-magnetic interactions. On the other hand, the DFT method based on unrestricted Kohn-Sham (UKS) with Becke(B)-Lee-Yang-Parr (LYP) functional, DFT UKS B-LYP, and semi-empirical INDO methods are successfully employed in order to calculate spin densities in relation to the SP term.

In addition to the KE, PE and SP terms given by APUHF, higher-order intermolecular interactions such as the van-der-Waals interactions and superexchange interactions may contribute to the effective exchange interactions.

$$J_{ab}(APUHF\ \ X) = J_{ab}(APUHF) + J_{ab}(higher-order\ \ term) \qquad (3.5)$$

where X denotes the post UHF, i.e., Møller-Plesset (MP) or coupled-cluster (CC), method. Since these post Hartree Fock calculations involve the higher-order interactions responsible for electron correlation effects, they improve J_{ab}(APUHF) values which often overestimate the SP effect. So, the J_{ab} values by APUMPn and APUCCSD(T) should have better agreement with the experimental results than the values by APUHF method. The reliability of these computational methods were examined previously, comparing with spin-restricted CASSCF and CASPT2(D) results.

SOMO-SOMO interaction

The condition $J_{ab}(KE) < 0$ means that the orbital overlap leads to a strong antiferromagnetic interaction between radical groups as understood intuitively. However for the condition of $S_{ab} \approx 0$, the first term in Eq. (3.1) vanishes and the J_{ab} is determined by the second and third terms. If the PE term remains, J_{ab} value is positive and ferromagnetic interaction appears. We already investigated the systems satisfying this condition, i.e., various stacking models of nitroxide derivatives and ionic crystals of *p*-carboxyl phenyl nitronyl nitroxide. We could successfully explain the strong ferromagnetic interaction in these crystals in terms of our orbital symmetry rule. For this hypothesis we carry out theoretical investigations and show the detailed results in the following chapter 4.

Weak interaction: with spin density and/or hydrogen bridge

For the last case, if not only the KE term but also the PE term is almost negligible because of a lack of the direct interaction between radical groups, the SP term dominates the sign and the magnitude of the J_{ab} value. Namely, indirect magnetic interaction by the SP effect through bonds and space plays an important role. For example, the β-phase of *p*-NPNN corresponds to this case.

Since the spin density on the hydrogen atom is usually small, the hydrogen atom was not taken into account for explanation of the ferromagnetic interaction in crystals. However, the weak magnetic interaction via the hydrogen bridging is a current interest in relation to the ferromagnetic phase transitions at low temperature in several organic ferromagnets recently discovered. Our previous theoretical calculations suggest that the hydrogen bridging is effective for the weak intermolecular ferromagnetic exchange interaction. Two different mechanisms for the effective exchange interaction via hydrogen bridging are conceivable. One is the hyperconjugation between the hydrogen atom and SOMO of nitroxide group, which is called as "hydrogen bridging hyperconjugative effect". The potential exchange between hyperconjugated SOMOs provides a ferromagnetic exchange interaction. The other is the spin polarization (SP) effect via the hydrogen atom bridging, though the spin density induced on the hydrogen atom by the nitroxide radical

group is small. This mechanism is referred to "the hydrogen bridging SP effect". For this hypothesis we carry out theoretical investigations and show the detailed results in the following chapter 5.

Table 3.1 Selection rules for organic ferromagnetism

case	KE	PE	SP	J_{total}	Notations
I_a	<0	>0	>0	<0	KE-forbidden
I_b	<0	>0	<0	<0	KE-forbidden
II_a	~ 0	>0	>0	>0	PE-allowed
II_b	~ 0	>0	<0	>0	PE-allowed
III	~ 0	~ 0	>0	>0	SP-allowed
IV	~ 0	~ 0	<0	<0	SP-forbidden

Chapter 4.

No-overlap and Orientation Principles

Section 4.1

Introduction

In previous chapter it was ensured that the KE and PE terms stabilize the antiferro- and ferro-magnetic spin states, respectively. Therefore, the net effective exchange interaction becomes ferromagnetic if the PE term overweighs the KE one. Thus, in order to accomplish ferromagnetic interactions between organic radicals, the KE-term should disappear, leading to the no-overlap between SOMOs. Therefore, the reverse principles, no-overlap and orientation principles, are required for achieving no covalent bonding between spins and ferromagnetic exchange interactions between organic radicals. Here, we wish to extend no-overlap and orientation principles for ferromagnetic exchange interactions between organic radicals in several cases.

In the following sections 4.2 and 4.3, let us first consider very simple examples of SOMO-SOMO interactions in hydrocarbon (section 4.2) and nitroxide (section 4.3) systems. The kinetic exchange (KE) interaction is orbital-symmetry-allowed in several orientations and the s-type bondings are feasible, leading to the case I in **Table 3.1**. The KE-interaction is also orbital-symmetry-allowed in another orientations accompanied by the p-type bondings, giving rise to the formation of antiparallel spin alignment, namely the singlet pair. On the other hand, it is orbital-symmetry-forbidden for the sp-type orientations, indicating that ferromagnetic interaction is KE-allowed. Moreover, the potential exchange (PE) term is not zero because of the orbital symmetry, together with close contact between SOMOs. The ferromagnetic interaction can be PE-allowed in suitable orientations, in conformity with the intermolecular Hund rule.

Following the intermolecular Hund picture, the effective exchange interactions have been believed to be antiferromagnetic in the case of parallel orientations of organic radicals because of the nonzero-overlap between SOMOs. However, the KE-term often becomes almost zero even in the parallel orientation because of the zero SOMO-SOMO overlap as the case II in **Table 3.1**. The π^*-nature of SOMO, which appears in ethelene anion open-shell system for example, may play an important role for ferromagnetic interactions since

the orbital overlap disappeared even in these parallel stacking modes. Similarly the nonbonding MO (NBMO) plays an important role for ferromagnetic interactions in the parallel orientations. The nitroxide and nitronyl nitroxide stable radicals have stable π^*-type SOMO potentially and exist in some crystalline ferromagnetic materials.

Especially, the section 4.3, these no-overlap and orientation principles for ferromagnetic interactions between nitroxides were discussed with more deep interest. The author will mention that the ferromagnetic exchange interactions can be feasible for rhombus conformations of nitroxide groups in parallel interplane syn- and anti-stackings modes by ab initio theoretical calculations with systematic insight, though the effective exchange interactions have been believed to be antiferromagnetic in the case of parallel orientations of organic radicals because of the nonzero-overlap between SOMOs. These theoretical results are found to be consistent with the recent experiment, though it is widely understood that the magnetic interaction is propagated with only the spin polarization (SP) effect in the known organic ferromagnets such as *p*-NPNN[49,50]. Here, detailed computations are carried out for nitroxide pairs with parallel interplane conformations in order to clarify the origin of ferromagnetic interactions.

In the last section 4.4, implications of our selection rules are discussed in relation to the ferromagnetism observed for crystals of nitroxides. For one of the most suitable real systems a certain ph-NN system is synthesized and detail experimental studies were carried out. Inoue and co-worker reported[7] synthesis of *p*-NNBA$^-$ (**1**) and its lithium-methanol ($\mathbf{1}^-$ · Li^+ · MeOH) (**2**) and lithium D-substituted methanol crystals ($\mathbf{1}^-$ · Li^+ · MeOD)) (**3**). They performed the magnetic measurements of the crystals **2** and **3**, which manifested that dimers have a short intermolecular contact between the oxygen atom in nitronyl nitroxide (NN) group and the alpha carbon atom in the nearest-neighbor NN group with T-shape conformation. These lithium salts provided not only the first example of ferromagnetic dimers of radical anions but also the largest J_{ab} value ever reported for exchange couplings between PNNO derivatives.

Judging from the scientific point of view, it is particularly interesting and important to investigate theoretically the origins of the large J_{ab} values in the crystals in order to design high-T_c organic ferromagnetic materials. Here, calculations based on molecular orbital (MO)[51] and density functional theory (DFT)[52] will be carried out in order to determine the intermolecular effective exchange integrals for clusters, whose detailed geometries are taken from the X-ray diffraction experiments.

Section 4.2

SOMO-SOMO direct interaction and orbital symmetry (I): For open-shell hydrocarbon groups

4.2.1 Various models and theoretical calculations

In order to confirm the no-overlap and orientation principles in **Fig. 4.1**, we here examined typical systems as illustrated in **Fig. 4.2**. Model A denotes the face-to-face interaction between the cation radical (m=+1) of ethylene or between anion radical (m=-1) of ethylene, where R_1 and R_2 are taken as the sliding and interplane distances, respectively. The orientations **3** and **11** correspond to the case R_1=0.0 and R_2 = 3.4 Å. On the other hand, model B shows the perpendicular approach between the cation radicals of ethylene, where R_1 and R_2 are also taken as the sliding and interplane distances, respectively. The orientation **9** corresponds to the case; R_1=0.0 and R_2 = 3.4 Å in model B. The models C and D show, respectively, the face-to-face interaction between dihydronitroxide and methyl radical, and between benzyl radical and methyl radical. The orientations **10**, **19** and **20** correspond to the specific geometries with ferromagnetic interactions at appropriate R_1 and R_2 values as shown below.

In addition to the KE, PE and SP terms in Eq. (3.1) given by APUHF, higher-order intermolecular interactions such as the van-der-Waals interactions may contribute to the effective exchange interactions. Here, the UHF Møller-Plesset (MP) and coupled-cluster (CC) SD(T) method followed by the approximate spin projection, APUMP4 and APUCC SD(T), were carried out for the low- and high-spin states of radical pairs, and the effective exchange integrals were obtained as previously[53,54]. The reliability of these

computational methods and the 4-31G basis set used in this work were examined previously, comparing with spin-restricted CASSCF and CASPT2(D) results.

Comparison between Parallel and Perpendicular Orientations

Both parallel and perpendicular conformations were examined in order to confirm the intermolecular Hund rule for radical pairs. The APUMP4(2)/4-31G calculations were performed for the cation radical dimer of ethylene in model A and B in **Fig. 4.2**. **Figure 4.3**-A and B illustrate, respectively, variations of effective exchange integrals (J_{ab}) for models A and B with the sliding distance R_1 at the fixed interplane distance R_2=3.4 Å.

From this figure, the following notices are available:

(1) The J_{ab}-values are negative (antiferromagnetic) throughout the sliding deformation in the parallel orientation in model A, whereas these are always positive (ferromagnetic) in the case of perpendicular orientation in model B. The APUMP4/4-31G calculations confirmed the intermolecular Hund rule.

(2) The magnitudes of the J_{ab} values are not so dependent on the computational methods in both cases, showing that the higher-order correlation corrections are not serious.

(3) The maximum magnitude for negative J_{ab} values is about -800 cm^{-1} for the parallel orientation A, whereas the maximum positive value for the perpendicular orientation is about 70 cm^{-1} at the APUMP4/4-31G level.

The positive J_{ab} value via the potential exchange (PE) mechanism is far larger than the spin polarization (SP) mechanism as shown in the case of β-phase of *p*-NPNN. The intermolecular Hund rules are recognized for **3** and **9**. The situations were similar in other cases in **Fig. 4.1**.

Importance of π-SOMO for Ferromagnetic Interaction*

In order to clarify the importance of π*-nature of SOMO for ferromagnetic interaction, let us consider the intermolecular interaction between dihydronitroxide and methyl radical as illustrated in **Fig. 4.2**C. Since the π*-type SOMO of nitroxide has a node near the center of the N-O bond, the pπ* orbital overlap $S_{p\pi^*}$ should disappear at a bridge structure as illustrated by **10**.

$$S_{p\pi^*} = S_{12} - S_{13} = 0 \qquad (4.1)$$

where $S_{12(3)}$ denotes the orbital-overlap between the atomic orbitals 1 and 2(3).

Therefore the effective exchange integral J_{ab} in Eq. (3.1) should become positive (ferromagnetic) at this structure because of the nonzero potential exchange. The J_{ab} values were calculated for this parallel interplane stacking mode by APUMP2(4) and APUCC/4-31G. **Figure 4.4** shows variations of the calculated effective exchange integrals with R_1.

From this figure, the following characteristics were drawn:

(1) The J_{ab} values are positive in the bridge structure **10**, whereas these values are negative at the no-bridge conformations. The post Hartree-Fock calculations involving correlation corrections support qualitative predictions by the no-overlap principle.
(2) The maximum positive J_{ab} value is about 65 cm^{-1} by the APUCC/4-31G method at the bridge structure with the sliding distance R_1 = 0.8 Å. The potential exchange interaction is rather strong even at the van der Waals contact between nitroxides.

The magnitude of positive J_{ab} value for the dihydronitroxide-methyl radical pair is quite larger than spin polarization (SP) term in Eq. (3.3). The parallel spin arrangement in **Fig. 4.2**C indicates that the potential exchange (PE) K_{ab} in Eq. (3.2), instead of the SP term, plays a dominant role for the ferromagnetic exchange interaction in a SOMO-SOMO contact region. The ferromagnetic exchange interaction between nitroxides and alkyl radical is feasible by the potential exchange (PE) term, even though the SOMO-SOMO direct contact is weak.

Three-center interactions **21-23** in the T-shape conformations satisfy the no-overlap principle because of the π*-nature for one of SOMOs, suggesting the ferromagnetic interactions. In fact, previous APUCC/4-31G and 6-31G* calculations showed that the ferromagnetic interaction is feasible for nitroxide dimer with the T-shape conformation **22**.

Importance of Rhombus Conformation for Ferromagnetic Interaction

In order to confirm the no-overlap but parallel orientation principle for ferromagnetic interactions, the face-to-face stacking of anion radical (m=-1) of ethylene (model A in **Fig. 4.2**) was examined by changing the sliding distance (R_1) at the fixed interplane distance (R_2=3.4 Å). Because of the π*-nature of SOMO for the species, the SOMO-SOMO overlap should disappear at the rhombus conformation as illustrated in **12** of **Fig. 4.1**.

$$S_{\pi^*\pi^*} = (S_{14} + S_{23}) - (S_{13} + S_{24}) = 0 \qquad (4.2)$$

Therefore the KE-term is almost zero, but the potential exchange (PE) term remains nonzero because of the close SOMO-SOMO contact. In order to confirm this prediction, the APUMP4(2) calculations were carried out. **Figure 4.5** shows variations of the calculated J_{ab} values with the sliding distance R_1.

From this figure, the following conclusions were drawn:

(1) The J_{ab} values become positive (ferromagnetic) near the rhombus conformation **12** in **Fig. 4.1**, whereas these are negative near the rectangular conformation **3**.
(2) The maximum positive J_{ab} value by the APUMP4/4-31G method is 93 cm^{-1} at the rhombus conformation with the sliding distance R_1 =1.4 Å.

The spin structure for triplet state for the rhombus dimer exhibits the parallel spin alignment **24**. Therefore, the potential exchange (PE) term overweighs the kinetic exchange (KE) term in the rhombus conformation, showing an important role of the no-overlap but parallel orientation for the ferromagnetic interaction between π*-SOMOs

Previous APUMP2/4-31G calculations showed that the ferromagnetic interaction is possible even for the parallel syn-stacking mode of dihyronitroxide ($0 < \theta < 90$ in model B of Ref. [51]). Previous calculations also showed that the ferromagnetic interaction is feasible even for the parallel anti-stacking mode of dihyronitroxide ($140 < \theta < 180$ in model C in Ref. [51]). Because of the π*-nature of SOMO for niroxide, the SOMO-SOMO overlap should disappear as shown in Eq. (4.2) at the rhombus conformations **25-27**. Then the J_{ab} value should be positive (ferromagnetic) because of the nonzero potential exchange at these compact stackings.

Importance of NBMO for Ferromagnetic Interactions

In order to check the no-overlap but parallel orientation principle, the face-to-face stacking mode between benzyl and methyl radicals was examined by changing the sliding distance (R_1) at the fixed interplane distance (R_2=3.4 Å) as shown in **Fig. 4.2**D. **Figure 4.6** shows variations of the J_{ab} values with the sliding distance R_1 calculated by the APUMP2/4-31G method.

From this figure, the following conclusions were obtained:

(1) The J_{ab} values become positive (ferromagnetic) at two conformations **19** and **20** because of zero SOMO-SOMO overlaps, whereas these are negative in other conformations.
(2) The magnitudes of the ferromagnetic interactions are 86 and 13 cm^{-1} at **19** with R_1=2.8 Å and **20** with R_1=1.0 Å, respectively.

The potential exchange term overweighs the kinetic exchange term at the conformations **19** and **20**, indicating the importance of the no-overlap but parallel orientation for the ferromagnetic interaction between NBMO and *p*-SOMO. The positive J_{ab} values via the PE mechanism are quite larger than those of the SP mechanism.

The ferromagnetic exchange interactions between NBMOs in ally and benzyl radicals were examined previously in details. It was found that the effective exchange interaction between allyl radical is ferromagnetic at the conformation **18**. Both the PE and SP mechanisms favor the ferromagnetic interactions between benzyl radicals in appropriate conformations where the KE-terms become zero. Therefore these are classified into the case II_a in **Table 3.1**.

4.2.2 Discussions

No SOMO-SOMO overlap principle is applicable to organic radical crystals which exhibit the ferromagnetic effective exchange interactions. Here, it should be emphasized that the π^*-nature (orbital symmetry) of SOMO for organic radicals plays an important role to reduce the orbital-overlap (OO) antiferromagnetic term even in parallel interplane orientations. On the other hand, the potential exchange (PE) term is still nonzero because of SOMO-SOMO through-space contacts in the orientations, giving rise to ferromagnetic intermolecular interactions. Thus no-overlap and orientation principles are required for ferromagnetic interactions as illustrated in several examples.

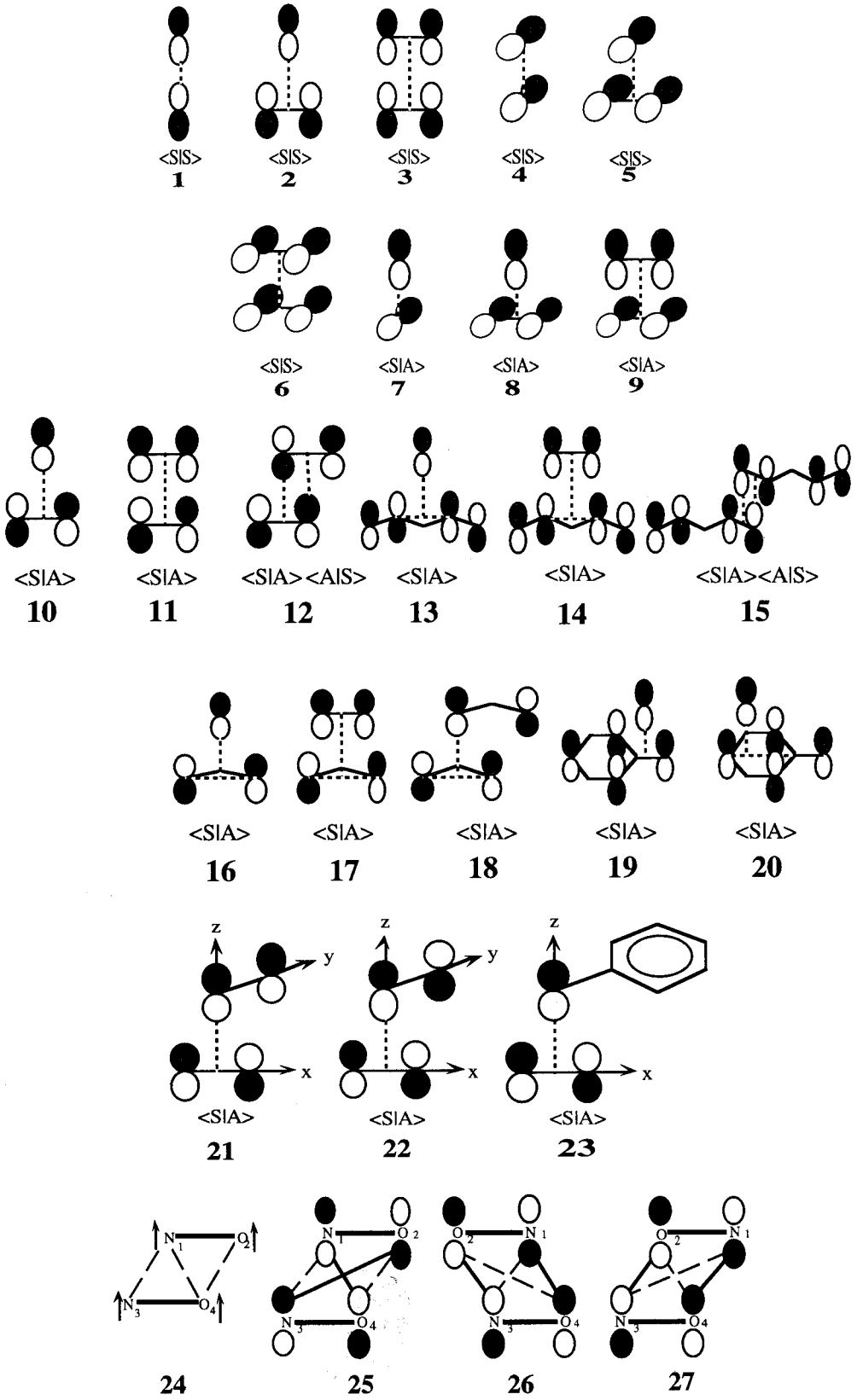

Figure 4.1 SOMO-SOMO interactions

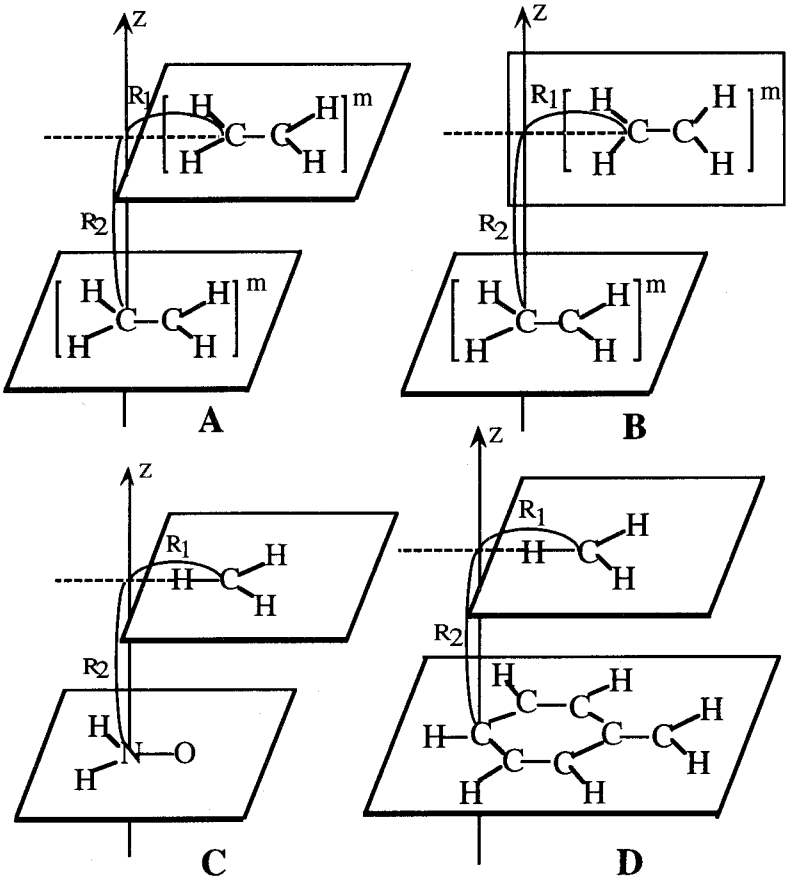

Figure 4.2 Conformations for radical pairs: parallel orientations A, C and D, and perpendicular one B.

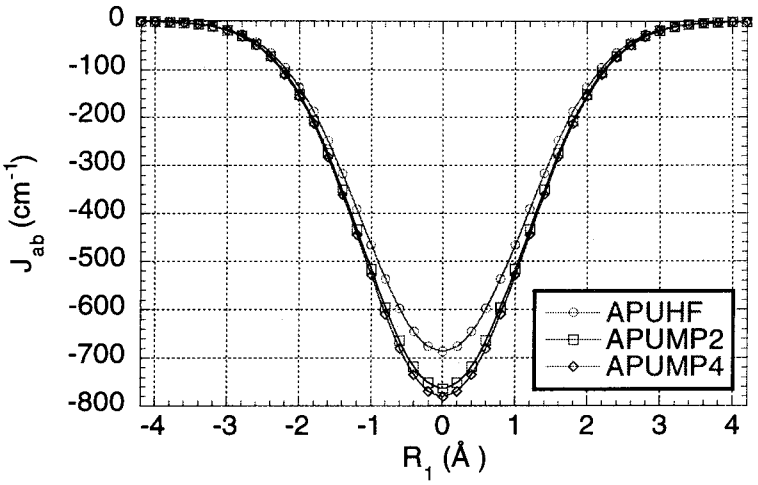

A

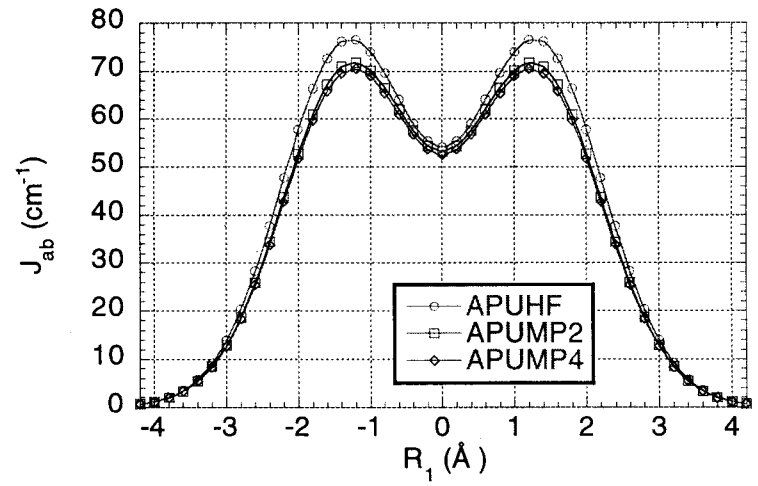

B

Figure 4.3 (A) J_{ab}-values for dimer of the cation radical of ethylene in **Fig. 4.2**A.
(B) J_{ab}-values for dimer of the cation radical of ethylene in **Fig. 4.2**B

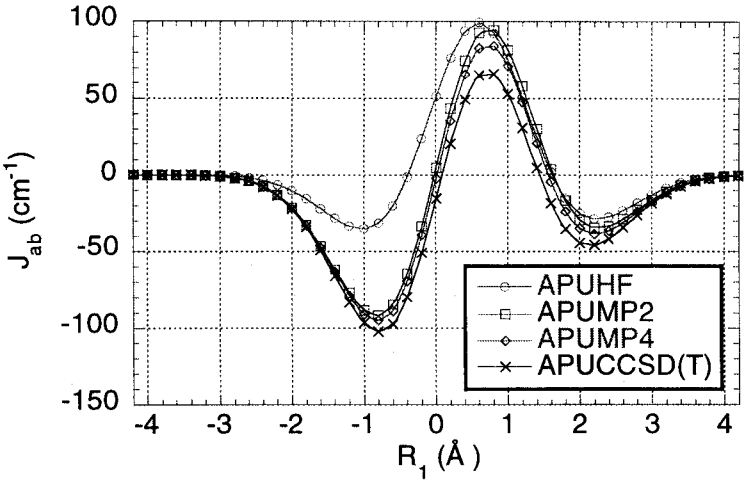

Figure 4.4 J_{ab}-values for the nitroxide-methyl radical pair in **Fig. 4.2**C

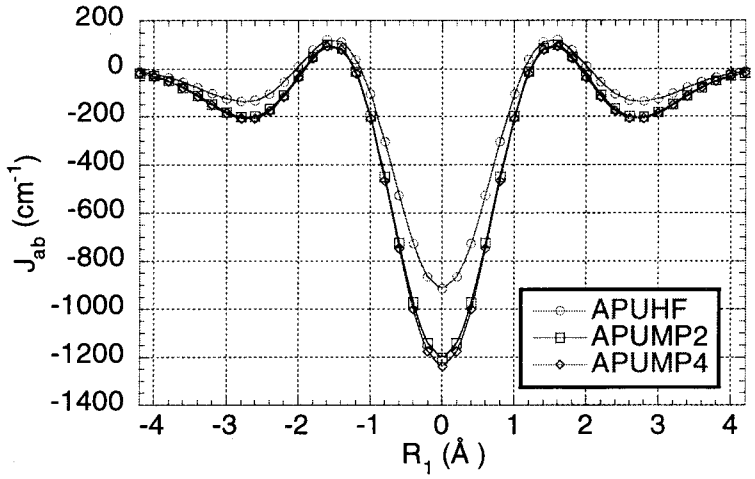

Figure 4.5 J_{ab}-values for dimer of anion radical of ethylene in **Fig. 4.2**A

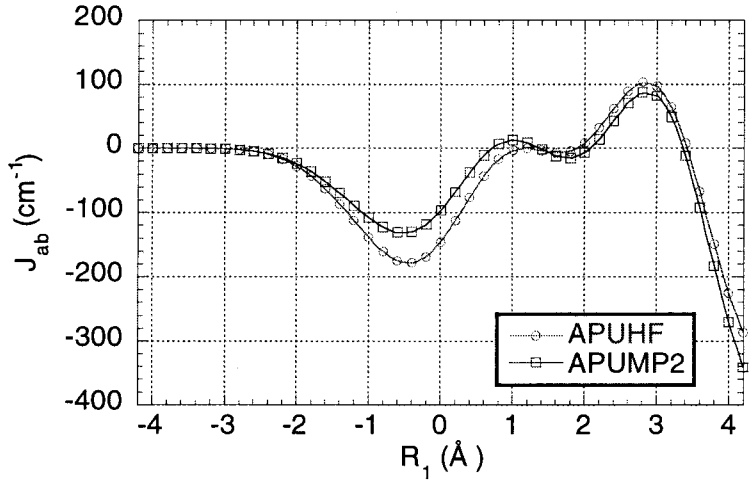

Figure 4.6 J_{ab}-value for benzyl and methyl radical pair.

Section 4.3

SOMO-SOMO direct interaction and orbital symmetry (II): For nitroxide groups

4.3.1 Importance of π*-SOMO of nitroxide

In order to clarify the importance of π*-nature of SOMO of nitroxide for ferromagnetic interaction, let us first consider the intermolecular interaction between dihydronitroxides in the orthogonal (T-shape) conformation as illustrated in I of **Fig. 4.7**. Since the π*-type SOMO of nitroxide has a node near the center of the N-O bond, the π*π* orbital overlap $S_{\pi^*\pi^*}$ should disappear at a bridge (T-shape) structure as illustrated in **Fig. 4.8**A

$$S_{\pi^*\pi^*} = S_{13} - S_{14} = 0 \tag{4.3}$$

where $S_{13(4)}$ denotes the orbital-overlap between the atomic sites 1 and 3(4). On the other hand, the PE term is given by

$$K_{ab} = \left\langle \pi_a^*(1)\pi_b^*(2) \middle| \pi_a^*(1)\pi_b^*(2) \right\rangle = \frac{1}{2} S_{13}^2 U > 0 \tag{4.4}$$

where the Mulliken approximation is employed for the atomic orbital overlap and U is the on-site Coulombic repulsion; U= U(N) = U(O). The parallel orientation is rather important for the nonzero overlap between atomic sites in Eq. (4.4). Therefore the effective exchange integral J_{ab} in Eq. (3.1) should become positive (ferromagnetic) at the structure because of

the nonzero potential exchange. In order to confirm this no-overlap and orientation principle, the orthogonal (T-shape) stacking mode of nitroxides was examined by changing the sliding distance (R_1) at the fixed interplane distance (R_2 = 3.4 Å) as shown in I of **Fig. 4.7**. The J_{ab} values were calculated for the parallel interplane stacking mode by APUMP2(4) and APUCC SD(T)/4-31G. **Figure 4.9** show variations of the calculated effective exchange integrals with R_1.

From this figure, the following characteristics were drawn:

(1) The J_{ab} values are positive in the bridge structure (**Fig. 4.8**A), whereas the values are negative at the no-bridge conformations (**Fig. 4.8**B). The post Hartree-Fock calculations involving correlation corrections support qualitative predictions by the no-overlap and orientation principle.

(2) The ferromagnetic regions are the smallest and the largest by APUCC SD(T) and APUMP2/4-31G methods, respectively. This means that the higher-order intermolecular interactions favors the low-spin state.

(3) The maximum positive J_{ab} value is about 4.5 cm^{-1} by the APUCC SD(T)/4-31G method at the bridge structure with the sliding distance R_1 = 0.6 Å. The potential exchange interaction is rather strong even at the van der Waals contact between nitroxides.

In order to examine the reliability of the 4-31G basis set, APUCC SD(T)/6-31G* calculation was performed for the bridged structure (R_1 = 0.6 Å) in **Fig. 4.8**A. **Table 4.1** shows the J_{ab} values. From this table, the magnitude of J_{ab} increases by about 1 cm^{-1} by an addition of the d-polarization function. The magnitude of positive J_{ab} value for the dihydronitroxide pair is quite larger than spin polarization (SP) term in Eq. (3.3), which favors a local antiparallel spin alignment in the β-phase of *p*-NPNN. The spin structure for the triplet state is shown in C of **Fig. 4.8**. The parallel spin arrangement indicates that the potential exchange (PE) in Eq. (3.2) plays a dominant role for the ferromagnetic exchange interaction. The ferromagnetic exchange interaction between nitroxides is certainly feasible via the potential exchange (PE) mechanism, even though the SOMO-SOMO direct contact is weak.

4.3.2 Parallel syn-stacking of nitroxides

Previous APUMP2/4-31G calculations showed that the ferromagnetic interaction is possible even for the parallel syn-stacking mode of dihydronitroxide ($0 < \theta < 90$ in model B of Ref. [51]). In order to confirm the no-overlap but parallel orientation principle for ferromagnetic interactions, the syn-stacking mode II in **Fig. 4.7** was examined by changing the sliding distance (R_1) at the fixed interplane distance (R_2 = 3.4 Å). Because of the π*-

nature of SOMO for nitroxide, the SOMO-SOMO overlap should disappear at the rhombus conformation as illustrated in **Fig. 4.8**D.

$$S_{\pi^*\pi^*} = (S_{14} + S_{23}) - (S_{13} + S_{24}) = 0 \tag{4.5}$$

$$K_{ab} = \langle \pi_a^*(1)\pi_b^*(2) | \pi_a^*(2)\pi_b^*(1) \rangle = \frac{1}{2}(S_{14}^2 + S_{23}^2 - S_{13}S_{24})U > 0 \tag{4.6}$$

Therefore the kinetic exchange (KE) term is almost zero, but the potential exchange (PE) term remains nonzero because of the close SOMO-SOMO contact in the parallel orientation. In order to confirm this prediction, the APUMP4(2) and APUCC SD(T) /4-31G calculations were carried out. **Figure 4.10** shows variations of the calculated J_{ab} values with the sliding distance R_1.

From this figure, the following conclusions were drawn:

(1) The J_{ab} values become positive (ferromagnetic) near the rhombus conformation D in **Fig. 4.8**, whereas these are negative near the rectangular conformation in **Fig. 4.8**E.
(2) The maximum positive J_{ab} value by the APUCC SD(T)/4-31G method is 9.5 cm^{-1} at the rhombus conformation in **Fig. 4.8**D with the interplane distance R_2 = 1.4 Å.
(3) Since the small negative spin density appears on the hydrogen atom, the spin polarization effect, namely McConnell's term, favors the ferromagnetic interaction at the hydrogen-bridge structure F in **Fig. 4.8** ($|R_1| > 1.5$ Å). However, the kinetic exchange (antiferromagnetic) term overweighs such a weak ferromagnetic interaction, giving rise to the net negative J_{ab} value in conformity with the case I in **Table 3.1**.

The J_{ab} values by APUCC SD(T)/6-31G* is 11.5 cm^{-1} for the rhombus conformation in **Fig. 4.8**D, supporting the 4-31G results. The spin structure for triplet state for the rhombus dimer exhibits the parallel spin alignment as illustrated in **Fig. 4.8**G. Therefore, the potential exchange (PE) term overweighs the kinetic exchange (KE) term in the rhombus conformation, showing an important role of the no-overlap but parallel orientation for the ferromagnetic interaction between nitroxides.

4.3.3 Parallel anti-stacking of nitroxides

(A) effective exchange interactions between dihydronitroxides

Previous APUMP2/4-31G calculations showed that the ferromagnetic interaction is feasible even for the parallel anti-stacking mode of dihydronitroxide ($140 < \theta < 180$ in model C in Ref. [51]). Because of the π*-nature of SOMO for nitroxide, the SOMO-

SOMO overlap should disappear as shown in Eq. (4.5) at the rhombus conformations as illustrated in H and I in **Fig. 4.8**. Then the J_{ab} value would becomes positive (ferromagnetic) because of the nonzero potential exchange at these compact stackings. In order to check the no-overlap and orientation principle, the anti-parallel stacking mode III in **Fig. 4.7** was examined by changing the sliding distance (R_1) at the fixed interplane distance (R_2=3.4 Å). **Figure 4.11** shows variations of the J_{ab} values with the sliding distance R_1 calculated by the APUMP4(2) and APUCC SD(T)/4-31G methods.

From this figure, the following conclusions were obtained:

(1) The J_{ab} values become positive (ferromagnetic) at the rhombus conformations H and I in **Fig. 4.8**, whereas these are negative near the rectangular conformation.
(2) The magnitudes of the ferromagnetic interactions are quite dependent on the higher-order correlation corrections at the rhombus conformation H in **Fig. 4.8**, whereas such variations are small on the other rhombus conformation I in **Fig. 4.8**.
(3) The maximal positive J_{ab} values by the APUCC SD(T) /4-31G method are 9.5 and 5.8 cm^{-1} at the rhombus conformations H (R_1 = -1.2 Å) and I (R_1 = 1.4 Å) in **Fig. 4.8**, respectively.

The APUCC SD(T)/6-31G* calculations also provides the positive J_{ab}-values for H and I as shown in **Table 4.1**. The spin structure for the high-spin (triplet) state for the rhombus dimer exhibits the parallel spin alignment as in the case of G in **Fig. 4.8**. Therefore, the potential exchange term overweighs the kinetic exchange term at the rhombus conformations, indicating the importance of the no-overlap but anti-parallel orientation for the ferromagnetic interaction between nitroxide groups.

(B) ferromagnetic interaction between dimethyl nitroxides

Here the anti-parallel stacking mode of dimethyl nitroxide was examined by changing the interplane distance (R_2) at the fixed sliding distance R_1 in **Fig. 4.7**-III (W = CH_3). **Table 4.2** summarizes the calculated results by the APUMP2/4-31G method. From this table, the J_{ab} values at R_1 = 1.6 Å decrease sharply with the increase of R_2, but they remain positive in sign even in the larger intermolecular region (R_2 > 4.2 Å). Thus the through-space ferromagnetic interaction via the potential exchange mechanism is feasible even at R_2 = 4.2 Å.

4.3.4 Discussions

Present *ab initio* calculations indicate that the ferromagnetic effective exchange interactions are feasible even in the parallel interplane orientations for nitroxide pairs since

the direct potential exchange (PE) interaction overweighs the kinetic exchange (KE) interaction. Since SOMO of nitroxide is the π^*-type, the SOMO-SOMO overlap disappears almost in the orthogonal (T-shape) conformation, and syn- and anti-stackings with rhombus conformations, satisfying the no-overlap principle. On the other hand, the potential exchange interaction (PE) is still nonzero because of the SOMO-SOMO contact in these parallel orientations. Therefore, no-overlap and orientation principles are consistent with the computational results. They also predict that ferromagnetic intermolecular interactions are feasible via direct potential exchange mechanism even for simple nitroxides such as dimethylnitroxide, unsubstituted nitronylnitroxide if stacking modes of these species are well-controlled as illustrated in **Figs. 4.7** and **4.8**. Similarly, π^*-type SOMOs should be also promising for ferromagnetic intermolecular interactions between anion radicals of vinyl group, carbonyl group, etc. In fact, previous semi-empirical calculations showed the ferromagnetic interaction between quinone anion radicals. Experimental examinations of crystals of these species are desirable.

Table 4.1 The effective exchange integrals calculated for key conformations (A, D, H, I) by the APUCC SD(T) / 6-31G* method.

System	Model [a]	R_1	R_2	Jab (cm^{-1}) UMP2	UMP4	UCCSD(T)
I	A	0.6	3.4	10.962	6.599	5.465
			3.8	3.773	2.320	1.758
II	D	1.4	3.4	17.061	13.745	11.522
			3.8	4.392	3.419	2.800
III	H	-1.2	3.4	30.204	21.451	15.503
			3.8	8.094	5.656	4.058
	I	1.4	3.4	4.839	4.912	5.412
			3.8	-0.161	-0.044	0.191

Table 4.2 Effective exchange integrals for anti-parallel stacking mode of dimethylnitroxide by the APUMP2/4-31G method.

R_2 \ R_1	1.2	1.4	1.6	1.8
3.4	-0.017	5.559	6.957	5.575
3.6	-0.802	1.805	2.704	2.358
3.8	-0.594	0.484	0.935	0.888
4.0	-0.290	0.097	0.284	0.297
4.2	-0.106	0.012	0.076	0.088
4.4	-0.029	0.000	0.018	0.023

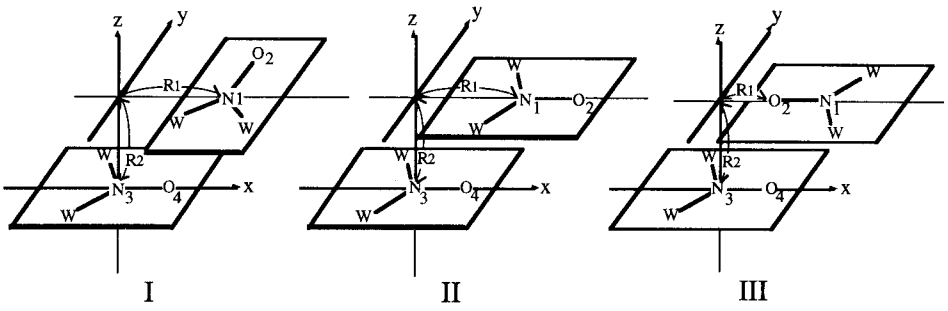

Figure 4.7 Three different orientation models for nitroxide pair (W = H, CH_3, etc.): (I) parallel orthogonal (T-shape) stacking mode, (II) parallel syn-stacking mode and (II) parallel anti-stacking mode. R_1 and R_2 denote, respectively, the sliding and interplane distances.

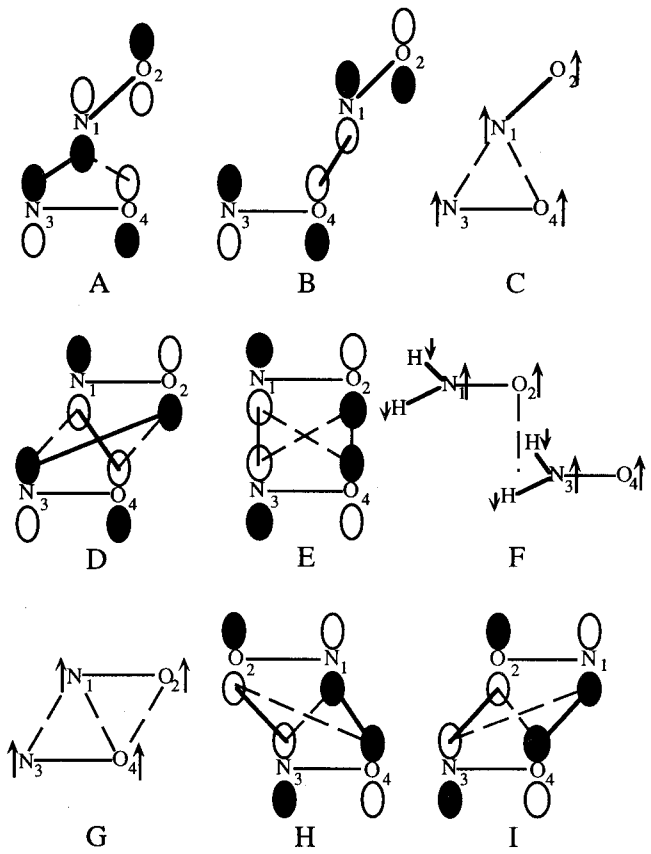

Figure 4.8 Schematic illustrations of the orbital-overlap (OO) interactions between nitroxides and the spin structures of the nitroxide pairs. A and B denote, respectively, the OO interaction at the bridge and no-bridge structures. C and G show the spin structures of the bridge and rhombus structures, respectively, whereas F denotes the spin structure via the hydrogen bridge in the parallel stacking mode. D, H and I are the OO interactions in rhombus conformations for nitroxide pairs with parallel and anti-parallel stacking modes.

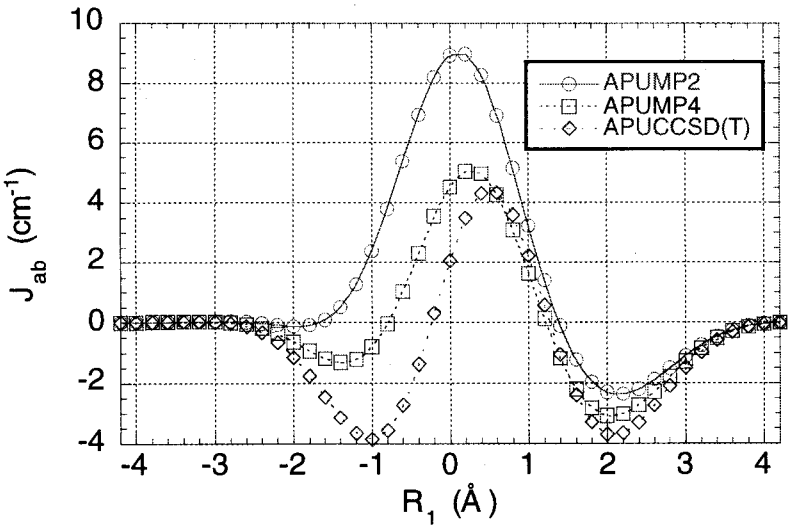

Figure 4.9 Variations of effective exchange integrals (J_{ab}) calculated for the T-shape orientation of nitroxide pair in I of **Fig. 4.7** by the APUMP4(2) and APUCC SD(T)/ 4-31G methods.

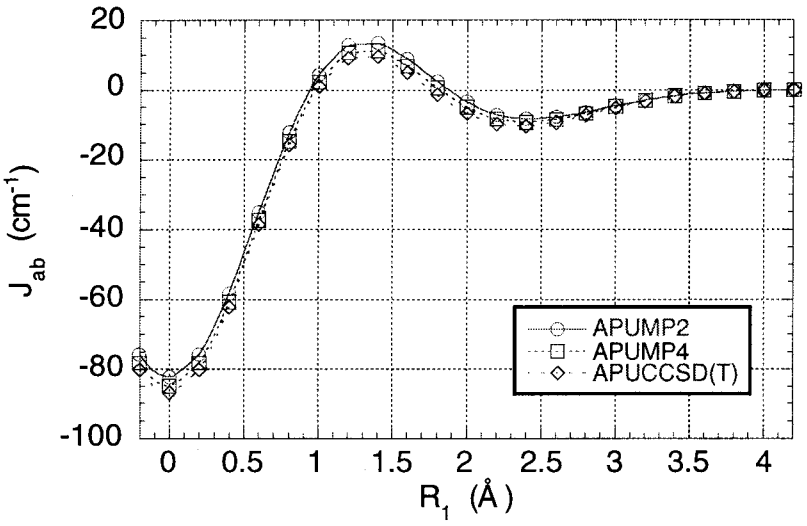

Figure 4.10 Variations of effective exchange integrals (J_{ab}) calculated for the parallel orientation of nitroxide pair in II of **Fig. 4.7** by the APUMP4(2) and APUCC SD(T)/ 4-31G methods.

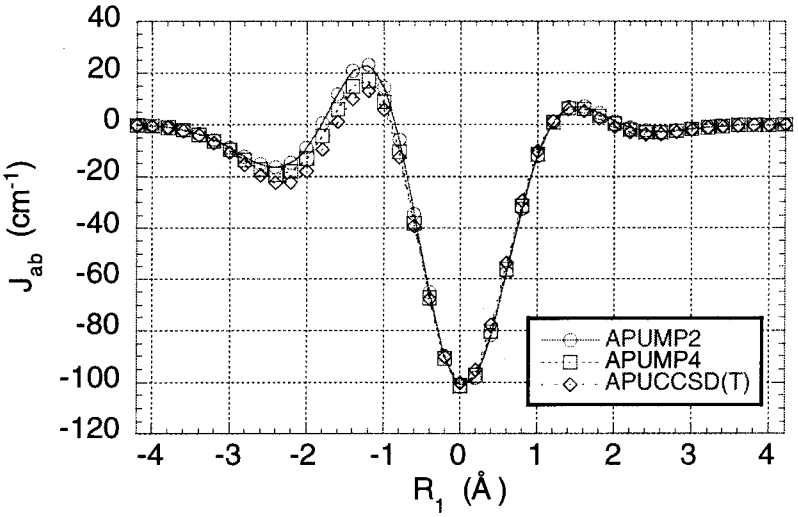

Figure 4.11 Variations of effective exchange integrals (J_{ab}) calculated for the anti-parallel orientation of nitroxide pair in III of **Fig. 4.7** by the APUMP4(2) and APUCC SD(T)/4-31G methods.

Section 4.4

Theoretical studies for real system: *p*-carboxylate phenyl nitronyl nitroxide

4.4.1 Crystal structure

Since dimer structures[7] were found in the crystals of **2** and **3**, an exchange-coupled dimer model was applied to elucidate the magnetic susceptibility data. **Figures 4.12**-A and B illustrate the orientations ($\mathbf{a_1}$,$\mathbf{b_1}$,$\mathbf{c_1}$,$\mathbf{d_1}$,$\mathbf{a_2}$,$\mathbf{b_2}$,$\mathbf{c_2}$,$\mathbf{d_2}$) of **2** and **3**, respectively, in their X-ray crystal structures. From **Fig. 4.12**, the following characteristics were drawn:

(1) Both the structures reveal that one of the terminal oxygen of the nitronylnitroxide approaches significantly the α-carbon atom of the other imidazolinyl unit. The nearest C-O distances between the radical groups are, respectively, 3.246 and 3.309 Å for the dimers $\mathbf{A_1}$($\mathbf{a_1}$-$\mathbf{b_1}$) and $\mathbf{A_2}$($\mathbf{a_2}$-$\mathbf{b_2}$) which are composed of monoanion of **1**.

(2) On the other hand, the second, third and forth nearest distances between $\mathbf{1}^-$ in **Fig. 4.12**A are 5.404, 6.087 and 7.360 Å, respectively, for the dimers $\mathbf{B_1}$($\mathbf{a_1}$-$\mathbf{c_1}$), $\mathbf{C_1}$($\mathbf{a_1}$-$\mathbf{d_1}$) and $\mathbf{D_1}$($\mathbf{a_1}$-$\mathbf{e_1}$) in the crystal **2**. While, the corresponding distances are 5.090, 5.378 and 5.538 Å, respectively, for the dimers $\mathbf{B_2}$($\mathbf{a_2}$-$\mathbf{c_2}$), $\mathbf{C_2}$($\mathbf{a_2}$-$\mathbf{d_2}$) and $\mathbf{D_2}$($\mathbf{a_2}$-$\mathbf{e_2}$) in the crystal **3**.

Here, we will perform the theoretical calculations of the dimers $\mathbf{A_1}$ and $\mathbf{A_2}$ which have the shortest distance between the monoanion $\mathbf{1}^-$ in **2** and **3**, respectively. First, we extracted the simplified models $\mathbf{A_1}$' and $\mathbf{A_2}$' from the X-ray structures, which remain the only two nitronyl nitroxide (ON-C-NO) skeletons. **Figure 4.13**A shows the molecular coordinates for one ($\mathbf{A_1}$') of these dimers, since their geometries are similar each other except for the intradimer distance. The C-H distances in these models were optimized by the PM3 semi-empirical method. From **Fig. 4.13**A, the simplified dimer exhibits the short intermolecular contact between the oxygen atom in nitronyl nitroxide (NN) group and the alpha carbon atom in NN group with vertical T-shape conformation. On the other hand,

Fig. 4.13B shows the full geometry of the dimer $\mathbf{A_1}$, where Li^+, MeOH and MeOD were neglected in order to clarify the direct effective exchange interaction between $\mathbf{1}^-$.

4.4.2 Calculations for simplied dimer models

Ab initio post Hartree-Fock and DFT calculations were carried out for the simplified dimers, $\mathbf{A_1}$' and $\mathbf{A_2}$', in order to elucidate the origin of the ferromagnetic effective exchange integral $|J_{ab}|$. **Table 4.3** gives the J_{ab} values obtained by several computational methods. From **Table 4.3**, the following conclusions are drawn:

(1) All the methods give the positive J_{ab} values and the absolute values of dimer $\mathbf{A_1}$' are larger than those of dimer $\mathbf{A_2}$' in each calculation. The ratios, J_{ab} ($\mathbf{A_1}$')/J_{ab} ($\mathbf{A_2}$'), by these computational methods are in good agreement with the ratio derived from experiment data[7].

(2)APUHF/4-31G methods overestimate the positive J_{ab} values because of the large SP effect. The Møller Presset (MP) perturbation methods cannot correct the overestimation occurred in the UHF calculation even at the fourth-order level.

(3) UNO CASCI by the use of the two active UNOs and two electrons {2,2} method involving only SOMO-SOMO direct interactions (KE and PE terms) gives the positive J_{ab} values which are in good agreement with the experimental values[7].

(4) The UNO CASSCF{2,2} method gives quite larger Jab values than UNO CAS CI {2,2}. It is essential to include orbital relaxations by the SCF procedure in the UNO CASCI {2,2} calculation.

(5) UNO CASCI and UNO CASSCF methods by the use of the six-active UNO and six-active electrons {6, 6} give similar J_{ab} values, which are smaller than that of UNO CASSCF {2,2}, but are close to the experimental values. The SP plus electron correlation (EC) terms given by the former two methods reduce the magnitude of J_{ab} arising from the direct PE effect.

(6) DFT UKS B-LYP 4-31G methods give quite larger J_{ab} values than UNO CASCI {6,6}, which is insufficient for quantitative calculations of intermolecular J_{ab} values.

(7) The J_{ab} values by INDO are close to the experimental values, although the calculations are performed for the simplied dimers.

In order to explain and understand the above conclusion (3), let us consider the shape of SOMO. **Figure 4.14**A illustrates the stacking of two SOMOs, and the solid and dotted lines indicate, respectively, the in-phase and out-of-phase combinations of the p-orbitals. From **Fig. 4.14**A, it can be seen that SOMOs have nodes and two nitronylnitroxide groups stack each other in balance to eliminate the SOMO-SOMO overlap, i.e., KE term, whereas the PE term still remains because of the short intradimer distance. This indicates that the direct potential exchange (PE) interaction between SOMO electrons plays an essential role for the ferromagnetic interaction between the nitronyl nitroxide group.

Figure 4.14B illustrates the spin densities calculated by the UB-LYP/4-31G method. The UKS B-LYP method can give the more reasonable spin densities for open shell species than the UHF method. From **Fig. 4.14**B it is found that positive densities populated on the N and O atoms of the nitronyl nitroxide (NN) group and the negative density is induced on its a-carbon atom. The terminal O atom with positive spin density on one NN group contacts with the a-carbon atom with negative spin density on the other NN group, indicating the ferromagnetic interaction via the intermolecular spin polarization (SP) mechanism. However, the positive J_{ab} value given by the SP effect is improved by the higher-order effects as confirmed by UNO CASSCF {6,6}. This in turn indicates that the direct potential exchange interaction is responsible for the large ferromagnetic interaction between the NN group in the crystals **2** and **3**, which supports our no-overlap and orientation principle for organic ferromagnetism.

4.4.3 Sliding between NN-groups

In order to investigate how conformations between two NN groups contribute the ferromagnetic interaction, J_{ab} values at many sliding conformations are obtained by UNO CASCI {2, 2} and APUHF/4-31G methods. Graphical presentations are depicted in **Fig. 4.15** and the definitions of the origin of the coordinate axes, sliding orientation and etc. are shown in this figure. From these results each method give resemble contour maps each other and the most large positive values are realized around the origin, where two molecules in the original nearest dimer contact each other. It is concluded that the spin polarized effects are not crucial, since the result by UNO CASCI {2, 2} methods can represent main contribution.

4.4.4 Calculations for full dimer models

(A) Electronic property of the monomer

The preceding model calculations indicated the essential role of the SOMO-SOMO interaction. Therefore, let us examine the magnetic orbitals of the monoanion $\mathbf{1}^-$. **Figures 4.16**-A, B and C illustrate the HOMO, SOMO and LUMO, respectively, determined by the UNO analysis. From **Fig. 4.16**B, it is noticed that SOMO orbital of $\mathbf{1}^-$ is localized with the nitronyl nitroxide (NN) group, ON-C-NO, as in the case of the above simplied model. Therefore, the SOMO-SOMO direct interaction should be expected even for the dimer $\mathbf{A_1}$ of the nearest neighbor monoanion $\mathbf{1}^-$.

Figures 4.16-D and E depict the spin density populations on monomer $\mathbf{a_1}$ in dimer $\mathbf{A_1}$ in **Fig. 4.12** by the UHF/4-31G and UBLYP/4-31G method, respectively. It is seen that

spin densities on the ON-C-NO group are similar to those of the model system in **Fig. 4.13**A. However, spin densities are induced even on the benzene ring because of the SP effect. As shown previously, the magnitudes of the induced spin densities by the B-LYP method are quite similar to those of the experiments obtained for PNNO derivatives by the neutron diffraction technique[6], although the UHF method largely overestimates them and the spin projection is crucial for the improvement.

(B) J_{ab} value for the full dimer models

In order to study magnetic properties observed for crystals of **2** and **3**, their full molecular skeletons must be taken into account because HOMO and LUMO are delocalized over not only the ON-C-NO group but also the benzene ring as illustrated in **Figs. 4.16**-A and C, indicating that indirect effective exchange interactions are operative. Since the J_{ab} values in **Table 4.3** showed that the INDO semiempirical method works well for qualitative calculations of J_{ab} values, it was applied to the dimers $\mathbf{A_1}$ and $\mathbf{A_2}$ in **Fig. 4.13**B, which have the nearest intradimer distance extracted from the X-ray study of the crystals of **2** and **3**. **Table 4.3** gives the calculated J_{ab} values for these dimers. The J_{ab} values by INDO correspond to about 55% of the experimental values. Interestingly, the calculated ratio, J_{ab} ($\mathbf{A_1}$)/J_{ab} ($\mathbf{A_2}$), is about 1.424/1, in good agreement with the ratio 1.412/1 derived from the magnetic measurements for the crystals **2** and **3**. Thus the semiempirical INDO calculation at least reproduces the observed tendency. The more reliable UNOCAS SCF calculations are in progress in our laboratory.

4.4.5 Calculations for the second, third and forth nearest dimers

Through the above section only the dimer $\mathbf{A_1}$ and $\mathbf{A_2}$ having the nearest intradimer distances have been taken into account and we could explain theoretically their magnetic behaviors. In this section, the INDO calculations were also performed for the second, third and forth nearest dimers in both crystals of **2** and **3** in order to elucidate their magnetic contributions. **Table 4.4** summarizes the calculated J_{ab} values. From **Table 4.4**, it is found that only the first nearest dimers have large J_{ab} values, and the second, third and fourth nearest dimers have smaller J_{ab} values than 1 cm^{-1}. These results may be explained by dependence of J_{ab} values on intermolecular distances (R) : J_{ab} values decrease with the increase of R in an exponential manner. Therefore the calculated results are understood intuitively from the crystal structures in **Fig. 4.12**. In fact, the effective interactions become weaker as R increase in the case of **2**. The interaction in dimer $\mathbf{B_1}$ is only 0.06 cm^{-1}, and the interactions in dimers $\mathbf{C_1}$ and $\mathbf{D_1}$ are negligible. On the other hand, the J_{ab} values of the

dimers $\mathbf{B_2}$, $\mathbf{C_2}$ and $\mathbf{D_2}$ in **3** exhibit the reverse dependency, showing that the orientations between the monoanion $\mathbf{1}^-$ become crucial. In summary, the tendency obtained by the INDO calculations is consistent with the experimental results derived form the exchange-coupled dimer models[7].

4.4.6 Discussions

Judging from the present ab initio and semiempirical calculations, the nearest intermolecular O-C(a) distance in the dimer was responsible for the difference between J_{ab} values of the crystals **2** and **3**. The difference between crystal structures of **2** and **3** was lattice constants and molecular packing style. The true isotope effect (H, D) might not contribute to the effective exchange interactions. In addition it will be reasonable to conclude that the Li cation and methanol play no important role for the ferromagnetic intradimer interaction of the monoanion $\mathbf{1}^-$ though they are not treated explicitly in our studies.

The simplied model extracting the nitronyl nitroxide groups could give a useful guide for theoretical understanding of the effective exchange interaction. The UNO CASSCF by the use of two SOMOs and two unpaired electrons {2,2} demonstrates that SOMO is essentially localized on this group, and the SOMO-SOMO potential exchange (PE) interaction is predominant for explaining the ferromagnetic interactions observed for the dimers $\mathbf{A_1}$ and $\mathbf{A_2}$. On the other hand, the spin polarization (SP) plus higher-order magnetic interactions estimated by the UNO CASCI{6,6} method rather reduce the positive J_{ab} value via the PE mechanism in the case of the molecular packings of $\mathbf{1}^-$ revealed by the X-ray diffraction experiments[7]. The *ab initio* UNO CASSCF of the full dimers is desirable in this regard.

The INDO method gives reasonable J_{ab} values which are about one half of the experimental values[7]. This is the same even for clusters of phenyl nitronyl nitroxide (PNNO) derivatives in general. The APUHF INDO method is useful for qualitative calculations of J_{ab} values for larger organic radical systems.

The J_{ab} values for the dimers $\mathbf{B_1}$, $\mathbf{C_2}$ and $\mathbf{D_2}$ by INDO remain positive, indicating the nonnegligible contributions to magnetic behaviors in the crystals. In fact, this may be the reason why the temperature dependence of the effective magnetic moments meff per molecule of the crystalline samples of **2** does not become 2.0 even at the near 0 K[7]. So, in order to study more explicit magnetic behaviors experimental studies at much lower temperature region are desirable than at already reported region.

Table 4.3 J_{ab} values calculated by several theoretical methods for both dimer $\mathbf{A_1}$ and $\mathbf{A_2}$.

methods	J_{ab} /cm^{-1} **2** (**1**$^-$•Li$^+$•MeOH)	**3** (**1**$^-$•Li$^+$•MeOD)
Simplied model	$\mathbf{A_1}$'	$\mathbf{A_2}$'
APUHF[a)]	27.88	22.37
APUMP2[a)]	23.98	19.98
APUMP3[a)]	25.75	21.22
APUMP4SDTQ[a)]	26.31	21.67
UNOCASCI{2,2}[a)]	10.08	7.42
UNOCASSCF{2,2}[a)]	16.40	13.46
UNOCASCI{6,6}[a)]	8.26	6.36
UNOCASSCF{6,6}[a)]	8.86	6.76
APUB-LYP[a)]	19.81	16.12
INDO	9.72	7.18
Full model with whole atoms	$\mathbf{A_1}$	$\mathbf{A_2}$
INDO	5.666	3.979
Experiment[b)]	10.219	7.239

a) 4-31G basis set were used.
b) an exchage-coupled dimer model were employed.

Table 4.4 J_{ab} values (INDO) for each dimers in **2** and **3**.

dimer		distance /Å	J_{ab} (INDO) /cm^{-1}
2 (**1**$^-$•Li$^+$•MeOH)			
dimer $\mathbf{A_1}$	($\mathbf{a_1}$-$\mathbf{b_1}$)	3.246	5.666
dimer $\mathbf{B_1}$	($\mathbf{a_1}$-$\mathbf{c_1}$)	5.404	0.061
dimer $\mathbf{C_1}$	($\mathbf{a_1}$-$\mathbf{d_1}$)	6.087	-0.001
dimer $\mathbf{D_1}$	($\mathbf{a_1}$-$\mathbf{e_1}$)	7.360	0.000
3 (**1**$^-$•Li$^+$•MeOD)			
dimer $\mathbf{A_2}$	($\mathbf{a_2}$-$\mathbf{b_2}$)	3.309	3.979
dimer $\mathbf{B_2}$	($\mathbf{a_2}$-$\mathbf{c_2}$)	5.090	0.005
dimer $\mathbf{C_2}$	($\mathbf{a_2}$-$\mathbf{d_2}$)	5.378	0.043
dimer $\mathbf{D_2}$	($\mathbf{a_2}$-$\mathbf{e_2}$)	5.538	0.111

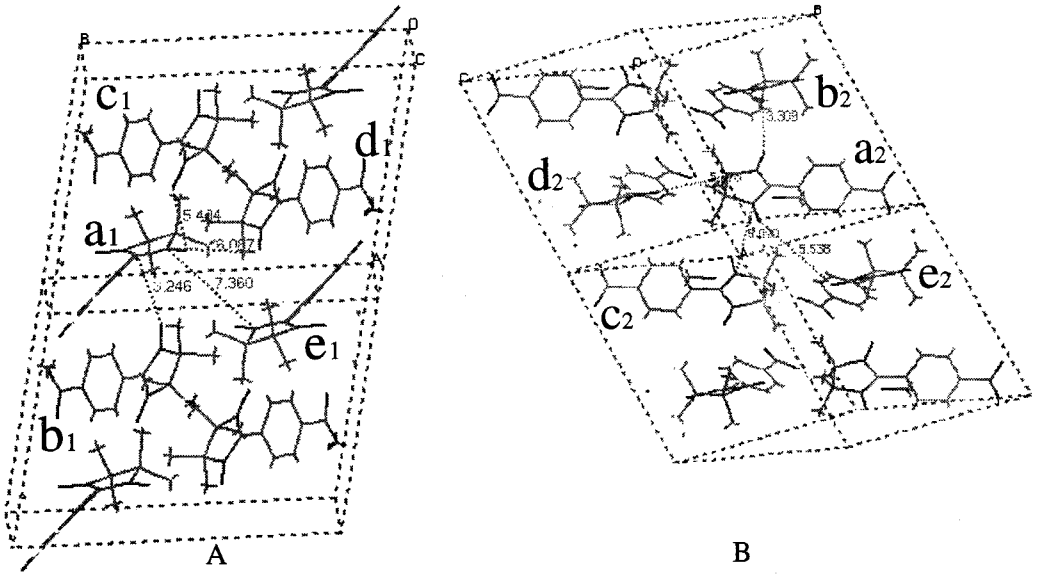

Figure 4.12 Crystal structures of **2** ($\mathbf{1}^-$ · Li^+ · MeOH) and **3** ($\mathbf{1}^-$ · Li^+ · MeOD).

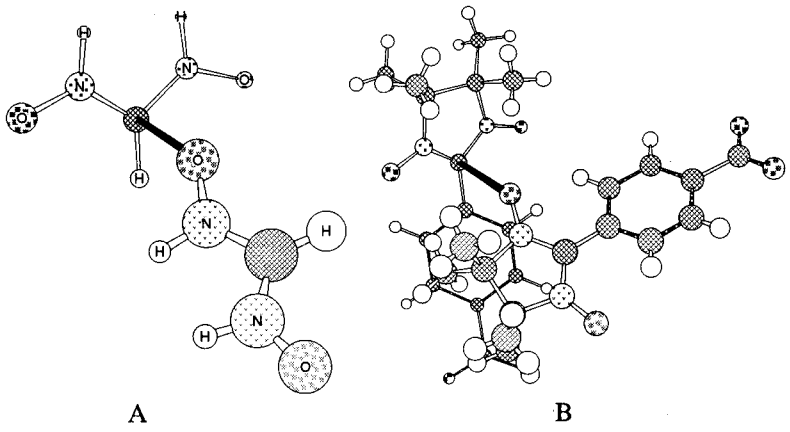

Figure 4.13 Simplified model $\mathbf{A_1}$' and Full model $\mathbf{A_1}$($\mathbf{a_1}$-$\mathbf{b_1}$).

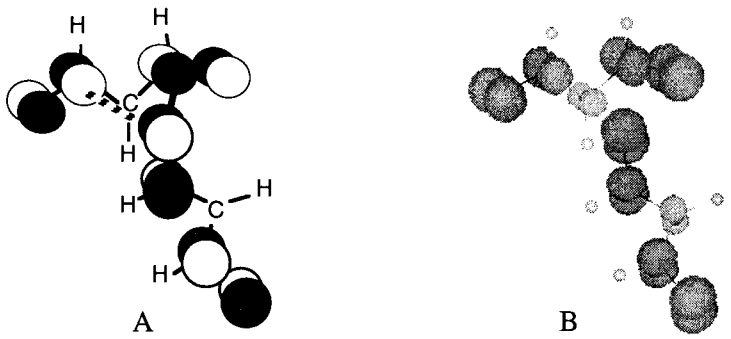

Figure 4.14 SOMO-SOMO direct interaction (A) and spin densities (threshold 0.01) by UBLYP/4-31G (B) in the simplified model $\mathbf{A_1}$'.

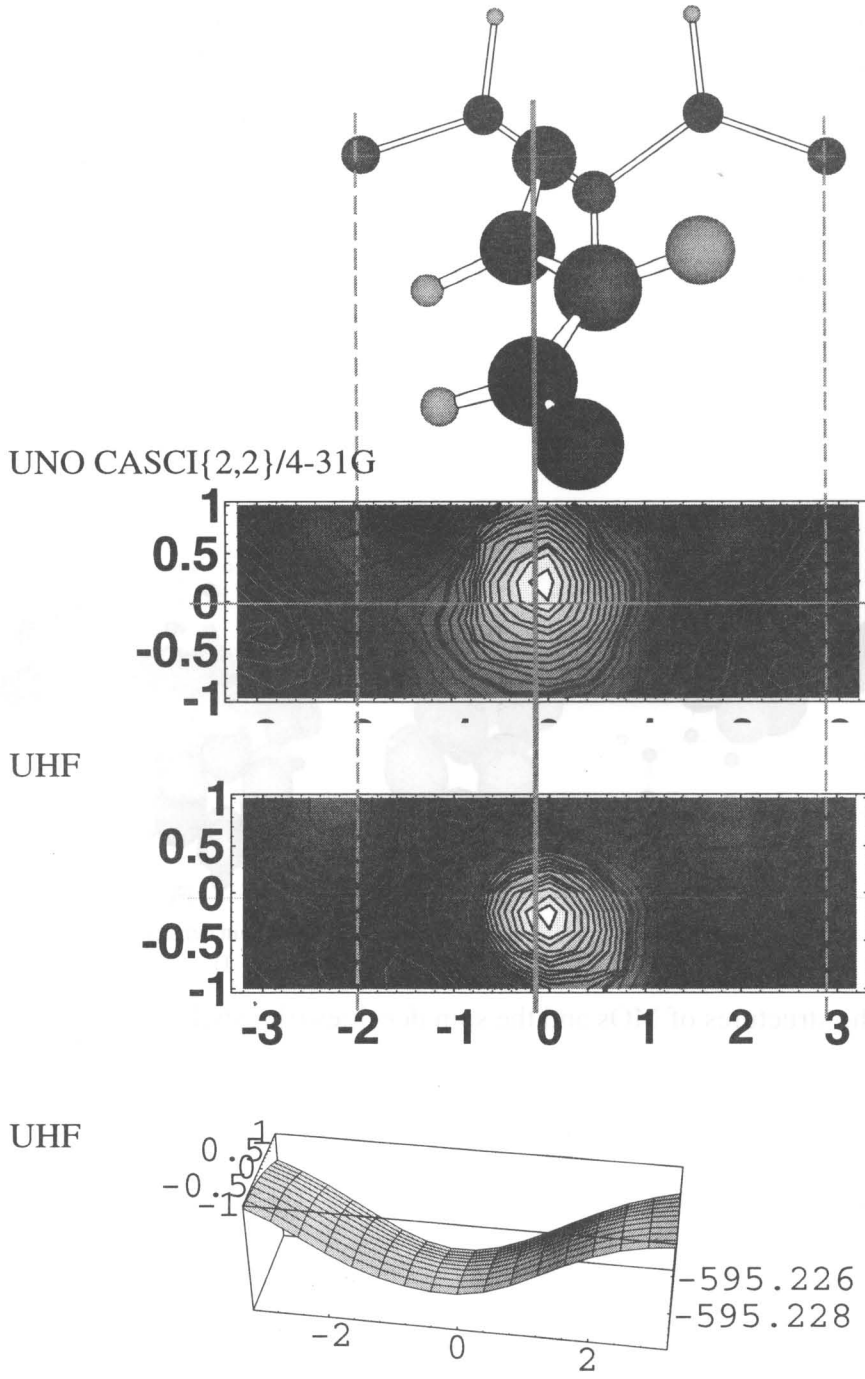

Figure 4.15 In order to investigate how conformations between two NN groups contribute the ferromagnetic interaction, graphical presentations of J_{ab} values by UNO CASCI {2, 2} and APUHF/4-31G method and energy curves by UHF/4-31G method at many sliding conformations are depicted. The definitions of the origin of the coordinate axes, sliding orientation and etc. are shown in this figure.

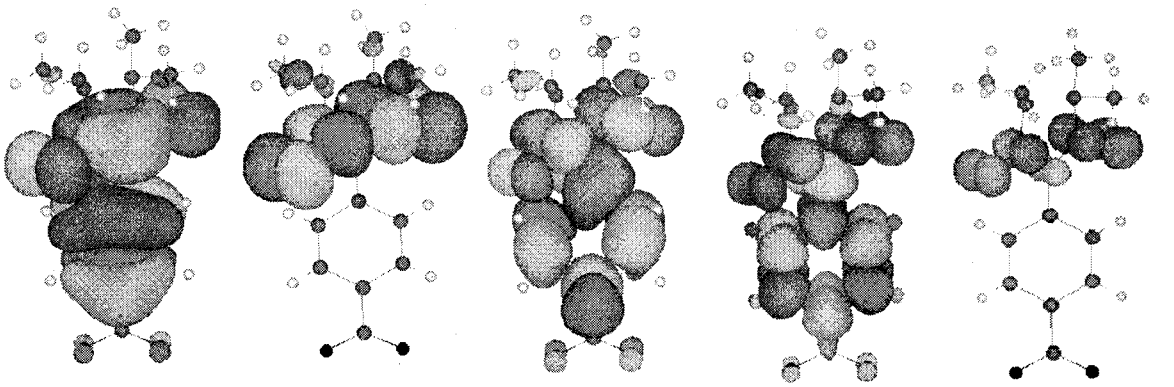

Figure 4.16 The structures of MOs and the spin densities (threshold 0.005) of the dimer $\mathbf{A_1}$.

Section 4.5

Conclusion

In conclusion, present and previous computations conclude that the no overlap and orientation principles in **Table 3.1** are useful guides for molecular design of organic ferromagnets. The orbital symmetry rules for kinetic exchange interactions are also derived for several cases. They are utilized for derivations of symmetry rules for organic ferromagnetism.

No SOMO-SOMO overlap and orientation principles is applicable to nitroxide crystals which exhibit the ferromagnetic effective exchange interactions. Here, it should be emphasized that the π^*-nature (orbital symmetry) of SOMO of nitroxide or nitronylnitroxide plays an important role to reduce the orbital-overlap antiferromagnetic term even in parallel interplane orientations. The situation is similar in the case of zero NBMO overlap in a zigzag but parallel conformation for ally radical dimer. On the other hand, the potential exchange (PE) term is still nonzero because of SOMO-SOMO through-space contacts in the orientations, giving rise to ferromagnetic intermolecular interactions. Thus, controls of spatial orientations of nitroxides or nitronyl nitroxides are also important for ferromagnetic intermolecular interactions between these species.

Chapter 5.

Role of "Hydrogen Bridge" for Interaction Path

Section 5.1

Introduction

Weak interchain or interplane three-dimensional interactions are essential for the long-range magnetic ordering at low temperature, since the exchange interaction networks in nitroxide crystals are low-dimensional. It has been suggested that hydrogen-atom bridges are effective for weak intermolecular ferromagnetic exchange interactions between nitroxides. Such weak interactions via hydrogen bridges attract current interest in relation to the ferromagnetic phase transitions in several crystalline organic ferromagnets discovered recently.

In the following section 5.2, as a continuation of our previous work, here the author investigates possibilities of the ferromagnetic interaction through bridge hydrogen atoms under adequate intermolecular stacking conditions and orientations. In addition, alkyl substituent effects on the exchange integral interactions are also examined. To this end, ab initio post-UHF, UNO CASCI and DFT computations are carried out for several idealized dimers of nitroxide in order to elucidate possible interaction mechanisms.

Theoretically, two different mechanisms for the effective exchange interactions via hydrogen bridges are conceivable: One is the hyperconjugation effect of methyl and alkyl groups with the SOMO of nitroxide, entitled "the bridge hydrogen hyperconjugative effect". The potential exchange between orthogonalized hyperconjugated SOMOs should provide ferromagnetic exchange interaction. The other is the spin polarization (SP) effect via hydrogen bridge, though the spin densities induced on hydrogen atoms by the magnetic field of nitroxide are small. This mechanism may be referred to as "the bridge hydrogen SP effect".

Recently, Nogami and co-workers reported ferromagnetic behavior of *ph*-CH=N-TEMPO. This crystal shows Weiss temperature of +0.74 K and undergoes ferromagnetic phase transition at T_c = 0.18 K. Related compounds of the TEMPO derivatives also show ferromagnetic behaviors. A common structural feature was found for these TEMPO derivatives: β-hydrogen atoms, i.e., methyl hydrogen atoms and/or methyene hydrogen

atoms, locate in close contact with the neighboring nitroxide (NO) radical group in the crystal.

In the section 5.3, we proposed the hydrogen bridging effect that the ferromagnetic interaction can be mediated by the hydrogen atoms in the real model[19]. A series of TEMPO derivatives seem a suitable system for the precise investigation of the hydrogen bridging effect. We here report the detailed theoretical studies on these species. Calculations based on molecular orbital (MO) theory were carried out to evaluate the intermolecular effective exchange integrals for pair molecules in the crystal. Particularly, we wish to elucidate the origin of the ferromagnetic interaction in the crystals in relation to designing the organic ferromagnetic materials.

Section 5.2

Magnetic interaction between nitroxides via hydrogen atoms

5.2.1 Spin polarization effect via bridge-hydrogens

Parallel orientation

The previous chapter 4 have shown that the sign and magnitude of effective exchange integrals are sensitive to the stacking modes of nitroxides such as parallel and perpendicular conformations. The roles of bridge hydrogens for effective exchange interactions are first studied by calculating the intermolecular interactions in simple model systems composed of planar dihydronitroxide (**1**) illustrated in **Fig. 5.1**-I, II. The molecules of model dimer I (**Fig. 5.1**-I(a)) are stacked parallel, and the hydrogen atom of one molecule is placed just above the oxygen atom of the other. The interplane distance is indicated by R. **Table 5.1** summarizes the effective exchange integrals (J_{ab}) calculated at several intermolecular distances R by the post-UHF methods using the 4-31G basis set, and **Table 5.2** shows numerical results at a fixed distance, R=3.4 Å. Overlap integrals ($-1 \leq S_{ab} \leq 1$) between the molecules are also calculated.

The following conclusions can be drawn from **Tables 5.1** and **5.2**.

(1) The J_{ab} values estimated by all the UHF-based methods are positive in the magnetic region (near R=3.4 Å). However, the magnitudes of J_{ab} values depend remarkably on the electron correlation corrections. They are reduced by including higher-order electron correlations, e.g., the J_{ab} values at 3.4 Å are 3.00 and 0.366 cm^{-1} by APUHF and APUCCSD(T), respectively.

(2) All J_{ab} values calculated by different methods decay exponentially as the intermolecular distance increases (R>3.4 Å), although APUCCSD(T) method gives negative J_{ab} values at shorter distances (R<3.2 Å).

(3) The UNO CASCI {2, 2} method which involves only the SOMO-SOMO direct interaction gives a positive J_{ab} value (1.11 cm^{-1}) at 3.4 Å, whereas the APUHF provides a much larger J_{ab} value (3.00 cm^{-1}).

(4) APUB-LYP gives an abnormally large negative value (-15.1cm^{-1}) for model I, showing that DFT is not reliable for computations of intermolecular effective exchange integrals via hydrogen bridge. This behavior may come from the emphasis of a small S_{ab} value.

Since the magnitudes of J_{ab} values are small, they may be sensitive to the basis sets employed. Therefore, the basis set dependence of J_{ab} is examined in detail. **Table 5.3** summarizes the results; all the calculated J_{ab} values except for the STO-3G values are positive (ferromagnetic) and the magnitudes of J_{ab} decrease with the electron correlation corrections when the same basis set is used. The combination of the largest basis set (6-311G**) and the best correlated method (APUCCSD(T)) gives a positive J_{ab} value (2.59 cm^{-1}), which is close to that of APUHF/4-31G. Judging from the present results, the 4-31G basis set can be used for qualitative purpose, though larger basis sets should be used for quantitative purpose.

In model I, two types of effective exchange interactions are feasible: One is the SOMO-SOMO direct interaction path, and the other is the indirect interaction path via the bridge hydrogen atom. As for the former, **1** has a π*-type SOMO which is essentially localized on the nitrogen and oxygen atoms, as shown in **Fig. 5.2**A. The π*-type SOMOs in model I interact with each other as shown in **Fig. 5.1**-I(b), where the solid and waved lines indicate the intermolecular in-phase and out-of-phase combinations of the orbital lobes, respectively; they lead to a very small SOMO-SOMO overlap integral (S_{ab} = 0.00297 in **Table 5.2**) and cancel the orbital interactions. Therefore, the KE term in Eq. (3.1) is estimated to be very small, though it is still nonzero. On the other hand, the PE term is much larger. Hence, the net J_{ab} value should be positive, as confirmed by UNO CAS CI {2,2} at R= 3.4 Å in **Table 5.2**.

Model I is suitable for studying the possibility of the other interaction path based on the SP effect via the bridge hydrogen atom, for example N_1-$H_1\cdots O_2$-N_2. To clarify whether the induced spin densities on the hydrogen atoms contribute to the effective exchange interactions, those in the high-spin state of the dimer are calculated by the UHF / 4-31G method as shown in **Fig. 5.1**-I(c); the size of arrows indicates their magnitudes. Positive spin densities are induced on the N_1 and O_1 atoms of **1** by the spin delocalization (SD) effect[55], whereas a small negative spin density is induced on H_1 because of the SP effect. Since the local effective exchange interaction between the induced spin and the delocalized spin (H_1 - O_2) is predicted as antiferromagnetic at parallel stacking, the high-spin state is preferred in total, as shown in **Fig. 5.1**-I(d). Therefore, the induced spin on H_1

is expected to play a significant role in addition to the pure SOMO-SOMO direct term. The J_{ab} value calculated by APUHF involving the SP effect is larger by 2 cm^{-1} at 3.4 Å than that of UNO CASCI{2,2}. Thus, the PE and SP terms are both ferromagnetic in model I. The ferromagnetic SP term is responsible for the so-called McConnell model. On the other hand, a J_{ab} value estimated by APUCCSD(T), which is smaller than that by UNO CASCI{2,2}, indicates that the electron correlation (EC) term reduces the J_{ab}.

Perpendicular orientation

Next, the perpendicular approach model II is studied to elucidate the relative contributions of the PE and SP terms in Eq. (3.1) to the effective exchange interactions. In this model the two molecular planes of **1** in **Fig. 5.1**-II(a) are oriented perpendicular to each other and the bridge hydrogen atom (H_1) contacts with the oxygen atom (O_2).

The following characteristics can be drawn from **Tables 5.1-5.3**.

(1) All the calculated Jab values in **Table 5.1** are negative in the magnetic region.

(2) The J_{ab} values calculated by APUHF and APUCCSD(T)/4-31G are -0.470 and -0.307 cm^{-1} at 3.4 Å, respectively, indicating only small correlation corrections.

(3) The UNO CASCI{2,2} and APUB-LYP methods give positive J_{ab} values, respectively.

(4) All the basis sets except for the STO-3G basis set give similar J_{ab} values; those derived from APUHF/4-31G and APUCC SD(T)/6-311G** are -0.470 and -0.307 cm^{-1}, respectively. This result indicates that the 4-31G basis set is useful for qualitative purpose, as in the case of model I.

As for conclusion (3), the SOMO-SOMO direct interaction should provide information on the possible mechanisms of the effective exchange interaction. **Figure 5.1**-II(b) shows that the no-overlap configuration between the SOMOs causes a small positive J_{ab} value, in conformance with the result using UNO CASCI{2,2} at R=3.4 Å. This can be understood by the cancellation of the orbital interactions denoted by the solid and waved lines in **Fig. 5.1**-II(b). The overlap integral S_{ab} in **Table 5.2** vanishes completely. From conclusion (1), the contributions except for SOMO-SOMO direct interaction are dominant because the J_{ab} values calculated by APUHF and post-HF are negative. This result can be explained by the spin densities in the low spin state by the UHF method shown in **Fig. 5.1**-II(c). The directly contacting spins prefer the parallel (ferromagnetic) spin alignment, as shown in **Fig. 5.1**-II(d), and the net spin alignment becomes antiferromagnetic. Therefore, the SP effect is reversed due to the perpendicular conformation, as expected from the McConnell model. This situation has been recognized for the local ferromagnetic interaction between the *p*-NO_2 and NO radical groups in the β-phase of *p*-NPNN.

In summary, the SOMO-SOMO direct interaction term (PE) and the indirect SP term are shown to contribute to ferro- and antiferromagnetic interactions, respectively. The latter term turns out to be stronger than the former in the magnetic region. Therefore, the

bridge hydrogen SP effect should play a predominant role in model II. Such interaction paths via hydrogen atoms may be important in many systems where the KE and PE terms are negligible.

5.2.2 Bridge-hydrogen hyperconjugative effect

Methylnitroxide (**2**) is examined so as to investigate the role of the α-hydrogen atoms placed below, above and on the plane. They are denoted as $H_{\alpha 1}$, $H_{\alpha 2}$ and $H_{\alpha 3}$, respectively, as shown in **Fig. 5.3**-III, IV. The bond lengths and angles in **2** are assumed to have standard values[55]. **Figure 5.2**B illustrates the SOMO of **2**, showing that the two hydrogen atoms above ($H_{\alpha 2}$) and below ($H_{\alpha 1}$) the plane have significant SOMO lobes arising from hyperconjugation between the methyl and nitroxide groups. The SOMO is regarded as the π*-type MO, since **2** involves five electrons in three p-type orbitals.

Figures 5.3-III(a), and IV(a) illustrate the stacking models III and IV, by which the roles of the methyl group for weak intermolecular interactions via the hyperconjugation effect are studied. In model III, the bridge $H_{\alpha 1}$ is fixed above the O_2 atom, whereas the bridge $H_{\alpha 3}$ is fixed above the O_2 atom in model IV.

The APUCCSD(T) method gives positive J_{ab} values for model III at all R values examined, as shown in **Table 5.2** and **Fig. 5.4**, which provide information on the dominant term in the effective exchange interactions in Eq. (3.1). **Figure 5.3**-III(b) illustrates the stacking mode of the hyperconjugated SOMOs for model III, where the SOMO-SOMO overlap integral is nearly zero (S_{ab} = 0.00034 in **Table 5.2**). Therefore, the UNO CASCI{2,2} method gives a positive J_{ab} value (0.120 cm^{-1}) at R = 3.4 Å and affords evidence that the orbital lobe on the bridge hydrogen atom plays an important role for the ferromagnetic interaction via the potential exchange mechanism.

Figure 5.3-III(c) shows the spin densities at the high-spin state. The ferromagnetic interaction path, C_1-$H_{\alpha 1}$···O_2-N_2, can be predicted from the SP rule for perpendicular planes, as illustrated in **Fig. 5.1**-II(d). In fact, the APUHF value including the SP effect is 0.234 cm^{-1}, being larger by 0.114 cm^{-1} than the UNO CASCI{2,2} value. This tendency is not altered by the addition of higher-order correlation corrections by APUCCSD(T). Thus, the ferromagnetic interaction via the bridge hydrogen hyperconjugative effect is feasible in appropriate conformations.

In contrast to model III, the UHF-based methods (UMPn, UCC) with electron correlations and the UNO CASCI{2,2} method give negative J_{ab} values for model IV, though APUHF gives positive J_{ab} values, as listed in **Table 5.2**. **Figure 5.3**-IV(b) illustrates schematically the orbital interaction between the SOMOs. The intermolecular contact between the hyperconjugated SOMO on $H_{\alpha 1}$ and SOMO on N_2 provides a nonzero (but very small) orbital overlap integral (S_{ab} = 0.00308 in **Table 5.2**). The J_{ab} value is calculated to be negative (-0.933 cm^{-1}) at R=3.4 Å by UNO CASCI{2,2}.

However, since APUHF gives a positive J_{ab} (0.747 cm^{-1}), a significant contribution of the SP effect must be considered. The spin densities by APUHF at the high-spin state are drawn in **Fig. 5.3**-IV(c). Here two effective exchange interaction paths are conceivable for the SP effect. The J_{ab} values via C_1-$H_{\alpha 1}\cdots N_2$-O_2 should be ferromagnetic in conformity with the spin alignment rule illustrated in **Fig. 5.1**-II(d), but that for C_1-$H_{\alpha 3}\cdots O_2$-N_2 is expected to be negative from the spin alignment rule illustrated in **Fig. 5.1**-I(d). Though model IV takes the $H_{\alpha 3}$ atom as a bridge atom, the distance of $H_{\alpha 1}$-N_2 is shorter than that of $H_{\alpha 3}$-O_2, and the spin density induced on $H_{\alpha 3}$ is smaller than that on $H_{\alpha 1}$. Therefore, it is reasonable to conclude that the former ferromagnetic SP path is predominant. Moreover, APUCCSD(T) is found to give a large negative value (-5.49cm^{-1}) even at R = 3.4 Å, showing that the electron correlation effect is important in view of a large van der Waarls interaction via the methyl group.

Finally, a remote intermolecular interaction through hydrogen bridges is studied by model V, where the molecules contact on the bridge hydrogen $H_{\beta 3}$, as illustrated in **Fig. 5.3**-V(a). The geometry of ethylnitroxide (**3**) is constructed from **2** by substituting $H_{\alpha 3}$ with a methyl group, and the bond length and angles are assumed to have standard values[55]. **Figure 5.2**C illustrates the SOMO of **3**, which indicates the hyperconjugation on the $H_{\beta 1}$ and $H_{\beta 2}$, although it is largely reduced as compared with that on the $H_{\alpha 1}$ and $H_{\alpha 2}$. On the other hand, the $H_{\beta 3}$ atom on the plane is not conjugated with the SOMO.

The SOMO on the $H_{\alpha 1}$ atom in **3** interacts with the SOMO of **1**, as indicated in **Fig. 5.3**-V(b), and there is a small orbital overlap integral, though this model is assumed for the direct contact between the O_2 and $H_{\beta 1}$ atoms. The nonzero (but very small) overlap integral (S_{ab} = 0.00099 in **Table 5.2**) should cause the antiferromagntic interaction, and a negative J_{ab} value by UNO CASCI{2,2} affords evidence of this SOMO-SOMO kinetic exchange interaction. This in turn indicates that the main contribution arises from $H_{\alpha 1}$ because of the large orbital lobe on it, though $H_{\beta 3}$ is assumed to be the bridge hydrogen atom. In this regard, model V is similar to model IV as to the hyperconjuagative hydrogen effect at $H_{\alpha 1}$.

Figure 5.3-V(c) illustrates the spin densities at high-spin state obtained by APUHF method. The SP effects are conceivable from the C_1-$H_{\alpha 1}\cdots O_2$-N_2 vertical-type path and the C_2-$H_{\beta 3}\cdots O_2$-N_2 parallel-type path. Judging from the spin alignment rules illustrated in **Figs. 5.1**-II(d) and I(d), these paths should provide ferromagnetic interactions. In fact, the J_{ab} value by APUHF is 0.087 cm^{-1} because of the SP effect, although that by UNO CASCI{2,2} is -0.207 cm^{-1}. However, APUCCSD(T) gives a negative J_{ab} value (-0.467cm^{-1}), showing that the electron correlation correction overweighs the SP effect, giving rise to an antiferromagnetic interaction. This characteristic behavior is common in models IV and V. Higher-order electron correlations are essential for remote effective exchange interactions via methyl and alkyl groups in general.

5.2.3 J_{ab} values for larger alkyl nitroxides models

A systematic study for RHNO - H_2NO (HNO-$(CH_2)_n$-H ... O-NH_2) (R = *n*-Pr, *n*-Bu, *n*-Pe), is carried out as shown in **Fig. 5.5** for R = H (model I), Me (model IV) and Et (model V). Theoretical calculations reveal that the $|J_{ab}|$ values decay drastically with the distance between the NO-radical sites. The APUHF method gives positive J_{ab} values for all systems except for the R = *n*-Pr system. However, this calculation may overestimate the SP effect, since APUMP4SDTQ and APUCCSD(T) including electron correlations should improve the J_{ab} values.

5.2.4 Discussions

The effective exchange interactions between nitroxides via the bridge hydrogen have been investigated in simple models I and II in **Fig. 5.1** including bridge hydrogen atoms at appropriate positions. In model I, the potential exchange (PE) and spin polarization (SP) terms are both ferromagnetic because of the parallel conformation (**Figs. 5.1**-I(b) and I(d)). The ferromagnetic SP effect in the parallel stacking mode is consistent with the McConnell model. To the contrary, the bridge hydrogen SP effect is antiferromagnetic in model II because of the perpendicular conformation (**Fig. 5.1**-II(d)). Thus, the sign of the effective exchange interaction via the SP effect depends strongly on the stacking orientation of radical molecules, in agreement with the systems examined previously and with the spin alignment rules.

The effective exchange interactions between alkyl nitroxide (**2** or **3**) and dihydronitroxide (**1**) have been examined in models III, IV and V in order to elucidate the hyperconjugative effect between alkyl and NO groups. The SOMO's of **2** and **3** are found to be the π^*-like hyperconjugated MO delocalized over hydrogen atoms. Since the SOMO lobes are delocalized on the hydrogen atoms, the interaction path via these atoms can be responsible for the non-zero SOMO-SOMO overlap integral (KE-term) as well as the potential exchange (PE) term. Such SOMO-SOMO direct exchange interactions in models III, IV and V may play important roles in ferromagnetic crystals of nitroxide derivatives discovered recently. Judging from the results by the UNO CASCI{2,2} method, which gives the KE and PE contributions, it can be ensured that the hydrogen atoms attached to NO radical play a role in ferromagnetic interaction as hyperconjugation. However, the interaction via the SP effect exceeds the hyperconjugation effect in alkyl substituted nitroxides. This in turn indicates that a careful theoretical examination is crucial for elucidation of the type of ferromagnetic interactions via hydrogen bridges.

In addition, the higher-order electron correlations play important roles for weak interactions between alkylnitroxides. Such corrections are sensitive to the size-inconsistent

error[53,54], and therefore, the present size-consistent APUCC SD(T) is one of the practical computational methods for this purpose. Unfortunately, the DFT method is not reliable for a theoretical treatment of such weak intermolecular interactions via hydrogen bridges. The size-consistent multireference (MR) CC[56,57,58] computations seem to be desirable for quantitative purpose.

Table 5.1 Effective exchange integrals (J_{ab} / cm^{-1}) calculated by UHF-based methods at several distances (R) for models I and II.

	I				II			
R /Å	APUHF	APUMP2	APUMP4SDTQ	APUCCSD(T)	APUHF	APUMP2	APUMP4SDTQ	APUCCSD(T)
3.0	9.07	4.40	0.948	-2.84	-1.52	-1.89	-1.58	-0.893
3.2	5.59	4.02	1.97	-0.145	-0.867	-1.10	-0.920	-0.538
3.4	3.00	2.60	1.47	0.366	-0.470	-0.612	-0.509	-0.307
3.6	1.45	1.43	0.860	0.327	-0.242	-0.321	-0.268	-0.165
3.8	0.641	0.707	0.448	0.211	-0.118	-0.159	-0.132	-0.083
4.0	0.263	0.323	0.213	0.116	-0.055	-0.074	-0.061	-0.040
4.4	0.036	0.053	0.037	0.026	-0.010	-0.013	-0.011	-0.007
4.8	0.004	0.006	0.004	0.004	-0.001	-0.002	-0.002	-0.002
5.5	0.000	0.000	0.000	0.000	0.000	-0.001	-0.002	0.000

[a] 4-31G basis set was used.

Table 5.2 Effective exchange integrals (J_{ab}) calculated by UHF-based methods at R=3.4Å.

Model	J_{ab} /cm^{-1}						S_{ab} [b]
	UNO CASCI{2,2}	APUHF	APUMP2	APUMP4SDTQ	APUCCSD(T)	APUB-LYP	
I	1.11	3.00	2.60	1.47	0.366	-15.1	0.00297
II	0.073	-0.470	-0.612	-0.509	-0.307	0.123	0.00000
III	0.120	0.234	0.377	0.307	0.235	-0.284	0.00034
IV	-0.933	0.747	-2.86	-3.75	-5.49	-38.0	0.00308
V	-0.207	0.087	-0.136	-0.285	-0.467	-4.89	0.00099

[a] 4-31G basis set was used.
[b] Overlap integrals (S_{ab}) between fragment molecules (**1**, **2** and **3**).

Table 5.3 Basis set dependencies of effective exchange integrals (J_{ab} / cm^{-1}) calculated by UHF-based methods at R=3.4Å for models I and II.

	I				II			
Basis set	APUHF	APUMP2	APUMP4SDTQ	APUCCSD(T)	APUHF	APUMP2	APUMP4SDTQ	APUCCSD(T)
STO-3G	-0.235	-0.354	-0.371	-0.371	0.000	-0.015	-0.015	-0.009
4-31G	3.00	2.60	1.47	0.366	-0.470	-0.612	-0.509	-0.307
6-31G*	4.65	4.76	3.06	1.68	-0.587	-0.596	-0.478	-0.296
6-31G**	4.39	4.41	2.79	1.48	-0.592	-0.592	-0.472	-0.292
6-311G**	5.15	5.47	3.91	2.59	-0.641	-0.613	-0.503	-0.307

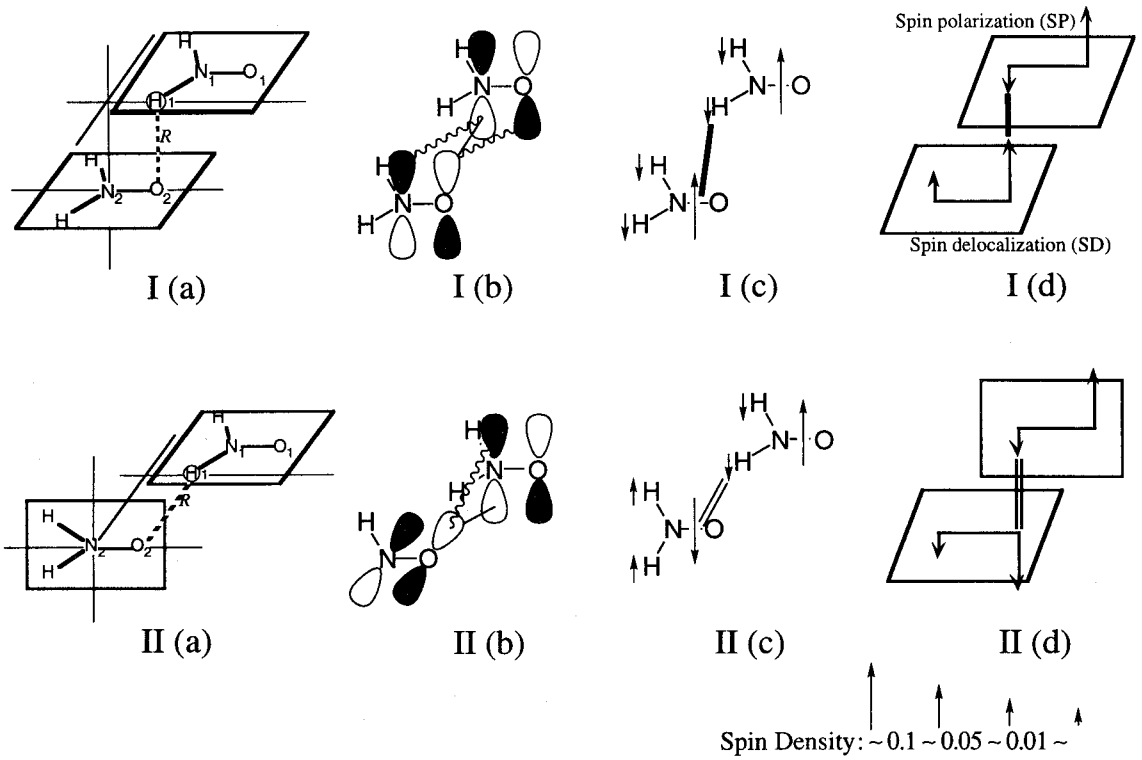

Figure 5.1 Parallel (I) and perpendicular (II) interaction models between dihydronitroxide molecules (**1**) via hydrogen atom bridge. (a): (I) One of the hydrogen atoms of one molecule is set above the O_2 atom, and (II) N_2 and O_2 atoms are coplanar with atoms with subscript 1. Broken lines indicate the interaction point. (b) : SOMO-SOMO direct interactions. Solid and waved lines indicate intermolecular in-phase and out-of-phase combinations of SOMO lobes, respectively. (c) : Spin structures and interaction paths with the SP effect. The sizes of arrows represent the magnitude of induced spin densities. Bold and parallel lines indicate antiparallel and parallel couplings of spin densities, respectively. (d) : Spin alignment rules in parallel- and perpendicular-type conformations.

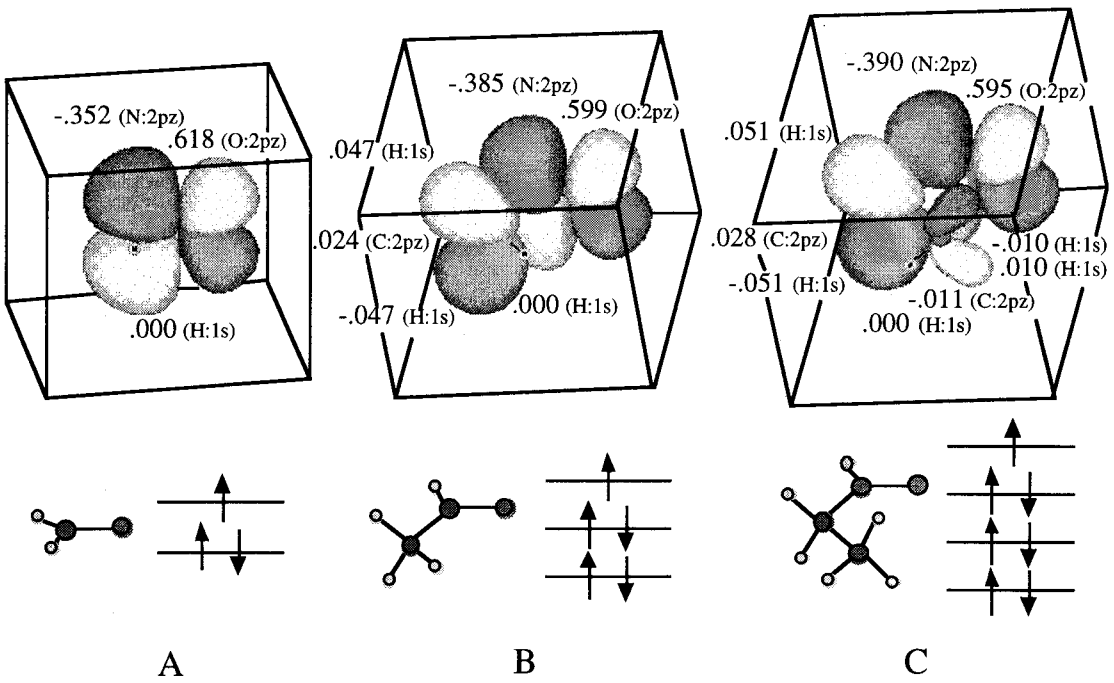

Figure 5.2 SOMOs of dihydronitroxides (1) (A), methylnitroxide (2) (B) and ethylnitroxide (3) (C), with coefficient numbers of 4-31G basis sets. B and C show the π*-type SOMO consisting of the hyperconjugation of methyl and ethyl groups with nitroxide group, respectively.

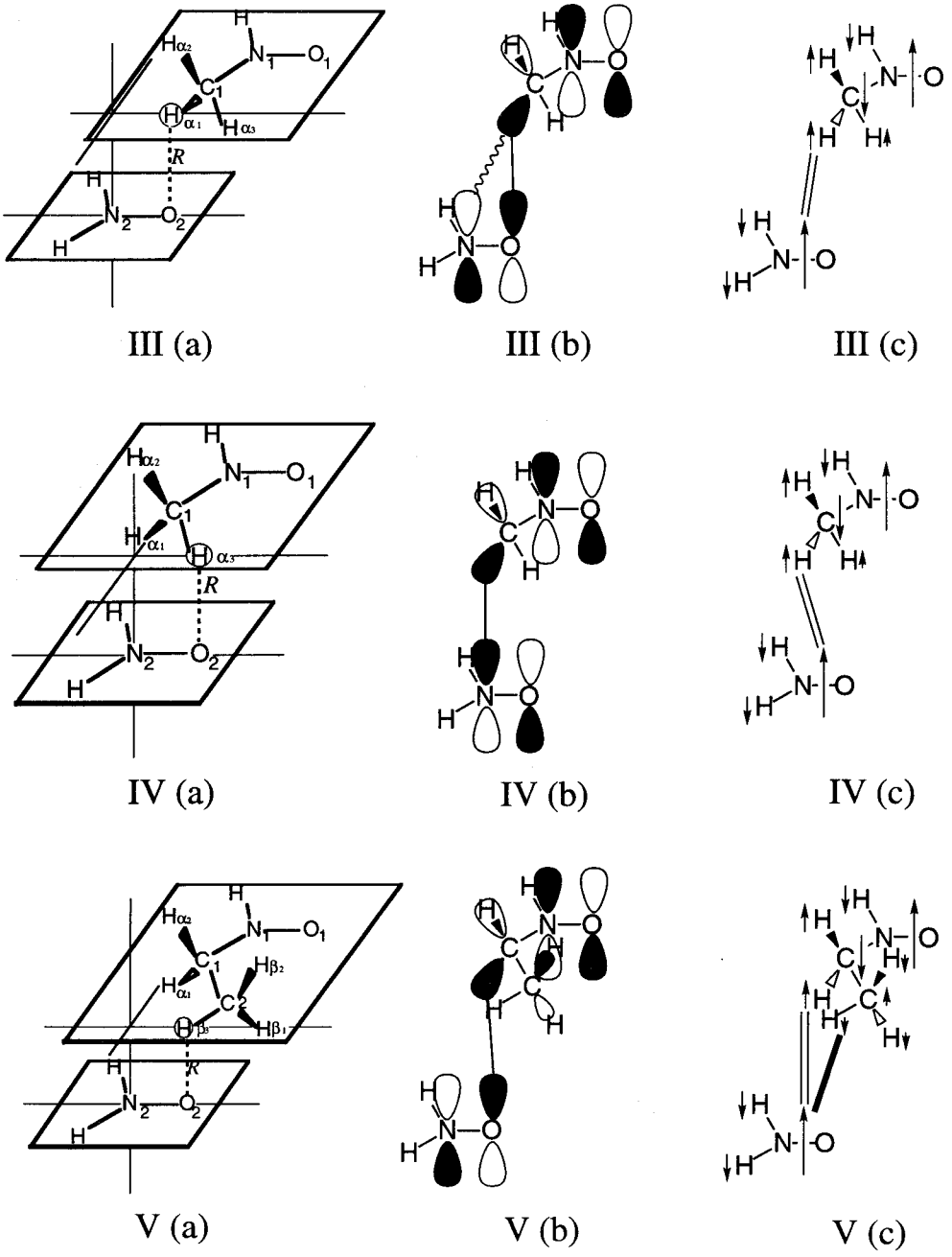

Figure 5.3 Intermolecular interaction models between nitroxides (**1**, **2** and **3** in **Fig. 5.2**). (a) : In model III, IV and V, bridge $H_{\alpha 1}$ and $H_{\alpha 3}$ of **2** and $H_{\beta 3}$ of **3** lie above O_2 of **1**, respectively. (b) : SOMO-SOMO direct interactions. (c) : Spin structures and interaction paths with the SP effect. See **Fig. 5.1** for definitions of the arrows.

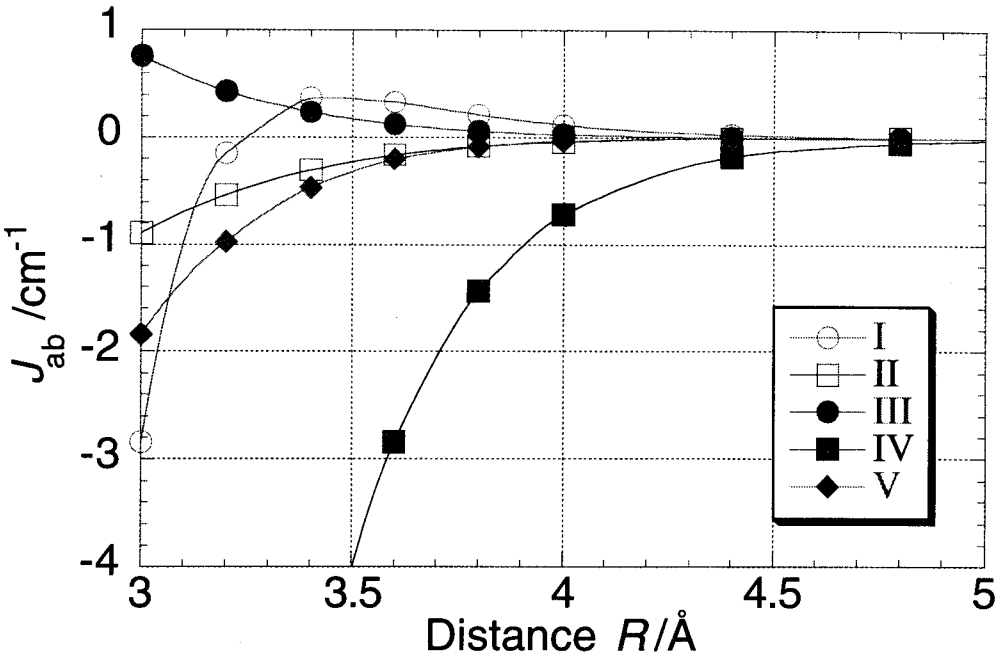

Figure 5.4 Effective exchange interactions (J_{ab}) calculated by APUCCSD(T)/4-31G. Models I and III show ferromagnetic interactions in the magnetic region.

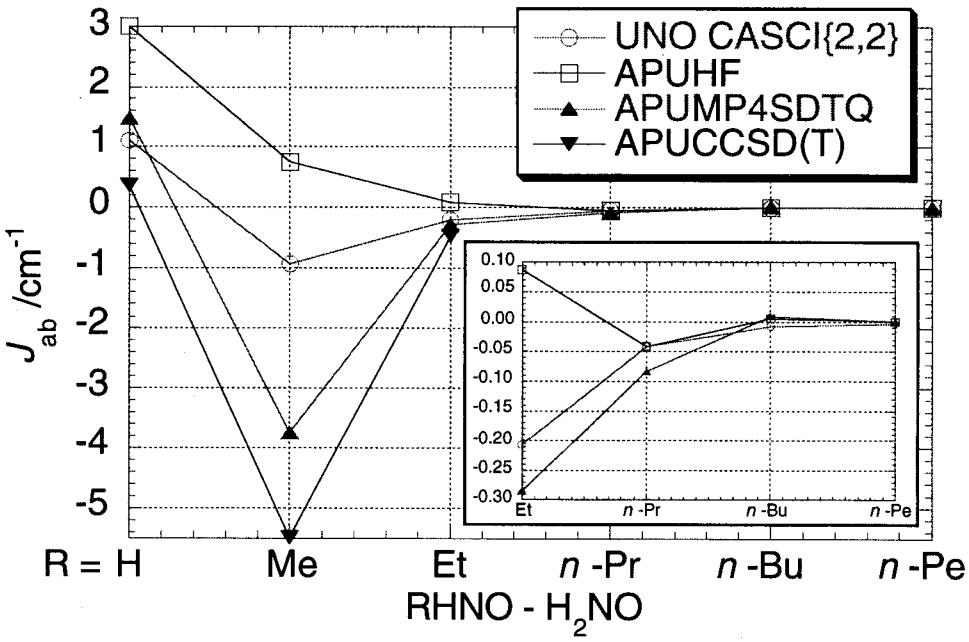

Figure 5.5 Dependence of the J_{ab} values on the alkyl substitutes for (HNO-$(CH_2)_n$-H ··· O-NH_2) (R = H : model I, Me : model IV, Et : model V, *n*-Pr, *n*-Bu, *n*-Pe).

Section 5.3

Theoretical studies for real system: Magnetic interaction via β-hydrogen atoms in TEMPO derivatives

5.3.1 The reported TEMPO derivatives

Nogami and co-workers have recently reported organic ferromagnets possessing a TEMPO group as shown in **Table 5.4** and interesting ferro- and antiferromegnetic interactions were found in these species[23]. Investigations of a possible mechanism of ferromagnetic coupling are required and molecular orbital calculations based on their crystal structures are also desired. In the following sections, the author treats the only *ph*-CH=N-TEMPO crystal.

5.3.2 Crystal structure

Figure 5.6 illustrates the two unit cells of the crystal. *Ph*-CH=N-TEMPO crystallizes in a monoclinic unit cell, $P2_1/c$, and cell parameters are a = 12.6835 Å, b = 11.7402 Å, c = 11.0236 Å and β = 111.399°[23]. In this figure, let us consider the molecule **A** as a reference. Molecular pair **A**-**B** is expected to have the largest intermolecular magnetic interaction, because two adjacent NO groups locate in close proximity. The theoretical calculations for this pair were carried out in detail. This pair is depicted in **Figure 5.7**, and it is shown that not only the direct interaction between N_1O_1 and N_2O_2 but also the indirect interaction paths I and II may be expected. The distances between the oxygen atom of NO group and the hydrogen atom of methyl group are 2.878 Å and 3.316 Å for

paths I and II, respectively. These hydrogen bridging paths are interesting for the ferromagnetic interaction in the crystal.

The nitroxide radical groups are arranged to construct a two-dimensional sheet, where the distances between the adjacent NO groups are 5.62 Å and 6.15 Å for the nearest and second nearest pairs, respectively. The intersheets distance is 11.89 Å. In addition to the pair **A-B**, pairs **A-C**, **A-D** and **A-E** were studied. The pairs **A-C** and **A-D** are the second and the third nearest neighbors, respectively. The pair **A-E** represents the intersheet interaction (see **Fig. 5.12**).

5.3.3 Calculations for pair A-B

Figure 5.8 illustrates simplified models of the pair **A-B**. Model I is the actual structure in the crystal. In model II *ph*-CH=N- group is replaced by a hydrogen atom to study the role of the phenyl ring for the magnetic interaction. In models III-$_{a, b}$ and $_{g}$ methylene frameworks are replaced by hydrogen atoms and only the CH_3CH_2NOH frame is considered in model IV_a. When we go through the process of the simplification, i.e., **A** → **A'**→**A"**→**A"'** and **B**→**B'**→**B"**→**B"'**, the interaction localized near the NO radical groups comes into the spotlight.

Ab initio UHF and INDO calculations were carried out for these models to elucidate the path of the ferromagnetic effective exchange interaction. Here, the 4-31G basis sets were used, since we performed calculations with various basis sets and it was concluded that the 4-31G basis sets can give relatively good result. For the simplified models III_a and IV_a the UNO CASCI{2,2} and UNO CASSCF{2,2} /4-31G methods were also employed, whereas these methods are not feasible for complicated models I and II. **Table 5.5** shows the J_{ab} values obtained by these computations. J_{ab} values for all models are positive, indicating a ferromagnetic interaction for pair **A-B**. It is noteworthy that similar J_{ab} values were obtained for all models I, II, III_a and IV_a. This result means that *ph*-CH=N- and methylene groups of TEMPO framework have negligible effect for the magnetic interaction. Judging from the spin density calculated by the INDO method, the induced spin density on the hydrogen atom is consistent with spin density expected from the SP rule, and therefore the explanation of the ferromagnetic interaction based on the SP effect may be feasible. In addition to the spin polarization mechanism, the SOMO-SOMO interaction seems to contribute to the ferromagnetic interaction through the hydrogen bridging. This was pointed out by the result that the UNO CASCI{2,2} and UNO CASSCF{2,2} methods gave relatively large J_{ab} values for models III_a and IV_a.

5.3.4 Calculations for simplified models

As mentioned in the previous section, two kinds of indirect magnetic interaction paths I and II are expected to exist in the nearest neighbor pair **A-B**. In order to investigate these contribution, simplified models with decomposing the two interaction paths were considered.

Figure 5.9 illustrates the simplified models, where molecules **A"** and **B"** in model III_a shown in **Fig. 5.8** are renamed as **a** and **b**, respectively. In model III_b one of the methyl groups of the molecule **b** was replaced by a hydrogen atom (marked by a cross), leading to the break of the hydrogen bridging path II of model III_a, while in model III_c a methyl group of molecule **a** was replaced by a hydrogen atom (marked by a cross), leading to the break of the hydrogen bridging path I of model III_a. In model III_d both interaction paths I and II are broken by replacing the methyl groups with hydrogen atoms (marked by crosses). The J_{ab} values calculated by the INDO method for model III_a through III_d are listed in **Table 5.6**. Although scatter of the calculated J_{ab} values is not small, the ferromagnetic interaction (J_{ab} = 0.009 cm-1) in model III_a decreased by breaking the hydrogen bridging paths I and II. The result suggests that the hydrogen bridging paths I and II contribute to the ferromagnetic interaction and the ferromagnetic interaction mediated by path I seems large compared with that of path II. As listed in **Table 5.6**, a similar trend was obtained for J_{ab} values of more simplified models IV_b through IV_d shown in **Fig. 5.9**. The model IV_b lacks in the hydrogen bridging path II, the model IV_c lacks in the path I and the model IV_d lacks in both paths I and II.

As discussed above, **Table 5.5** suggests that the SOMO-SOMO interaction through the hydrogen bridging seems to contribute to the ferromagnetic interaction and **Table 5.6** indicates that hydrogen bridging paths I and II contribute to the ferromagnetic interaction. Combining these two results, it is concluded that in addition to the spin polarization mechanism hyperconjugated SOMO should spread over the hydrogen atoms of the methyl groups. The spin polarization and hyperconjugation mechanism may be also affected by chemical modification of molecular group outside the interaction path. In order to investigate the secondary effect of the methyl group outside the hydrogen bridging, J_{ab} value was calculated for model pairs III_e through III_i shown in **Fig. 5.10**. In model III_e methyl group **ii** of model III_a is replaced by a hydrogen atom, while in model III_f methyl groups **i** and **ii** are replaced by hydrogen atoms. In model III_g methyl group **iii** is replaced by hydrogen atom, in model III_h **iv** is replaced and both **iii** and **iv** are replaced by hydrogen atoms in model III_i. J_{ab} values calculated by the INDO method are listed in **Table 5.7**. Chemical modification of the methyl group **ii** (model III_e), which locates in proximity with the methyl group participating in the intermolecular ferromagnetic interaction, gave a significant change of J_{ab}. In addition, model III_f lacking the interaction path I, too, gave almost the same J_{ab} value as III_c. Other modifications of the remote methyl groups from

the interaction path (methyl group **i**) gave no effect on J_{ab} (III_g through III_i) and gave the same tendency as III_a. Those calculations suggest that supplement of the methyl group near the interaction path modifies the spin polarization and/or hyperconjugation.

In the calculations described above, the methyl groups participating in the interaction path were replaced by hydrogen atoms. It is clear that the methyl group i is important for the intermolecular ferromagnetic interaction. However, it is not clarified which one of the carbon and hydrogen atoms of the methyl group is essential for the magnetic interaction.

Finally, in order to discuss this point the rotation of the methyl group around the C-C bond was considered as shown in **Fig. 5.11**A. The INDO calculation was carried out for several rotation angles between -60 and 120 degree. Origin of the rotation angle corresponds to the geometry of the pair determined by X-ray diffraction experiments. **Figure 5.11**B depicts the result of calculation and remarkable angle dependence of J_{ab} was found. The maximum of J_{ab} appears at about -15 degree (0.026 cm^{-1}) and the minimum appears at about +45 degree (0.002 cm^{-1}). The distances between β-hydrogen and oxygen atom of adjacent NO group are 2.774 Å and 3.128 Å, respectively. The distance between β-carbon atom and oxygen atom is fixed at 3.736 Å. This result clearly indicates that orientation of the hydrogen atoms is important for the intermolecular magnetic interaction. It is noted that "the hydrogen bridging hyperconjugative effect" and/or "the hydrogen bridging SP effect" occurs in this system. More accurate calculations for this system are in progress in our laboratory.

5.3.5 Calculations for the other pairs

Discussion of the pair **A-B** was described in the previous sections. In this section we investigate theoretically other pairs to elucidate bulk magnetic behavior. In **Fig. 5.12** positions of the molecules **A** through **E** shown in **Fig. 5.6** are illustrated. J_{ab} values calculated by the INDO and *ab initio* UHF/4-31G methods are also shown. In a two-dimensional sheet effective exchange interaction of pair **A-B** is ferromagnetic, while J_{ab} value of pair **A-C** is antiferromagnetic. A ferromagnetically interacted molecules construct a chain. The nearest interaction between the ferromagnetic chains is antiferromagnetic and intersheet interaction is very weak. Our theoretical calculations suggest that bulk ferromagnetism of the *ph*-CH=N-TEMPO crystal is difficult to predict and will be delicate in nature. Experimentally, a ferromagnetic phase transition at 0.18 K and positive Weiss temperature of +0.74 K in the high temperate phase were reported.

Table 5.4 Magnetic properties of TEMPO derivatives and complexes, which were reported by Nogami and co-workers.

Substances	Weiss temperature /K	Magnetic properties
phenyl-TEMPO	+0.74	ferromagnet, T_c=0.18K
p-biphenyl-TEMPO	+0.62	ferromagnet, T_c=0.4K
p-chlorophenyl-TEMPO	+0.69	ferromagnet, T_c=0.4K
p-phenoxyphenyl-TEMPO	+0.39	ferromagnet, T_c=0.2K
3,5-dichlorophenyl-TEMPO	+0.71	metamagnet, TN=0.12K
3-pyridyl-TEMPO	+0.42	no phase transition down to 30 mK
Naph-TEMPO	+0.30	metamagnet, TN=0.3K
p-bromophenyl-TEMPO	+0.32	no phase transition down to 40 mK
p-fluorophenyl-TEMPO	–2.6	antiferromagnetic

Table 5.5 J_{ab} values for pair **A-B** and its simplified models.

	J_{ab} /cm^{-1}			
methods	I	II	III_a	IV_a
INDO	0.010	0.010	0.009	0.021
UHF [a)]	0.164	0.170	0.155	0.125
UNO CASCI{2,2} [a)]			0.149	0.120
UNO CASSCF{2,2} [a)]			0.145	0.110

a) 4-31G basis set was used.

Table 5.6 J_{ab} values for simplified III_a through III_d and IV_a through IV_d shown in **Figs. 5.8** and **5.9**.

	J_{ab} /cm^{-1} [a]			
	subscript (a)	(b)	(c)	(d)
III	0.009	0.003	-0.005	-0.001
IV	0.021	0.018	0.000	0.000

a) INDO method was used.

Table 5.7 J_{ab} values for models III_e through III_i shown in **Fig. 5.10**.

	J_{ab} /cm^{-1} [a]				
	subscript (e)	(f)	(g)	(h)	(i)
III	0.019	-0.004	0.008	0.008	0.008

a) INDO method was used.

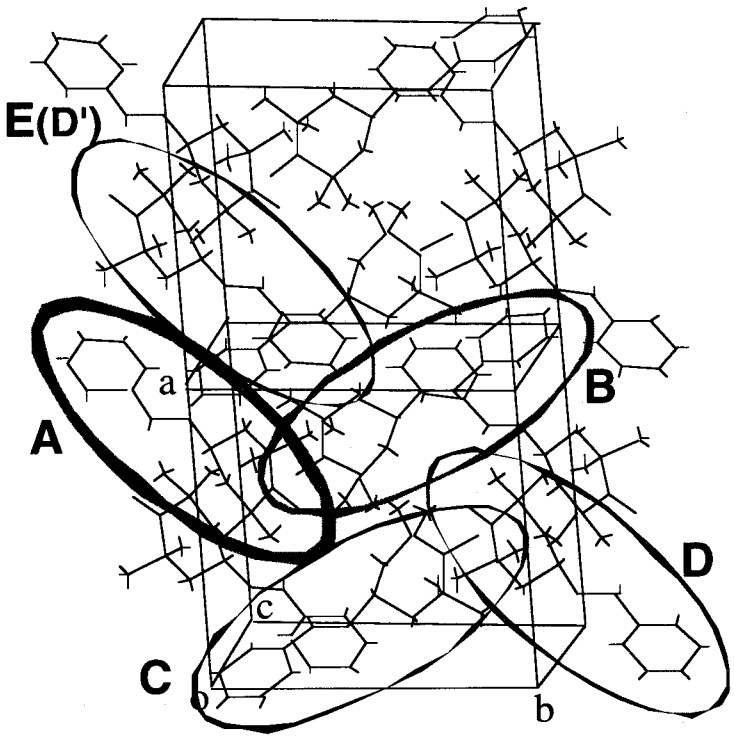

Figure 5.6 The crystal structure of phenyl-CH=N-TEMPO.

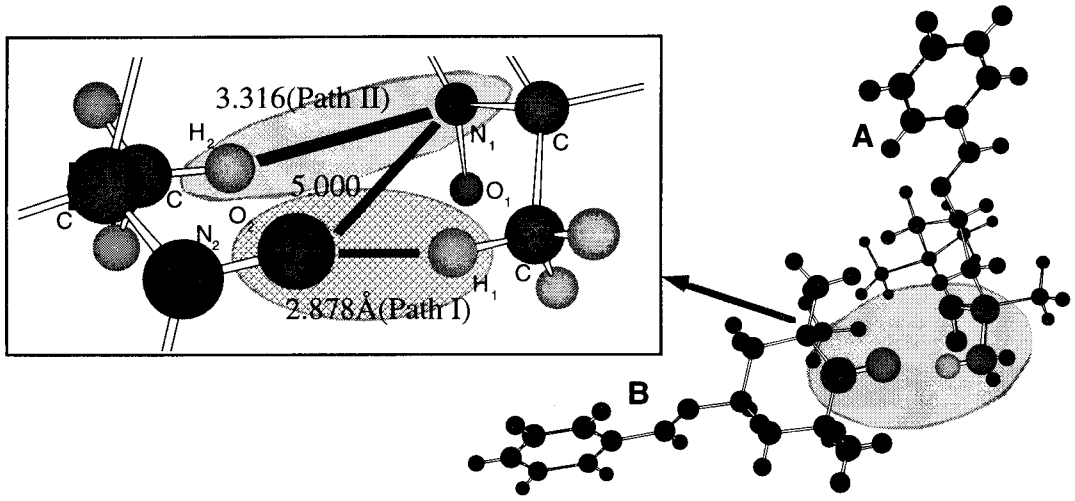

Figure 5.7 Direct and indirect interaction paths in the nearest neighbor pair **A**-**B**.

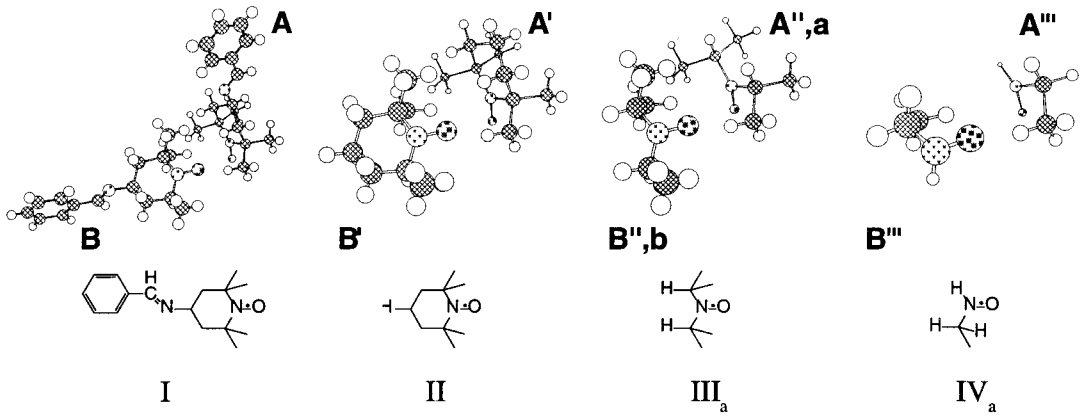

Figure 5.8 Simplified models of pair **A-B**.

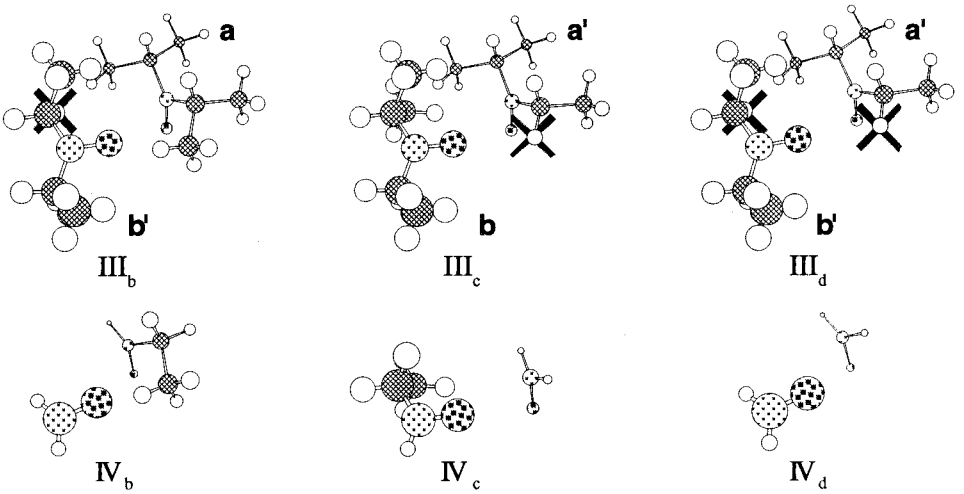

Figure 5.9 Simplified models of III_a and IV_a in **Fig. 5.8**, to study contribution of Paths I and II.

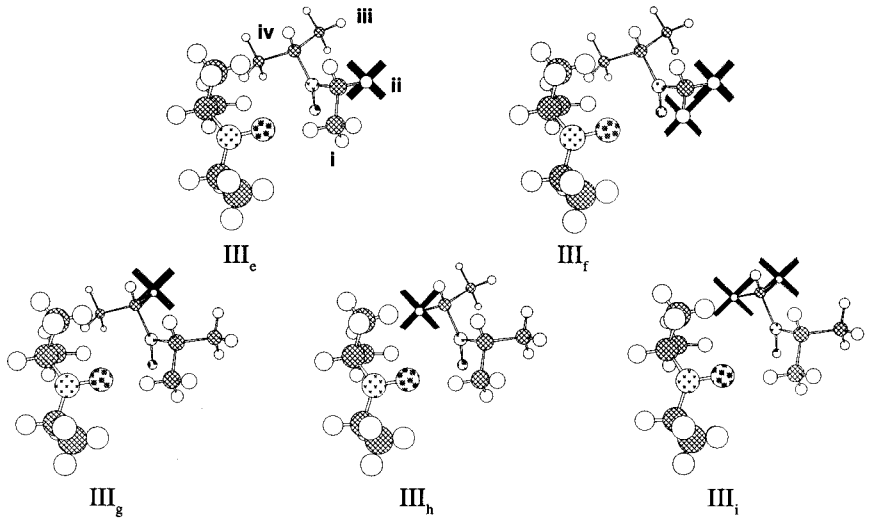

Figure 5.10 Models to elucidate the effect of the other β-methy group.

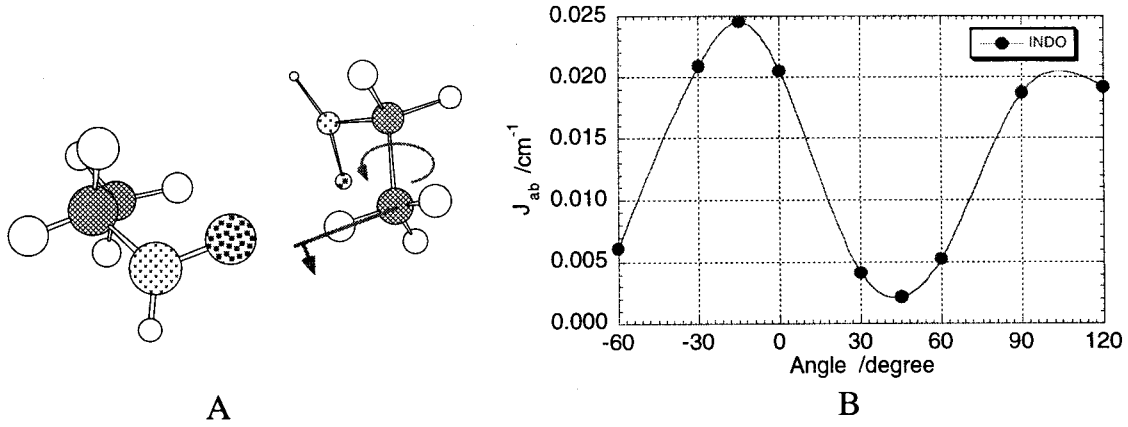

Figure 5.11 J_{ab} as a function of the rotation angle of the methyl group **i**.

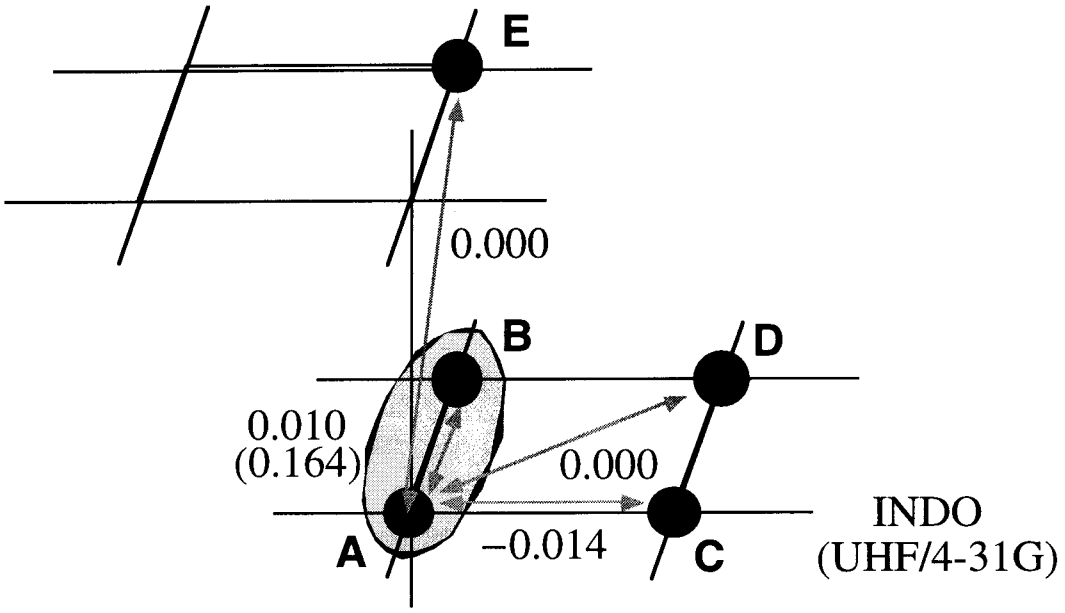

Figure 5.12 Various pairs **A**-**B**, **A**-**C**, **A**-**D** and **A**-**E** in the crystal.

Section 5.4

Conclusion

In the chapter 5.2, theoretical calculation based on both simple nitroxide model molecules and real system are carried out. And we can successfully study "the hydrogen hyperconjugative effect". I hope these investigation clarify newer magnetic interaction paths in ferromagnetic materials.

Especially, in the last section 5.3 we could apply our opinions to real organic crystal. Semiempirical and *ab initio* calculations were carried out for evaluating the effective exchange interaction for the pairs of adjacent molecules in the *ph*-CH=N-TEMPO crystal. Direct interaction of adjacent naked NO radical groups is weak. It was found that the hydrogen bridging between methyl hydrogen atom and adjacent NO group is essential for the ferromagnetic interaction. The ferromagnetic interaction runs along a chain. Interchain interaction is calculated to be antiferromagnetic. These two conflicting interactions exist in a molecular sheet and intersheet interaction is very week. Our theoretical calculations suggest that the bulk magnetism of this crystal is delicate in nature because the ferromagnetic and antiferromagnetic interaction coexists and is almost the same magnitude. More accurate and advanced calculations are required.

Also not only hydrogen atoms but also methyl groups are essential to magnetic interaction path. We guess a rotation of methy group can vary the sign and/or induce magnitude of effective exchange integrals and it may occur in real organic crstals. The author carried out the related discussions about importance of these groups in the section 6.2. Pressure-induced magnetic transition may be caused by the shortening or rotation of these groups under pressure. The author also discuss these pressure effects in the section 7.2.

Chapter 6.

Coupling of Intra- and Inter-Molecular Interactions in TMAO Crystal

Section 6.1

Introduction

In the previous chapters the author introduced only through-space ferromagnetic interaction and assume that each molecule had only one radical site. In this chapter the author takes into account not only inter- but also intra-molecular magnetic interaction and discuss coupling among these interactions.

Recently, Rassat and co-workers reported experimental measurements of α- and β-phases of a crystalline nitroxide biradical, that is, TMAO (**1**) and showed that for α-phase it had a positive Weiss constant of 10 K and exhibited a ferromagnetic transition at 1.48 K[14,17]. This biradical contains two NO radical groups at the opposite sides in one molecule and magnetic coupling between each site can be propagated through carbon atoms. In this point this crystal differs from other previous ferromagnetic crystals which contain only one NO radical site[7,13,19,1,23]. On the other hand, one NO radical site locates in close contact with one site on the next molecule without forming the local dimer bonding which is familiar for *p*-NNBA^{-}, *ph*-CH=N-TEMPO and so on, and linear zigzag NO paths appear. Two molecules on each chain also approach each other closely on NO radical sites and it is expected that spatial networks of magnetic interactions appear. Thus, two types of magnetic interactions, that is, intra- and inter- magnetic interactions are expected in this crystal and coupling between these magnetic interactions is worth evaluating.

Section 6.2

Theoretical studies for real system: Spatial networks for TMAO crystal

6.2.1 Crystal structure

The TMAO compound which consists of a purely organic non-ionic material has been reported in detail by Rassat and co-worker and their papers propose that it exhibits two crystalline forms (α- and β- forms) where packing styles are different from each other[14,17]. The α-form crystal undergoes a ferromagnetic transition at low temperature and the data of magnetic measurement were reported in their papers. It possess a Curie temperature of 1.48 ± 0.02 K and a positive Curie-Weiss temperature ($\theta = 10$ K), while the magnetic behavior in the β-form crystal was not reported. In addition, X-ray structural measurement was carried out in their papers and particularly the last paper contained accurate positions of not only heavy atoms, such as carbon, nitrogen and oxygen atoms, but also hydrogen atoms. Here, we employed the most accurate structural data for the a-form particularly, since its detailed magnetic behavior had been researched. The TMAO crystal in the a-form has unit cells classified by a space group of *C2/c* and cell parameters are a = 8.381(3) Å, b = 14.495(3) Å, c = 10.351(3) Å, and β = 105.35(2)

Figure 6.1A illustrates a unit cell of the a-form crystal, for which theoretical calculations will progress. In this figure, let us consider molecule **A** as reference and two radical NO sites indicate **i** and **ii**. In addition to molecule **A**, the adjacent molecules are also indicated as **B**, **C**, **D**, **E** and **F**. Each NO group has three close NO neighbors, i.e. one is located on the opposite side of the same molecule and the others occupy the adjacent side of the next molecules. Distances between oxygen atoms on each NO-group are 5.698 (**i** to **ii** on A), 4.091 (**i** to **iii** on **B**) and 4.654 Å (**i** to **iv** on **C**). The NO's network with intra- and inter- molecular chains will compose spatial magnetic interactions. Much detailed

theoretical studies depended on quantum chemistry techniques will be made on the following sections.

6.2.2 Intra-molecular ferromagnetic interaction

First of all, we have to investigate intra-molecular magnetic interaction in a TMAO molecule. **Figure 6.2** illustrates real TMAO and several modified models. Here, model I is actual structure without simplification in the crystal. In model II and III two (**a** and **b**) and four (**a**, **b**, **c** and **d**) methyl groups, which are close to one side and both sides of NO groups, are replaced by hydrogen atoms respectively in order to elucidate effects of β-hydrogen atoms and/or methyl groups etc. Here, C-H bond lengths in the models II and III were recalculated by the PM3 optimization method in the MOPAC program package under the condition that all another atoms are fixed. The last model IV implies only direct through-space interaction, though through-bond interactions with carbon atoms are expected in the other models. It is worth paying attention that difference between indirect coupling through bond and direct one through space comes into the spotlight, when we go through the process of these calculations.

The obtained J_{ab} values are summarized in **Table 6.1**. Here, INDO, *ab initio* UHF, CASSCF and DFT calculations are carried out and 4-31G basis set is employed for the purpose. The DFT techniques depend on the spin-unrestricted Kohn-Sham (UKS) equation with suitable exchange functionals and correlation functionals. In this investigation UBLYP and UB3LYP methods were employed in order to compare behavior of DFT methods. Though the other DFT methods are also feasible with the GAUSSIAN94 program package, our previous papers reported that the method combined Becke-88 for exchange functional and LYP for correlation functional could give the most accurate values. UNO CASCI{2,2} and UNO CASSCF{2,2} methods are also performed to evaluate only SOMO-SOMO direct interaction. In addition, for the model IV, UMP2 and UMP4 methods, which are Møller-Plesset perturbation theory, and UCCSD(T) method were applied, whereas these methods were not feasible for model I, II and III because of the large size of models.

First, let us analyze the evaluated data for model I. All the calculated J_{ab} values for model I are positive, indicating all methods support ferromagnetic interaction. Magnitude of the J_{ab} values are near to the experimental results, that is, Curie-Weiss temperature (θ = 10 K $\approx$ 7 cm^{-1}). UHF method gives about eight times as large a value as INDO method. Judging from our previous papers, UHF method tends to give too large values because of overestimation of the spin polarization (SP) effect, although values with INDO method are usually slightly small. This tendency also can be realized and a intermediate values between those derived by UHF and INDO methods may be often suitable. In addition, DFT methods, especially UB3LYP method, give similar J_{ab} values to the UHF method and

the balance of both reliability of result and CPU time is very good. The J_{ab} values derived with UNO CASCI{2,2} and UNO CASSCF{2,2} methods are positive, about 4 cm^{-1}. This positive values show that SOMO-SOMO direct interaction is essential. Judging from the positive values with UNO CASCI{2,2} method, interaction between two SOMOs delocalizing on both NOs seems to contribute to ferromagnetic interaction.

Figure 6.3A illustrates shapes of SOMOs and occupation numbers given with natural orbital (NO) analyses. Here, for model I each SOMO corresponds to 61th and 62th MOs. In this figure each orbital can be classified into σ-, π-, π*-, π'- and σ'- type. The marks ' (prime) indicate higher order orbitals because of double zeta orbitals of the employed 4-31G basis set. Occupation numbers on the SOMOs are equal to 1.00 and imply single occupation of electrons. Two localized MOs of each radical site are oriented to each other perpendicularly and have *C2* symmetric operation. From this figure SOMOs are delocalized over the connecting α- and β- carbons as can be recognized from the remaining small lobes. The orbitals spread over α- and β- C atoms enable two radical sites to couple each other. Magnetic interaction given by UNO CASCI{2,2} method turns out to be positive.

Pairs of 60th and 63th MOs, 59th and 64th MOs, etc. indicate pairs of natural orbitals. These MOs as well as SOMOs may play an important role of magnetic interactions and higher order effects beyond only direct couplings between SOMOs are also expected. Thus, these *ab initio* calculations support existence of this higher contribution. For this purpose, spin density analysis would help us to investigate magnetic coupling between each NO site. In **Fig. 6.3**B results by UHF methods for model I are showed. This figure can point out remarkable contribution of inserted atoms, that is, existence of α- and β- C atoms enable two radical sites at both ends to interact each other.

Next, studies for models II and III need to be made. It is noteworthy that similar J_{ab} values are obtained for models I, II and III by each method, though the values for model I are slightly larger than those for the II and III. Same tendency is found in the result by UNO CASCI{2,2} and CASSCF{2,2} methods. These results mean that methyl groups (**a**, **b**, **c** and **d**) of a TMAO molecule have negligible effect for ferromagnetic intramolecular interaction and variation of shape of SOMOs and spin densities are small.

Finally, we discuss model IV since it has no through-bond interaction. It is notice that the absolute values of J_{ab} obtained by INDO and UHF methods are about ten times as small as those for model I. UNO CASCI{2,2} and UNO CASSCF{2,2} methods give also small positive values. These results say that direct interaction through space between both H_2NOs is very small and through-bond path in model I is essential.

6.2.3 Inter-molecular ferromagnetic interaction

In the above section only intra-molecular magnetic interaction which appears in each TMAO molecule has been taken into account and we can explain theoretically their magnetic behaviors. Here, let us develop the investigation of magnetic interactions to inter-molecular magnetic coupling in this section. In α-form crystal, six TMAO molecules are packed in monoclinic unit cells and the four are shared by the next cells. **Figure 6.1**B illustrates straightforwardly how each molecule occupies its spatial position, where one ball indicates one TMAO molecule and shaded and white balls are individually packed into same unit cells. This figure is equivalent to **Fig. 6.1**A and the notations **A**, **B**, **C**, **D**, **E** and **F** are common to both figures. Let us consider molecule **A** as a reference. Orientation and relation between two molecules can be studied efficiently with crystal symmetry. In **Table 6.2** the J_{ab} values calculated by INDO and UHF/4-31G method for each molecular pair are summarized. From this table, it is found that only pairs **A-B** (=**A-H**) and **A-C** have small ferromagnetic interaction, although J_{ab} values derived for the other pairs are almost zero and it is suitable to neglect contribution of them. In this regard, it is noteworthy to discuss implications of the calculated results in relation to the spatial ferromagnetism observed for crystals. The suitable orientation and shortening of intermolecular distances may turn out to be essential factors for the non-zero J_{ab} values, as compared with the other no-coupled pairs such as pairs **A-D** and so on. Spatial relations of these molecules are extracted and illustrated in **Fig. 6.4**A. Crystal symmetry reproduces equivalent pairs such as pair **A-H** to pair **A-B** etc. and zigzag chains propagate ferromagnetic coupling periodically. The other pair **A-C** makes two chains combine each other. Thus, these networks in the α-form TMAO crystal are necessary to accomplish spatial organic ferromagnetic interactions of two dimensions at least. Moreover, though pair **A-E** has a very small positive J_{ab} value, i.e. 0.001 cm^{-1}, three dimensional networks may be formed.

Next, we must look more carefully into studying for pair **A-B** which have positive J_{ab} value in order to elucidate the origin of the inter-molecular ferromagnetism. **Figure 6.4**B illustrated models V and VI, though model V is equivalent to pair **A-B**. In this pair two NO radical sites stack in anti-parallel manner and three interaction paths, i.e., NO ··· NO, α-H ··· O and β-H ··· O are expected. Model VI was employed in order to eliminate the β-H interaction. To this end, the -CH_2 groups were replaced with -NH groups as isoelectronic structures. The obtained data are summarized in **Table 6.2** additionally. The minus and smaller J_{ab} values for model VI may indicate the β-hydrogen path (NO ↑ – C ↓ – C ↑ – H ↓ ··· NO ↑) is essential for the intermolecular ferromagenetic interaction.

Table 6.1 J_{ab} values for model I, II, III and IV.

Methods	J_{ab} /cm^{-1}			
	I	II	III	IV
INDO	2.162	1.783	1.527	-0.126
UHF [a)]	16.141	14.594	13.437	1.966
UMP2 [a)]				3.857
UMP4 [a)]				3.689
UCCSD(T) [a)]				3.340
UNO CASCI{2,2} [a)]	4.502	4.257	4.076	0.327
UNO CASSCF{2,2} [a)]	4.244	3.991	3.813	0.410
UBLYP [a)]	18.344	17.819	17.809	-0.059
UB3LYP [a)]	16.470	15.700	15.274	2.145

a) 4-31G basis set was used.

Table 6.2 J_{ab} values for various molecular pairs in TMAO crystal. Models V and VI are illustrated in **Fig. 6.4**B.

	J_{ab} /cm^{-1}	
	INDO	UHF/4-31G
A-B (V) (=**A-H**)	0.008	0.700
A-C	0.013	0.129
A-D	0.000	0.000
A-E	0.000	0.001
A-F (=**B-C**)	0.000	0.000
A-G	0.000	0.000
VI	-0.008	0.253

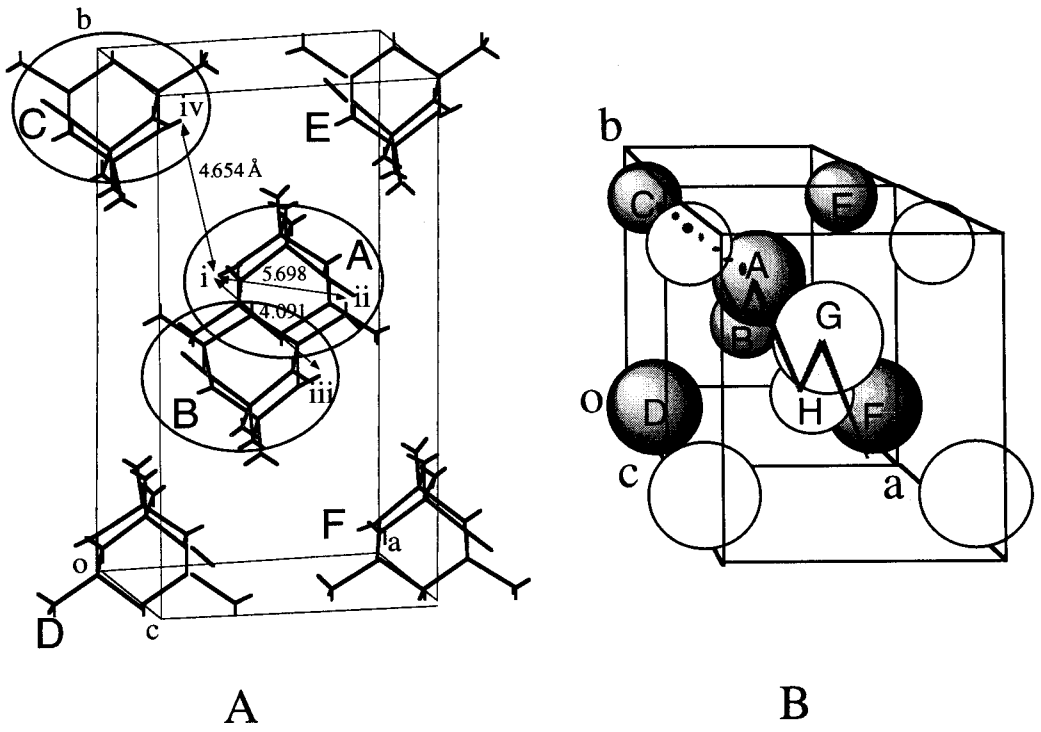

Figure 6.1 Crystal structure of TMAO

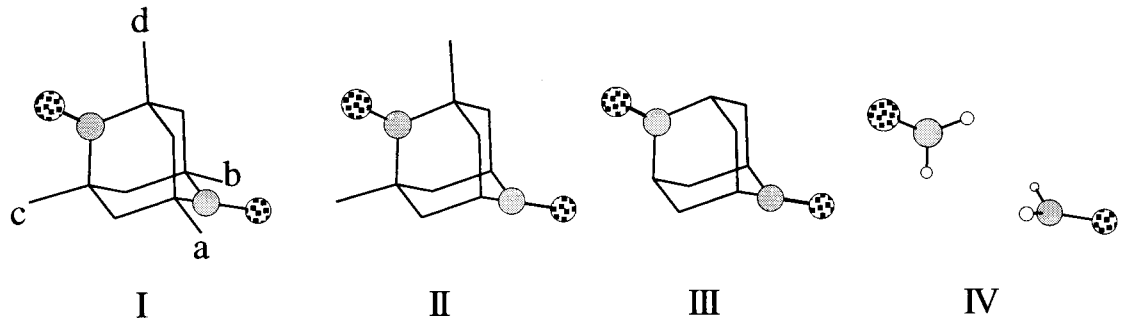

Figure 6.2 Models for studying intra-molecular magnetic interactions

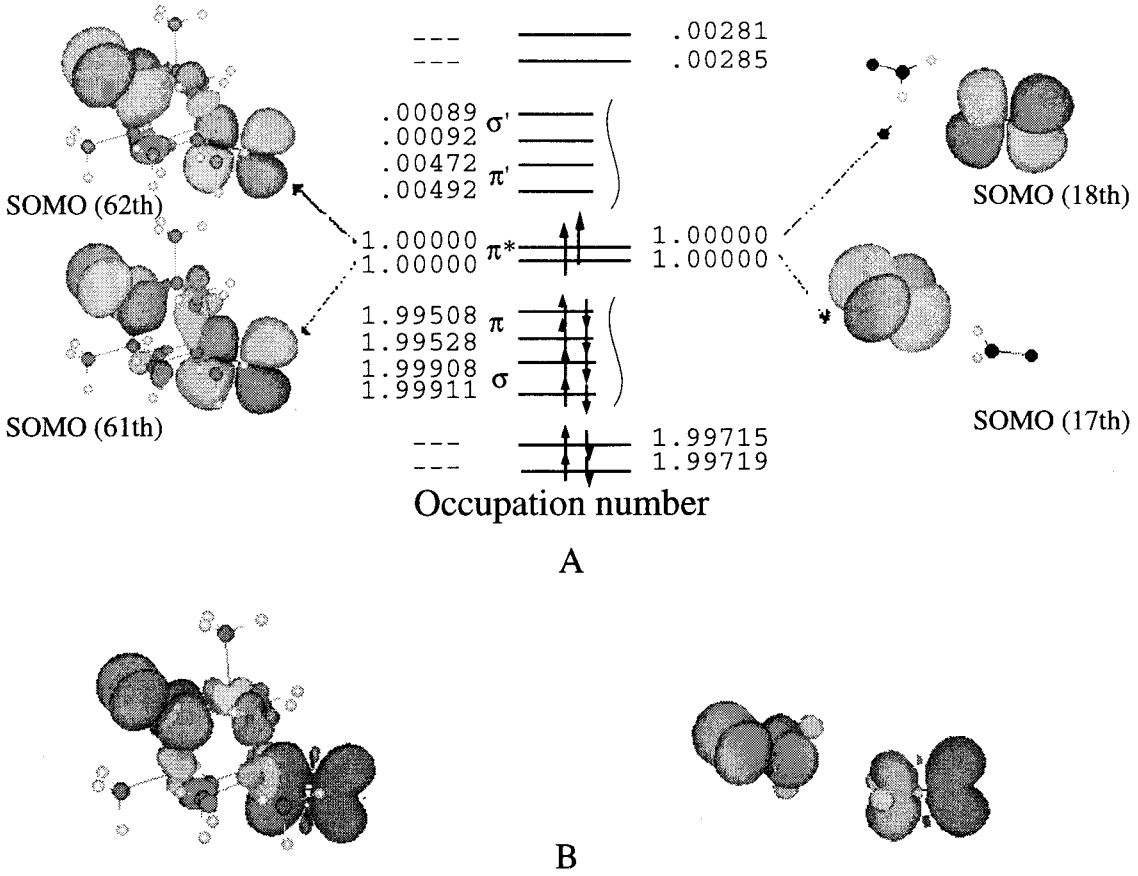

Figure 6.3 (A) Occupation numbers and shape of SOMOs for eath models (B) Graphical representation of spin densities by UHF/4-31G method.

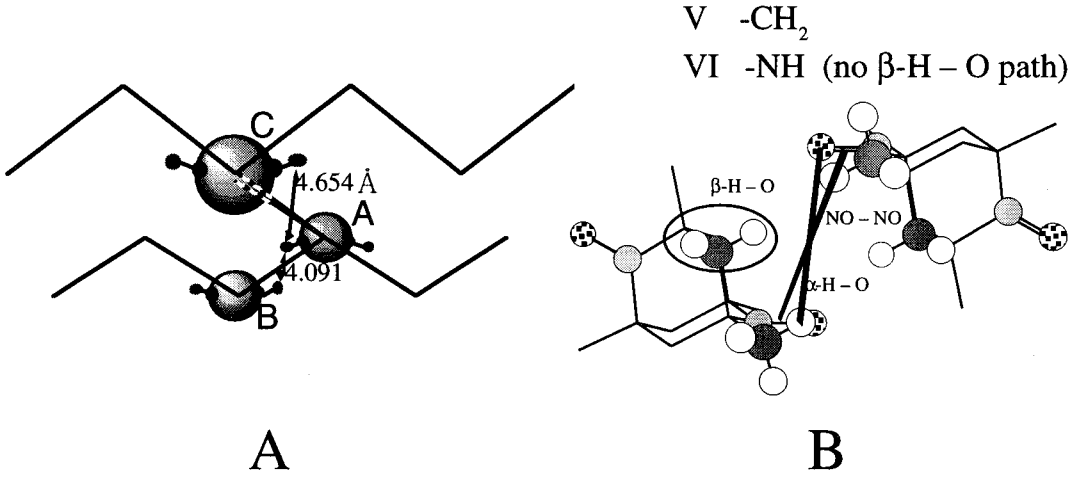

Figure 6.4 (A) Zigzag magnetic interactions (B) Models V (= A-B) and VI.

Section 6.3

Conclusion

Semiempirical INDO, *ab initio* UHF, CASSCF and DFT calculations were carried out for evaluating the effective exchange integrals J_{ab} for both intra- and inter- molecular magnetic interactions in α-form TMAO crystal. Through-bond coupling in one molecule corresponds to the former and relatively large ferromagnetic interaction is realized. On the other hand, through-space couplings between two molecules correspond to the latter and only small ferromagnetic interactions for pairs **A-B** and **A-C** and no interaction for the others are made clear. These cooperation might run in ferromagnetic intermolecular networks of three dimensions, at least two dimensions without pair **A-E**. These agree with the experimental measurements by Rassat et al. Our theoretical calculations suggest that the bulk magnetism of this crystal is delicate in nature because the magnitude of the intermolecular exchange integrals is not large. It is important to analyze and control magnetic coupling for all essential molecular pairs to design macroscopic organic ferromagnetic crystalline species. With regard to this, existence of two radical groups in one molecule is essential. Intra-molecular ferromagnetic interaction accelerates the radical spins induced on one side to be transmitted to the other side. The TMAO crystal has the advantage of bulk ferromagnetism owing to its symmetry, though dimerization of two molecules often occurred in another familiar organic ferromagnetic species.

In addition, in relation to the series of TEMPO compounds (the previous section 5.3), the orbital and/or spin polarization on the β-position hydrogen (β-H) of $-CH_3$ or $-CH_2$ groups is found to play an important role recently[19]. Here, this β-H effect was also studied by calculating J_{ab} values.

Chapter 7.

Ferromagnetic Interaction in β-*p*-NPNN Crystal under Pressure

Section 7.1

Introduction

Active control of electronic, magnetic and optical properties by external conditions such as the high pressure is challenges in molecule-based materials[59]. Theoretical computations have indeed revealed such possibilities. For example, Yamaguchi, Okumura and co-workers showed[51,60] that the sign and magnitude of effective exchange integrals (J_{ab}) were highly variable by rotation of nitroxide group in the cluster of para-nitropheyl nitronylnitroxide (*p*-NPNN) or with change of the intermolecular distance (R) between *m*-N-methylpridinium nitronyl nitroxide (*m*-MPYNN$^+$). These results suggest that the molecular magnetism sensitive to the structural changes. In fact, the sharp decrease of the magnitude of J_{ab} by the elongation of the intermolecular distance was observed for *m*-MPYNN$^+$ crystal[10]. In addition, in the previous section 5.3, theoretical studies have also elucidated important roles of conformations of methyl group and hydrogen bonds to determine the sign and magnitude of effective exchange integrals (J_{ab}) in TEMPO derivative crystals.

Very recently[61,62], the pressure effect on the intermolecular effective exchange interactions in the β-phase of *p*-NPNN was investigated by the simultaneous measurements of magnetic susceptibility and heat capacity under the high pressure. From these experiments, it was found that the effective exchange integrals were dramatically changed from positive (ferromagnetic) to negative (antiferromagnetic) depending on the pressure conditions. Here, this pressure effect has not been theoretically explored yet. Secondly, in the chapter 7.2, the author wishes to perform the MO calculations of the clusters of *p*-NPNN for theoretical understanding of the pressure-induced ferro-to-antiferromagnetic transition.

Section 7.2

Pressure effects for magnetic interaction

7.2.1 Structures

Figure 7.1 illustrates the crystal structure of the β-phase of *p*-NPNN with the Fdd2 space symmetry with a = 12.36, b = 19.36 and c = 10.97 Å. From **Fig. 7.1**, twelve nearest-neighbour *p*-NPNN molecules exist around the central *p*-NPNN. They are classified into three groups, which are denoted by the white, shaded and black circles. The effective exchange integrals between the central *p*-NPNN and the nearest neighbours in each group are equivalent, and therefore one of them is explicitly defined as J_{1n} (n = 2–4) without loss of generality. The corresponding J_{ab} values are also defined by J_{12}, J_{13} and J_{14} as shown in **Fig. 7.2**(a).

7.2.2 The previous works

Previously, the effective exchange integrals for the clusters of *p*-NPNN at the normal pressure were calculated with the INDO UHF method by Yamaguchi, Okumura and co-workers. The low-spin (LS) and high-spin (HS) solutions with semiempirical INDO UHF method for the clusters with the experimental structures in the β-phase of *p*-NPNN were constructed by taking the fragment (monomer) orbitals as the initial guess of the SCF calculations. Each value for the dimer were calculated and reported as $J_{12} = 0.167\text{cm}^{-1}$, $J_{13} = 0.078\text{cm}^{-1}$ and $J_{14} = -0.014\text{cm}^{-1}$.

The semiempirical computations indicated three-dimensional ferromagnetic exchange interactions, which were crucial for the occurrence of the long-range magnetic order in the Heisenberg model. This in turn indicated that the SP mechanism was operative for occurrence of the organic ferromagnetism. It is reasonable that the organic ferromagnetism could be expected in the low-temperature region for crystals. The SP rule proposed

previously is applicable to ferromagnetic interactions in clusters of the crystalline organic ferromagnet composed by *p*-NPNN.

7.2.3 Uniform compression model

Since the X-ray structure of the β-phase under the high-pressure at low temperature is not known, we here consider plausible models for structure changes which would be essential for qualitative understanding of the pressure effect. Takeda and co-laboratories reported relations between induced pressures (kPa) and cell parameters (a, b, c). All the cartesian coordinates (i.e., both of the molecular geometries and intermolecular distances) were first shortened assuming the uniform compression of lattice constants under the high pressure. **Figure 7.4** illustrates variations of the calculated J_{ab} values with the pressure. The calculated results were not consistent with the experimental tendency, because the sign and magnitude of the J_{ab} values varied independently under condition of the compression. Therefore, it was difficult to explain the pressure-induced ferro-to-antiferromagnetic transition by the simplest model.

Next, we examined a lattice compression model that lattice constants were varied so as to account for the decrease of intermolecular distances for the model clusters, but the molecular geometry itself was not changed. The calculation results are shown in **Fig. 7.5**. While the absolute values of three types of J_{ab} values are increasing with increase of induced pressure, the signs of J_{ab} values are not changed in contradiction to the experiments. Thus the situation is quite different from the usual cases in inorganic magnetic solids. This in turn suggests that the changes of stacking modes and/or the rotations of substituents must be considered for explanation of the pressure-induced change of the magnetism.

7.2.4 Sliding deformations

Several sliding models of *p*-NPNN along the several lines were examined to elucidate variations of three J_{ab} values shown in **Figs. 7.2**-(a) and (b). **Table 7.1** summarizes the calculated results. The magnitude of the J_{12} value was variable with the sliding along the x- or z-axis, but its sign was not changed by this type of deformations. The ferromagnetic spin alignment within the ac plane remains after the sliding deformation of *p*-NPNN along the x- or z-axis.

The J_{13} value is responsible for the effective exchange interaction between the ac-planes. As a model for the pressure effects for the interplane interaction, *p*-NPNN (3) in **Fig. 7.2** was shifted to the central *p*-NPNN (1) on the xy-plane (i.e., the interplane distance between the ac planes was retained to be constant). The intermolecular distance (R) was

expressed by the interatomic distance between the central carbon atoms of the nitronyl nitroxide groups, and the negative ΔR means the decrease of the intermolecular distance (see **Table 7.1**). From **Table 7.1**, the sign of J_{13} remained unchanged since this deformation did not affect the contacting points interactions. On the other hand, the sliding of *p*-NPNN along the z-axis altered the sign of J_{13}. Since the key contacting sites are the O-C_1 and O-C_2 atomic pairs in the β-phase, the sign of J_{13} is determined by the subtle balance of these two terms: the ferromagnetic O-C_2 interaction overweighs the antiferromagnetic O-C_1 interaction in the normal condition. The latter became predominant if R was elongated, namely in the case of ΔR= 0.2 ~ 1.0 Å as shown in **Table 7.1**.

The sign and magnitude of J_{14} were almost constant by the sliding deformations along the 1-4 line on the xy-plane and z-axis as shown in **Table 7.1**. The J_{14} term is not essential for variations of the magnetism because its magnitude is quite small.

7.2.5 Rotational deformations

The rotations of substituents provide another possibilities for modeling conformational changes under the high pressure conditions. We here examined variations of the interplane angle between nitronyl nitroxide and nitroxide groups. The side view of the rotational process was illustrated in **Fig. 7.3**. The deformations were restricted to retain the crystal symmetry by assuming the concerted rotations of both components. **Figure 7.6** shows variations of J_{12} with the rotational angle (θ). The J_{12} value certainly became negative by the rotation of nitroxide group at the ranges of the rotational angle from –10° to –20° and from 30° to 75°; note that the region θ < –20 is out of consideration because of strong steric repulsion. Thus the ferromagnetic interaction within the ac plane can be destroyed if the rotation of nitroxide group is variations of J_{12} with the rotational angle. **Figure 7.7** shows variations of J_{13} with the rotational angle. The calculated J_{13} values, which exhibited antiferromagnetic behavior at the ranges of the rotational angle from 5° to 40° and from –50° to –90°. Therefore, the ferro- to antiferromagnetic transition for the interplane interaction was caused by the rotation which would be reasonable from the view point of the lattice compression by the high pressure. The experimental examinations are desirable in future.

Table 7.1 Effective exchange integral J_{ab} (cm^{-1}) of the shifted stacking models of β-phase *p*-NPNN by UHF INDO method.

	J_{12}		J_{13}		J_{14}	
ΔR /A	x-axis	z-axis	xy-plane	z-axis	xy-plane	z-axis
-1.0	27.739	0.205	-0.276	0.271	-0.288	0.000
-0.8	10.430	0.205	0.311	0.316	-0.190	-0.001
-0.6	3.773	0.202	0.407	0.325	-0.111	-0.004
-0.4	1.338	0.196	0.295	0.286	-0.059	-0.008
-0.2	0.472	0.185	0.170	0.202	-0.030	-0.012
0.0	0.167	0.167	0.086	0.086	-0.014	-0.014
	(0.439)[a)]		(0.595)[a)]			
+0.2	0.060	0.142	0.040	-0.042	-0.063	-0.015
+1.0	0.001	0.028	0.001	-0.254	-0.002	-0.007

a)UB3LYP/4-31G

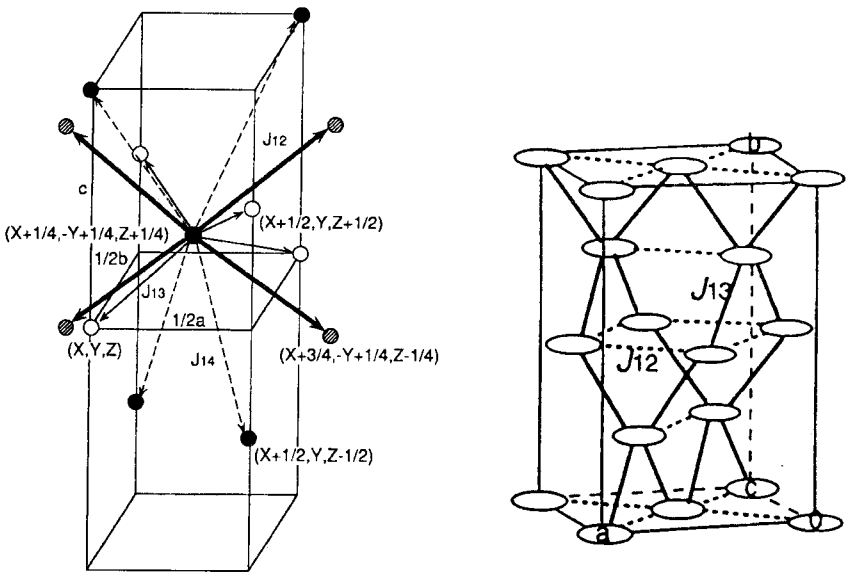

Figure 7.1 The crystal structure of the β-phase of *p*-NPNN with the *Fdd2* space symmetry. (a) The four equivalent *p*-NPNN are denoted by the white, shaded and black circles. J_{1n} (n = 2–4) denotes the effective exchange interaction. (b) Schematic drawing of the crystal structure of β-*p*-NPNN. Each ellipse represents the radical molecule.

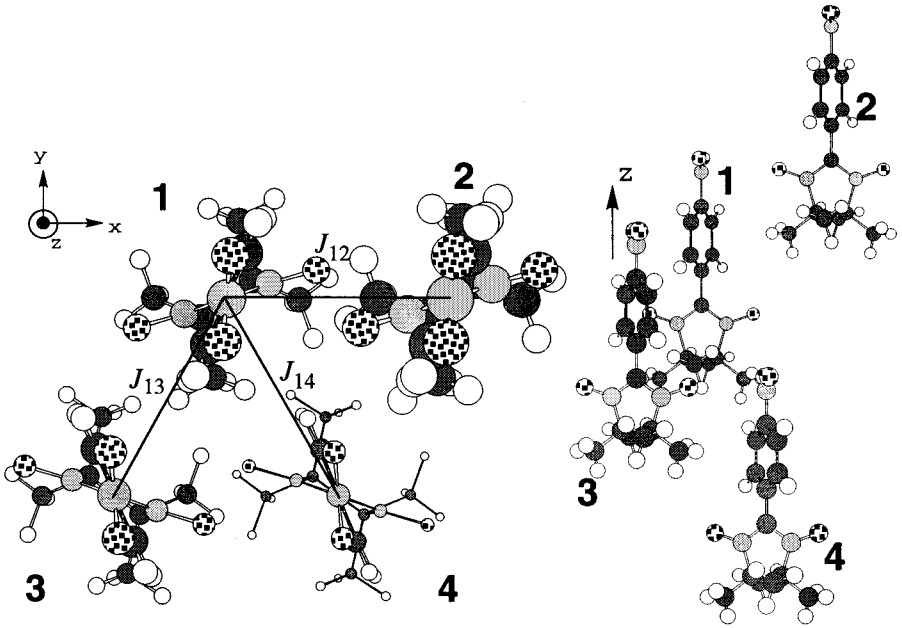

(a) (b)

Figure 7.2 (a) The crystal structure of the β-phase of *p*-NPNN with the *Fdd2* space symmetry where 1-4 denote the nearest neighbor *p*-NPNN molecules. J_{1n} (n =2-4) denote the effective exchange integrals between them. (b) Sliding modes of *p*-NPNN along the lattice axes.

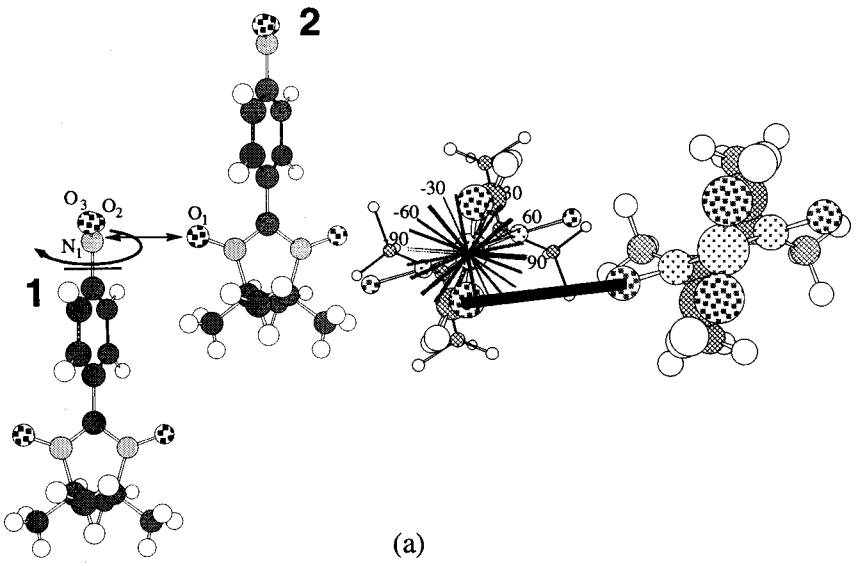

(a)

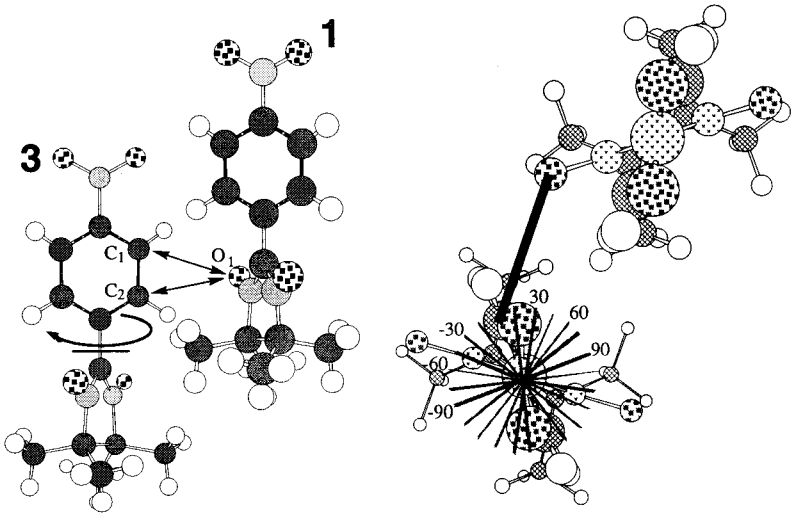

(b)

Figure 7.3 (a) Rotational deformation of nitroxide group of *p*-NPNN which is responsible for variation of J_{12}. (b) Rotational deformation of nitrophenyl group of *p*-NPNN which is responsible for variation of J_{13}.

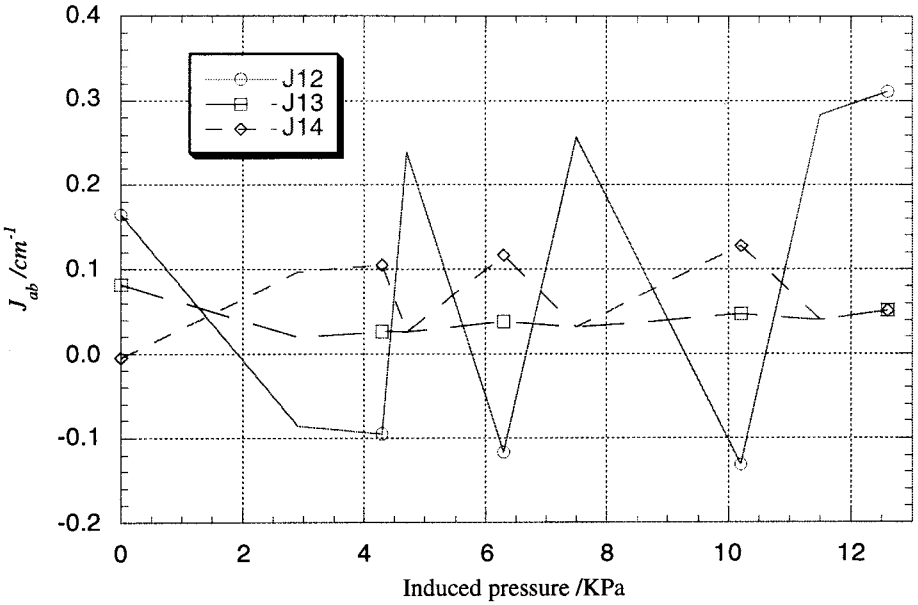

Figure 7.4 The schematic illustrations of variations of the effective exchange integrals between *p*-NPNN by the uniform compression model, which is one of the possibilities for the pressure effect.

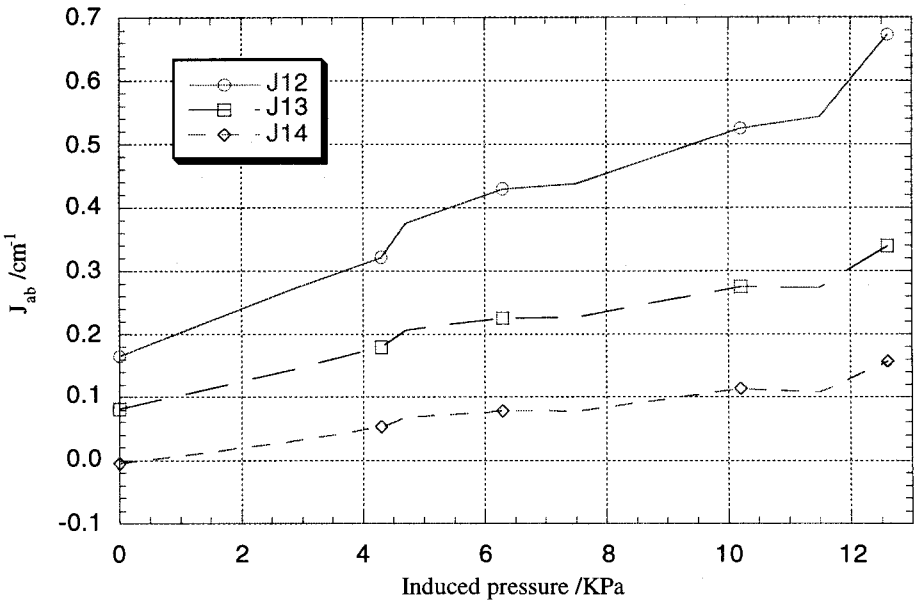

Figure 7.5 The schematic illustrations of variations of the effective exchange integrals between *p*-NPNN by the lattice compression model, which is one of the possibilities for the pressure effect.

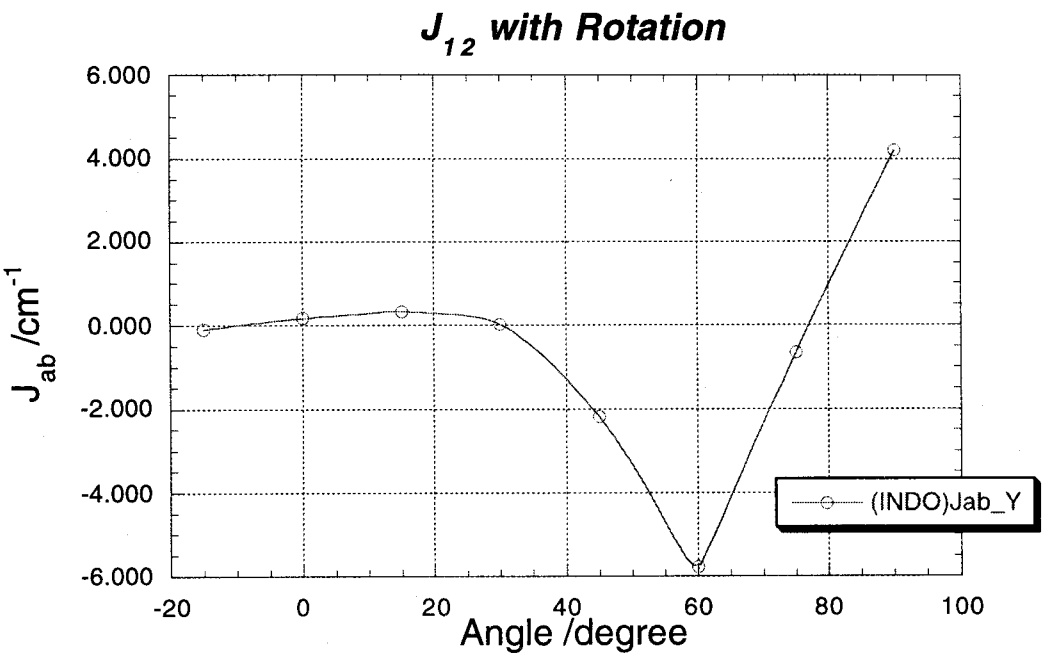

Figure 7.6 Variations of the J_{12} values with the rotational process of nitroxide group of *p*-NPNN molecules; two nitroxide groups were rotated concertedly in **Fig. 7.3**(a) to retain the *Fdd2* space symmetry.

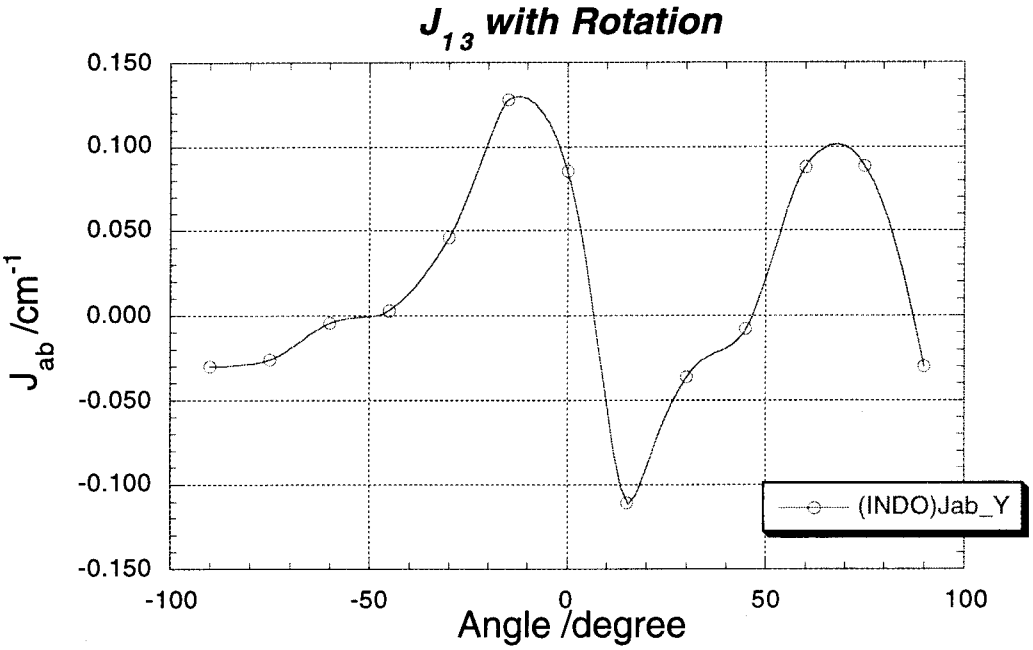

Figure 7.7 Variations of the J_{13} values with the rotational process of nitrophenyl group of *p*-NPNN molecules; two nitrophenyl groups were rotated concertedly in **Fig. 7.3**(b) to retain the *Fdd2* space symmetry.

Section 7.3

Conclusion

In summary, we found three characteristic modes to understand the observed pressure-induced ferromagnetic to antiferromagnetic transition in the β-phase; (1) the sliding of *p*-NPNN along the z-axis to alter the sign of the interplane exchange integral (J_{13}), (2) the rotation of nitrophenyl group to provide the negative J_{13} and (3) the rotation of nitro group to inverse the sign of the intraplane exchange integral (J_{12}). However, the first makes the lattice constant larger, so it is hardly acceptable unless other conformational changes are coupled together. The second induces the antiferromagnetic interaction between the ac-planes, while the third destroys the two-dimensional (2D) ferromagnetic interaction in the ac-plane. These are the simplest model for possible theoretical explanation of the pressure effect in the β-phase of *p*-NPNN. Although the real conformational changes in the β-phase under the high pressure are probably more complex, the present model calculations clearly demonstrated that the signs of effective exchange integrals are variable by conformational changes of component radicals in organic ferromagnets.

Since rotations of substituents group are feasible by the high pressure, the present calculations suggest that the pressure-induced ferro to antiferro-magnetic (vice versa) transitions would be equally anticipated for many other organic ferromagnets composed of alkylnitroxides and other organic radicals.

Chapter 8.

Concluding Remarks in Part I

Section 8.1

Organic Ferromagnetic Insulators

The research of genuine organic ferromagnets has its long history, but discovery of ferromagnetic crystals was achieved very recently. And, following this, various organic ferromagnets have been reported because of this breakthrough. In addition, in the present many experimental studies by many scientists reveal novel and peculiar organic crystals. However, in concerning to theoretical approach to these "molecular magnetism" many essential and interesting problems exist as open questions. The author has been challenging this problem with quantum chemistry in this study. In this chapter the author will summarize the results derived in each chapter briefly and make future discussion in order to develop this study to next stages.

First, about computational schemes, the formalism of effective exchange integrals (J_{ab}) were derived in order to carry out quantitative evaluation (Section 1.5). The magnetic interaction between organic radicals can be characterized quantitatively by the effective exchange integral (J_{ab}). Recent development of *ab initio* MO and DFT methods expands the new science field: "computational chemistry" (Section 1.4) and the author employs these methods based on quantum mechanics. In Chapter 2 the verification of J_{ab} formalism are ensured with methylene and nitrogen radical clusters. Character and application limit of these computational methods are successfully made clear because these model molecules contain essential properties for magnetic interaction between radical fragments. Thus, it is found that theoretical treatment to elucidate the mechanism of the magnetic interaction are crucial in cooperation with experimental studies. The author established the fundamental theoretical way to attack organic magnetism.

About spin alignment rules the author has expanded investigation into several contributions to magnetic interaction, such as through-space, through-hydrogen bond. Twelve types of magnetic interaction are proposed, and the classification of ferro- and antiferro-

magnetic coupling between radical spins and induced spin (with spin polarization effect and/or spin delocalization effect) (Section 1.3). In addition, decomposition of effective exchange integral were carried out and selection rules could be extracted. Essential and simple spin alignment rules to ferromagnetic interactions in organic crystals are established (Chapter 3). The results derived new two principles, that is, "No-overlap and orientation principles" (Chapter 4) and "Hydrogen bridge effect" (Chapter 5) and these are applied to both model and real molecular systems in order to confirm these legitimacy. Theoretical calculation with model systems are useful for evaluating the classification principle of the mechanisms for ferromagnetic interactions.

In Chapter 4, the author first considers very simple examples of SOMO-SOMO interactions in hydrocarbon (Section 4.2) and nitroxide (Section 4.3) systems. The KE-term often can become almost zero even in close distance because of the zero SOMO-SOMO overlap, though orbital overlap between most of radical pairs remains. For example, the π^*-nature of SOMO may play an important role for ferromagnetic interactions since the orbital overlap disappeared even in these parallel stacking modes. Thus, orbital symmetry rules for kinetic exchange interactions are useful guides for molecular design of organic ferromagnets. As development of these rules to real systems the detailed studies for *p*-NNBA$^{\cdot}$ ferromagnetic crystals are one of suitable examples (Section 4.4). In these systems, it is found that a short intermolecular contact between the oxygen atom in the nitronyl nitroxide group and the alpha carbon atom in the nearest-neighbor NN group with T-shape conformation is essential. These crystals provided not only the first example of ferromagnetic dimers of radical anions but also the largest J_{ab} value ever reported for exchange couplings between PNNO derivatives. The author's approach with theoretical MO methods achieved successfully and pointed out possibility of higher ferromagnetic interaction.

In Chapter 5, it has been suggested that hydrogen-atom bridges are effective for weak intermolecular ferromagnetic exchange interactions between nitroxides. The author shows the possibilities of ferromagnetic interaction through bridge hydrogen atoms under adequate intermolecular stacking conditions and orientation (Section 5.2). Here, simple and essential models were employed for this purpose. Such weak interactions via hydrogen bridges attract current interest in relation to the ferromagnetic phase transitions in several real crystalline organic ferromagnets discovered recently. Thus, the author could apply these effects to real organic crystal, i.e. TEMPO derivatives (Section 5.3). Several theoretical calculations were carried out and reveal that the hydrogen bridging between methyl hydrogen atom and adjacent NO group is essential for the ferromagnetic interaction. Here, it is found that existence of methyl groups as well as hydrogen atoms cannot be bypassed for magnetic interaction. In addition the author guess a rotation of methy group can be vary the magnitude of effective interaction integrals.

Applications to real crystals are carried out in Chapters 6 and 7, though, of course, theoretical treatment which were discussed in above chapters have already applied to real molecular systems in Sections 4.4 and 5.3. Recent many experimental studies by many scientists reveal novel organic crystals. In addition, numerical analysis of ferromagnetic interaction in "real" crystalline organic ferromagnets become feasible because of recent remarkable progress of computer technology. The author thinks the analytical and numerical investigations in theoretical quantum studies may lead to experimental studies, and vice versa.

In Chapter 6, coupling of intra- and inter-molecular interactions were discussed theoretically. Here, TMAO crystal with remarkable high T_c temperature was employed for this purpose. This unique crystal has two NO radical groups at the opposite sides in one molecule and magnetic coupling between each site can be propagated through-bond. On the other hand, one NO radical site locates in close contact with one site on the next molecule and magnetic coupling can be propagated through-space. Theoretical calculation concluded that both interactions are ferromagnetic, and supported the experimental studies. Moreover, it suggest that the bulk magnetism of this crystal is delicate in nature because the magnitude of the intermolecular exchange integrals is not large.

In Chapter 7, β-*p*-NPNN crystal with ferro- to antiferro-transition under pressure were employed. Active control of magnetic properties by high pressure is very interesting and theoretical computations have indeed revealed such possibilities. The author assumed several structural deformation or rotation, that is, the sliding of *p*-NPNN along the z-axis, the rotation of nitrophenyl group and the rotation of nitro group. From the results derived J_{ab} values, the structural rotation is conceivable as the simplest model for possible theoretical explanation of the pressure effect, although the real conformational changes in the β-phase under the high pressure are probably more complex.

Section 8.2

Future Prospect:

Organic Ferromagnetic Conductors

In order to introduce one of the author's future studies, the following few pages will be used. Recent many experimental studies by many scientists reveal novel organic crystals. Sugimoto and co-workers reported that ferromagnetic behavior at room temperature was observed in the tetramethylammonium (NMe_4^+) and cesium (Cs^+) salts of tetracyanoquinodimethane (TCNQ) and its radical anion ($TCNQ^{-\bullet}$) in a molecular ratio of 1:2. The saturation magnetizations and coercive forces are 0.79 emu/mol and about 300 Oe for (NMe_4^+ • $TCNQ^{-\bullet}$)•1/2TCNQ (see **Fig. 8.1**), and 1.46 emu/mol and about 100 Oe for (Cs^+•$TCNQ^{-\bullet}$)•1/2TCNQ, respectively. In contrast, the 1:1 TCNQ/$TCNQ^{-\bullet}$ mixed tetraethylammonium (NEt_4^+) salt (NEt_4^+ • $TCNQ^{-\bullet}$) • TCNQ, exhibited no ferromagnetic behavior at room temperature nor at lower temperatures.

For (NMe_4^+ • $TCNQ^{-\bullet}$)•1/2TCNQ crystal, the crystal structure is depicted in **Fig. 8.2** and it is found that simplified packing view along c-axis indicates peculiar stacking. Each column composed of 1:2 TCNQ/$TCNQ^{-\bullet}$ molecules in ab-plane, and one NMe_4^+ column intervenes between neighboring TCNQ/$TCNQ^{-\bullet}$ columns. The molecules **A** and **B** form a tight dimer and the interplane distance is remarkably short (3.15 Å). The dimer makes contact with one molecule **S** by separation of the interplane distance of 3.22 Å.

Theoretical calculations were carried out by semiempirical INDO method and the derived results were summarized in **Table 8.1**, though the results evaluated by other method (*ab initio* MO and DFT) were omitted. From this table it is found that molecular pair **AB** has a large absolute minus value (about -650 cm^{-1}) which indicates creation of single pair coupling. Its energy gap is larger than excitation energy at room temperature and this singlet pair is very stable. Thus, most of radical spins may vanish. However, we must notice

that very small magnetic couplings occur in the other pairs, for example J_{ab}(AP-INDO) = 0.135 cm^{-1} in pair **AC**.

These result may imply appearance of very very weak ferromagnetism in a certain mechanism. Canting ferromagnetic mechanism may be possible, that is, the spins are not completely antiparallel but slightly canted by Dzialoshinsky-Moriya antisymmetric exchange interaction. For another point of view, fractured spins in half-filled electron structure may contribute to its peculiar behaviors. In this case, hole doping in *t-J* model is suitable model. On the other hand, impurity in these crystal may disturb antiferromagnetic interaction unfortunately. Studying mechanism for these crystal will be important to future organic magnetic crystals, though expected ferromagnetism is very small in any case.

Table 8.1 The J_{ab} values calculated by semiempirical INDO UHF method are summarized. Molecular pair **AB** has a large absolute minus value which indicates creation of single pair coupling.

Molecular Pair		J_{ab}**(INDO)**	J_{ab}**(AP-INDO)**
AB		–682.464	–651.511
AC		0.135	0.135
AD		0.047	0.049
BC		0.002	0.002
AE		0.002	0.002
AF		0.001	0.001
ASE	[↑ · ↓(↑)]	–0.678	–0.678
ASF	[↑ · ↓(↑)]	4.512	4.514
ASTE	[↑ · · ↓(↑)]	–5.722	–5.721
CE		0.001	0.001
CF		0.002	0.002
CSE	[↑ · ↓(↑)]	–1.102	–1.102
CSF	[↑ · ↓(↑)]	4.142	4.143

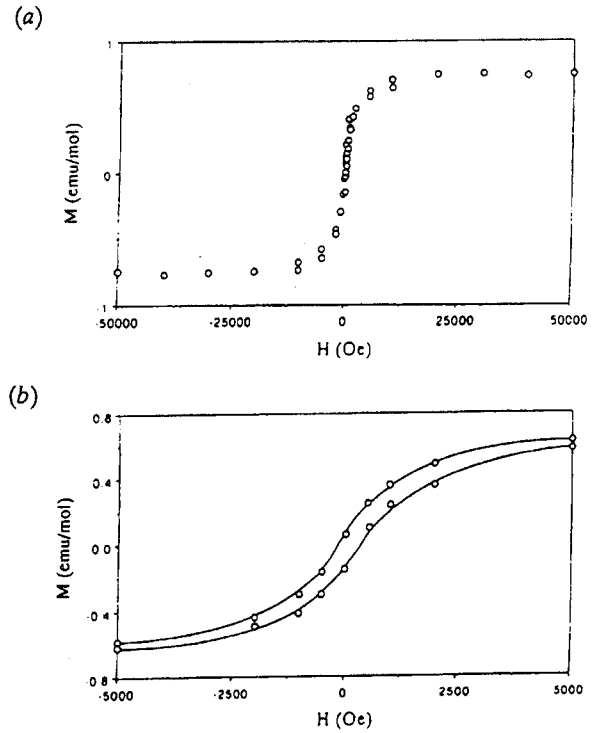

Figure 8.1 The magnetization curves of (NMe4+•TCNQ-•)•1/2TCNQ in the applied field range of (a) ±50 kOe and (b) ±5 kOe at room temperature. (Sugimoto and co-worker reported)

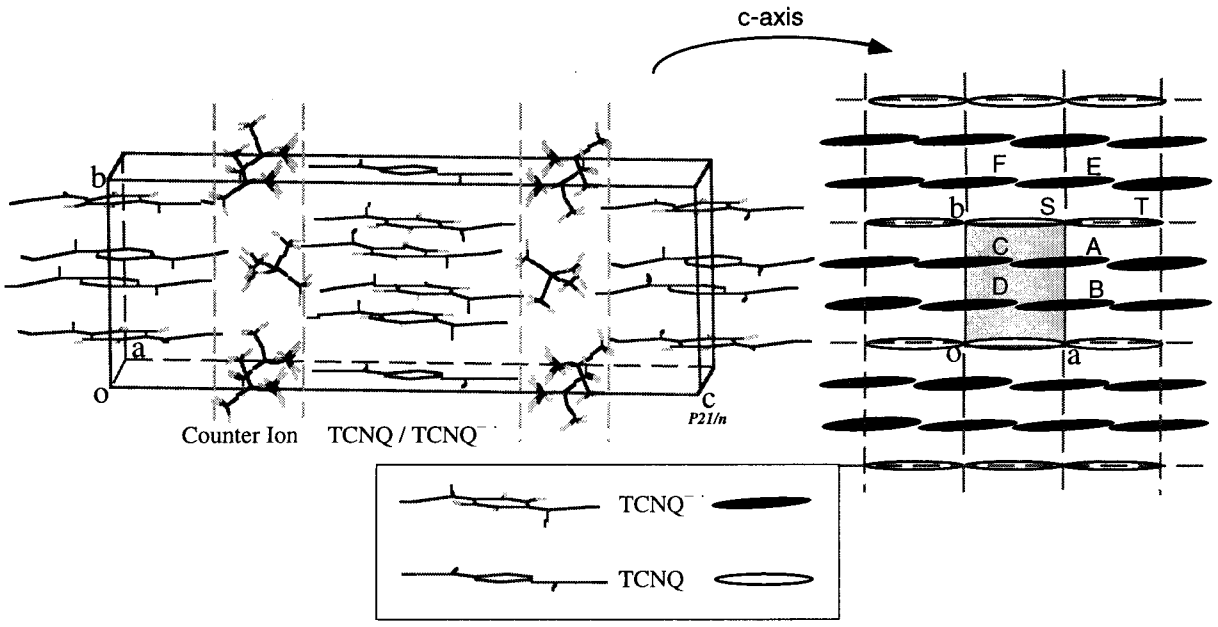

Figure 8.2 The crystal structure and its simplified packing along c-axis for (NMe_4^+ • $TCNQ^{-\bullet}$)•1/2TCNQ crystal are depicted. Each column composed of 1:2 TCNQ/$TCNQ^{-\bullet}$ molecules in ab-plane, and one NMe_4^+ column intervenes between neighboring TCNQ/$TCNQ^{-\bullet}$ columns.

Part II

Chapter 1.

Statistical Approach to Magnetic Interaction

Section 1.1

Introduction

In recent years there have been several attempts to study many spin phenomena, with success for simple systems. The path integral was introduced by Feynman[63,64,65]. The theory has been successfully applied to many problems[66,67,68,69,70] in quantum mechanics and has also applied to the many-electron systems in quantum chemistry[71,72,73]. In this path integral formulation of field theory fermions are represented by anti-commuting c-number fields[73]. As a result, it is not possible to make direct numerical evaluations of the path integrals. Suzuki[74] suggested that this fundamental problem might be solved by using a generalization[75] of the Trotter formula[76]. He showed that the partition function of a d-dimensional spin-1/2 model is obtained as the limit of a sequence of well-defined approximation. Each approximant can be interpreted as the partition function of a (d+1)-dimensional Ising-type lattice model with complicated 4-spin interactions. Formally this approach is closely related to the path integral formulation of quantum statistical mechanics[67,77]. Here, a statistical method such as the Monte Carlo (MC) method[78] has been attempted, because we cannot directly compute the integration by ordinary ways of the numerical integrations. The standard approach to the MC simulation of the field theory has been progressed through Feynman's path integral formulation. This means that one can be really studying finite temperature statistical mechanics.

Our group presented the path integral formulation based on a molecular orbital picture by means of the Thouless parametrization. It was applied to the theoretical studies of the magnetic properties, e.g., magnetization, and we have been progressing the numerical treatment of it. In our treatments the numerical partition function can be calculated directly and be applied for the calculations of the magnetization from the *ab initio* MO Hamiltonian. Numerical calculations were performed with the Monte Carlo (MC) method. This method can calculate exact magnetic properties including temperature effects as infinite MC steps.

Employed Hamiltonian contains both *ab initio* MO Hamiltonian and Zeeman Hamiltonian. Here, the g-factor fixed to 2.0 for simplicity, though it represents the isotropic effects in actual crystals, etc. That is, it is noteworthy that the calculations based on the molecular orbital picture can be performed in contrast to the Heisenberg spin picture.

It is difficult to carry out the calculations which involve many electron excitations because of need for very long running time. Therefore, we modified our program so as to deal with only important electrons, that is, limited excitation spaces of the electrons. This treatment is similar to the complete active space (CAS) in the *ab initio* MO calculation methods. The definition of Monte Carlo Active Space (MC-AS) between the radical pairs is represented as the abbreviated notation : (α-hole, α-particle, β-hole, β-particle space). For example, MC-AS : (1, 1, 1, 1) is suitable if we consider the only SOMO-SOMO interaction to study the dominant role to magnetic behaviors as a first approximation.

Here, this method is applied to simple systems (**Figs. 1.1**-A, B, C and D) of hydrogen(H), methyl(CH_3), titanium(Ti) and copper(Cu) radical pair systems as basic models for our future studies. In these systems the magnetic interaction between s-, p- and d-orbitals can be take into account. Especially, the author employed two systems as shown in **Figs. 1.1**-B and D and the studies of the hydrogen molecule (**Fig. 1.1**A) were already discussed by Nagao and co-workers. These results obtained by this method seems to clarified the scope and limitation. The dependence on the number of division with respect to the partition function is discussed. The characters and the physical properties under various situations as to temperatures and external magnetic fields are also examined.

In the following section 1.2, the author mentions theoretical backgrounds for our statistical approach to magnetic interaction with path integral methods. In the section 1.3 the author introduces the simple but essential models and attempts the detailed calculation with it. This treatment gives another point of view to our previous treatments of magnetic interaction.

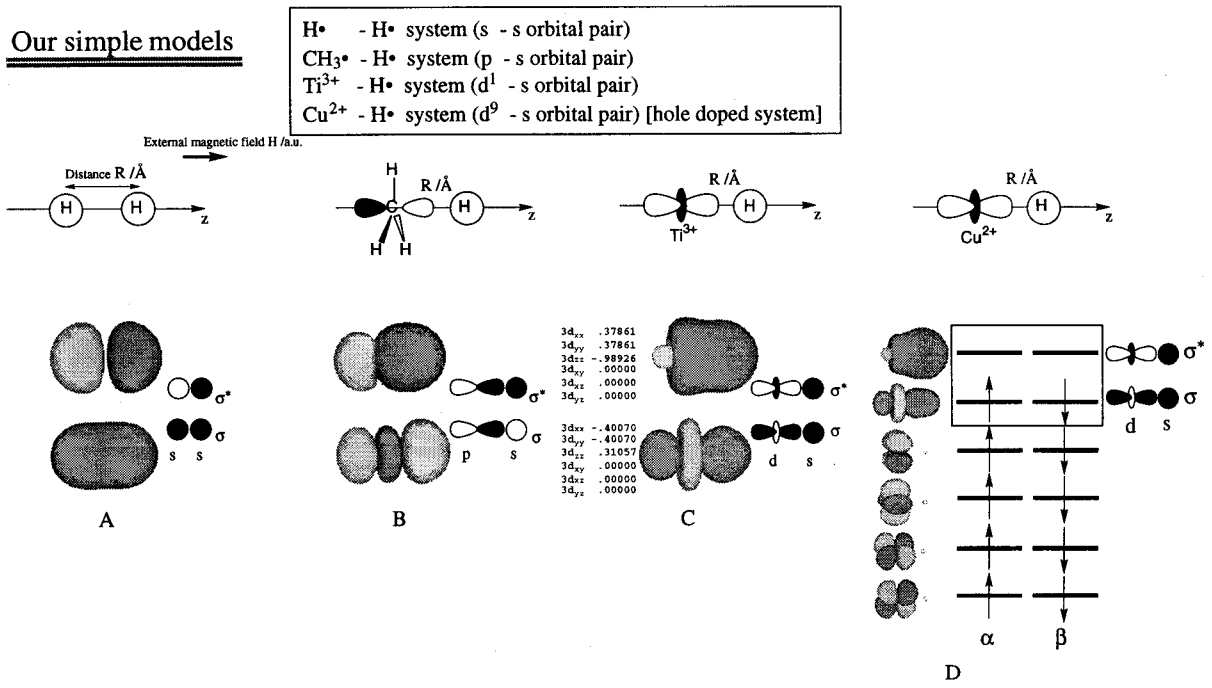

Figure 1.1 Simple models for evaluation for our statistical method.

Section 1.2

Theoretical background

1.2.1 Generalized coherent states

In order to formulate a path integral for the partition function to apply to molecular systems, first, we mention properties of the generalized coherent states of the Thouless parametrization including the spin space. Next, the path integral formulation is derived by using the generalized coherent states.

A Slater determinant composed of N orbitals (hole-orbitals) is written by

$$|\phi\rangle = \prod_{\sigma=\alpha,\beta} \prod_{h=1}^{N_\sigma} a_{h\sigma}^\dagger |0\rangle \tag{1.1}$$

where N_σ means the number of hole-orbitals with a spin σ, and N is $N_\alpha+N_\beta$. Slater determinant $|Z\rangle$ is written in terms of complex coefficients Z_{ph}^{σ} as

$$\begin{aligned} |Z\rangle &= \prod_{\sigma=\alpha,\beta} \det(1+Z^{\sigma\dagger}Z^{\sigma})^{-1/2} \\ &\quad \times \exp\left[\sum_{\sigma=\alpha,\beta} \sum_{p=1}^{M-N_\sigma} \sum_{h=1}^{N_\sigma} Z_{ph}^{\sigma} a_{p\sigma}^\dagger a_{h\sigma}\right] |\phi\rangle \end{aligned} \tag{1.2}$$

$$\begin{aligned} &= \prod_{\sigma=\alpha,\beta} \det(1+Z^{\sigma\dagger}Z^{\sigma})^{-1/2} \\ &\quad \times \prod_{\sigma=\alpha,\beta} \prod_{h=1}^{N_\sigma} \left(a_{h\sigma}^\dagger + \sum_{p=1}^{M-N_\sigma} Z_{ph}^{\sigma} a_{p\sigma}^\dagger\right) |0\rangle \end{aligned} \tag{1.3}$$

where M is the number of the base. The p labels denote the particle orbitals that orthogonal to the hole orbitals h, and Z^{σ} is a matrix whose elements are Z_{ph}^{σ}. The Slater determinants may be considered to be an expression of generalized coherent state. **Figure 1.2** depicts a

picture in relation to energy levels and hole- and particle-spaces by the Thouless parametrization. The following closure relation may be constructed :

$$1=c\int \prod_{\sigma=\alpha,\beta}\prod_{p=1}^{M-N_\sigma}\prod_{h=1}^{N_\sigma}\frac{dZ_{ph}^{\sigma}\,dZ_{ph}^{*\sigma}}{2\pi i} \times \prod_{\rho=\alpha,\beta}|\det(1+Z^{\rho\dagger}Z^{\rho})|^{-N_\rho}|Z\rangle\langle Z| \tag{1.4}$$

The constant c may be evaluated by taking the expectation value of Eq. (1.4) in the reference state $|\phi\rangle$

$$c^{-1}=\int \prod_{\sigma=\alpha,\beta}\prod_{p=1}^{M-N_\sigma}\prod_{h=1}^{N_\sigma}\frac{dZ_{ph}^{\sigma}\,dZ_{ph}^{*\sigma}}{2\pi i} \times \prod_{\rho=\alpha,\beta}|\det(1+Z^{\rho\dagger}Z^{\rho})|^{-N_\rho+1}. \tag{1.5}$$

1.2.2 Path integral for the partition function

partition function X is written by

$$\Xi=\mathrm{Tr}[e^{-\beta H}] \tag{1.6}$$

The symbol Tr implies a trace operation, and $\beta=(k_B T)^{-1}$ with the Boltzmann constant k_B and a temperature T(K). In order to construct a path integral representation of the partition function, we start by dividing $e^{-\beta H}$ into n factors

$$e^{-\beta H}=e^{-\tau H}e^{-\tau H}\cdots e^{-\tau H} \tag{1.7}$$

where $\tau=\beta/n$. The trace of Eq. (1.7) may be written as

$$\begin{aligned}\mathrm{Tr}[e^{-\beta H}]&=\int d\mu(Z)\langle Z|e^{-\beta H}|Z\rangle\\ &=\int d\mu(Z(0))d\mu(Z(1))\cdots d\mu(Z(n-1))\\ &\quad\times\langle Z(0)|e^{-\tau H}|Z(n-1)\rangle\langle Z(n-1)|\\ &\quad\times e^{-\tau H}|Z(n-2)\rangle\cdots\langle Z(1)|e^{-\tau H}|Z(0)\rangle,\end{aligned} \tag{1.8}$$

where

$$d\mu(Z(k))=c\prod_{\sigma=\alpha,\beta}\prod_{p=1}^{M-N_\sigma}\prod_{h=1}^{N_\sigma}\frac{dZ_{ph}^{\sigma}(k)\,dZ_{ph}^{*\sigma}(k)}{2\pi i}$$
$$\times\prod_{\rho=\alpha,\beta}|\det(1+Z^{\rho\dagger}(k)Z^{\rho}(k))|^{N_\rho}. \tag{1.9}$$

An expression is obtained by inserting a closure relation in Eq. (1.4) on the left of each factor $e^{-\tau H}$. When a large number n of factors is taken on the right-hand side of Eq. (1.7), τ is small and we approximate

$$\langle Z(k)|e^{-\tau H}|Z(k-1)\rangle$$
$$=\langle Z(k)|Z(k-1)\rangle e^{-\tau H(Z^*(k),Z(k-1))}+O(\tau^2) \tag{1.10}$$

where

$$H(Z^*(k),Z(k-1))=\langle Z(k)|H|Z(k-1)\rangle \tag{1.11}$$

Equation (1.8) then becomes

$$\mathrm{Tr}[e^{-\beta H}]=\int\prod_{k=1}^{n}d\mu(Z(k))\langle Z(k)|Z(k-1)\rangle$$
$$\times e^{-\tau\Sigma_{k=1}^{n}H(Z^*(k),Z(k-1))} \tag{1.12}$$

with

$$|Z(0)\rangle=|Z(n)\rangle \tag{1.13}$$

Equation (1.13) corresponds to the periodic boundary condition by the trace in the partition function. The expression in Eq. (1.12) may be viewed as a discretized path integral representation of the partition function, a path being defined as a set of states $|Z(k)\rangle$ and $\langle Z(k)|$ with k=1,2,...,n. To the extent that the terms of order τ^2 do not contribute, the expression in Eq. (1.12) is exact. However, as it stands, it is not very useful, except possibly for numerical computation. Indeed, from the expression in Eq. (1.13), we will derive a expression of the ensemble average of any operator to numerically calculate that of the total energy.

1.2.3 Further discussion

From essential discussions of the path integral in the previous subsection, we mention more analytical derivations. A more useful form is obtained by setting

$$|\delta Z(k)\rangle = |Z(k)\rangle - |Z(k-1)\rangle \tag{1.14}$$

so that Eq. (1.12) reads

$$\mathrm{Tr}[e^{-\beta H}] = \int \prod_{k=1}^{n} d\mu(Z(k)) \times e^{\sum_{k=1}^{n} \ln(1-\langle Z(k)|\delta Z(k)\rangle) - \tau H(Z^*(k),Z(k-1))} \tag{1.15}$$

Among the paths which contribute to Eq. (1.15), let us isolate the continuous paths, which are such that $|\delta Z(k)>\approx\tau$ for all values of k. For such paths we may write, in the limit of small t,

$$\langle Z(k)|Z(k-1)\rangle = 1 - \langle Z(k)|\delta Z(k)\rangle \approx e^{-\langle Z(k)|\delta Z(k)\rangle} + O(\tau^2) \tag{1.16}$$

and

$$\tau H(Z^*(k),Z(k-1)) \approx \tau H(Z^*(k),Z(k)) + O(\tau^2) \tag{1.17}$$

Neglecting the contribution of all the other paths, the partition function in Eq. (1.12) becomes

$$\mathrm{Tr}[e^{-\beta H}] = \lim_{n\to\infty} \int \prod_{k=1}^{n} d\mu(Z(k)) \times e^{-\tau \sum_{k=1}^{n} [\langle Z(k)|\delta Z(k)\rangle/\tau + H(Z^*(k),Z(k))]} \tag{1.18}$$

In the limit $\tau=(\beta/n) \to \infty$ the sum in the exponential may be replaced by an integral and the partition function in Eq. (1.18) becomes

$$\mathrm{Tr}[e^{-\beta H}] = \int D(Z^*,Z) e^{-S(Z^*,Z)} \tag{1.19}$$

where the effective action is a functional of the paths $|Z(\tau)>$ and $<Z(\tau)|$ defined by

$$S(Z^*,Z) = \int_0^\beta d\tau \langle Z(\tau)|(\partial_\tau + H)|Z(\tau)\rangle \tag{1.20}$$

and where the measure is

$$D(Z^*,Z) = \prod_\tau d\mu[Z(\tau)] \tag{1.21}$$

1.2.4 Matrix elements of Hamiltonian

In order to apply the path integral with the generalized coherent states to the quantum chemistry, we consider the *ab initio* Hamiltonian for molecular systems. In the Born-Oppenheimen (BO) approximation, the Hamiltonian is written by

$$\begin{aligned} H=&\sum_{\sigma=\alpha,\beta}\int d\mathbf{r}\,\Psi_\sigma(\mathbf{r})^\dagger\left[-\frac{1}{2m}\nabla^2\right]\Psi_\sigma(\mathbf{r}) \\ &+\frac{1}{2}\sum_{\sigma,\rho=\alpha,\beta}\int d\mathbf{r}\,d\mathbf{r}'\,\Psi_\sigma(\mathbf{r})^\dagger\Psi_\rho(\mathbf{r}')^\dagger\frac{1}{|\mathbf{r}-\mathbf{r}'|}\Psi_\rho(\mathbf{r}') \\ &\times\Psi_\sigma(\mathbf{r})+\sum_a^{N_a}\sum_{\sigma=\alpha,\beta}\int d\mathbf{r}\,\Psi_\sigma(\mathbf{r})^\dagger\left[-\frac{Z_a}{|\mathbf{r}-\mathbf{R}_a|}\right]\Psi_\sigma(\mathbf{r}), \end{aligned} \tag{1.22}$$

where the first term means the kinetic part, the second is the electronic interaction part and the third is the nuclear-electron interaction part. $\Psi_\sigma(\mathbf{r})^\dagger(\Psi_\sigma(\mathbf{r}))$ means the field operator which is the creation (annihilation) operator for an electron with a spin σ at three-dimensional spatial coordinate $\mathbf{r}$. $\mathbf{R}_a$ means a spatial coordinate of the a-th nucleus, and N_a is the number of the nucleus. Z_a indicates the positive electron charge of the a-th nucleus. The field operator is satisfied with the anticommutation relation

$$[\Psi(\mathbf{r})_\sigma,\Psi(\mathbf{r}')^\dagger_{\sigma'}]_+=\delta(\mathbf{r}-\mathbf{r}')\delta_{\sigma\sigma'} \tag{1.23}$$

$$\text{Others}=0 \tag{1.24}$$

Here, we introduce an orthogonal basis set $\varphi_i(\mathbf{r})$ such as a HF molecular orbitals (MO). Then, the field operators are expanded in terms of the basis set $\varphi_i(\mathbf{r})$ as

$$\Psi_\sigma(\mathbf{r})=\sum_{i=1}^{M}\varphi_i(\mathbf{r})a_{i\sigma} \tag{1.25}$$

where $a_{i\sigma}{}^\dagger(a_{i\sigma})$ is the creation (annihilation) operator for the i-th MO. These operators are also satisfied with the anticommutation relation. Then, the Hamiltonian in Eq. (1.22) becomes

$$\begin{aligned} H=&\sum_{\sigma=\alpha,\beta}\sum_{i,j=1}^{M}h_{ij}^\sigma a_{i\sigma}^\dagger a_{j\sigma} \\ &+\frac{1}{2}\sum_{\sigma,\rho=\alpha,\beta}\sum_{i,j,k,l=1}^{M}V_{ijkl}^{\sigma\rho\rho\sigma}a_{i\sigma}^\dagger a_{j\rho}^\dagger a_{k\rho}a_{l\sigma} \end{aligned} \tag{1.26}$$

where

$$h_{ij}^{\sigma}=\int d\mathbf{r}\ \varphi_i(\mathbf{r})^*\left[-\frac{1}{2m}\nabla^2-\sum_{a}^{N_a}\frac{Z_a}{|\mathbf{r}-\mathbf{R}_a|}\right]\varphi_i(\mathbf{r}) \tag{1.27}$$

and

$$V_{ijkl}^{\sigma\rho\rho\sigma}=\int d\mathbf{r}\,d\mathbf{r}'\ \varphi_i(\mathbf{r})^*\varphi_j(\mathbf{r}')^*\frac{1}{|\mathbf{r}-\mathbf{r}'|}\varphi_k(\mathbf{r}')\varphi_l(\mathbf{r}) \tag{1.28}$$

We derive the matrix elements $\langle Z(k)|H|Z(k\text{-}1)\rangle$ of the Hamiltonian in Eq. (1.26)

$$H(Z^*(k),Z(k-1))=H_0(Z^*(k),Z(k-1))+H_I(Z^*(k),Z(k-1)) \tag{1.29}$$

where

$$\begin{aligned}H_0(Z(k)^*,Z(k-1))=&\sum_{\sigma=\alpha,\beta}\sum_{i,j=1}^{M}\sum_{\xi=\alpha,\beta}\sum_{h,h'=1}^{N_\xi}h_{ij}^{\sigma}\times\left(\delta_{jh'}\delta_{\sigma\xi}+\sum_{p'}^{M-N_\xi}Z_{p'h'}^{\xi}(k-1)\delta_{jp'}\delta_{\sigma\xi}\right)\\&\times[1+Z^{\xi}(k)^{\dagger}Z^{\xi}(k-1)]^{-1}_{h'h}\left(\delta_{ih}\delta_{\sigma\xi}+\sum_{p=1}^{M-N_\xi}Z_{ph}^{\xi*}(k)\delta_{ip}\delta_{\sigma\xi}\right),\end{aligned} \tag{1.30}$$

$$\begin{aligned}H_I(Z^*(k),Z(k-1))=&\frac{1}{4}\sum_{\sigma,\rho=\alpha,\beta}\sum_{i,j,k,l=1}^{M}\sum_{\xi,\xi'=\alpha,\beta}\\&\times\sum_{h,h',h'',h'''=1}^{N_\xi}\Gamma_{ijkl}^{\sigma\rho\rho\sigma}\times\left(\delta_{kh'}\delta_{\rho\xi}+\sum_{p'}^{M-N_\xi}Z_{p'h'}^{\xi}(k-1)\delta_{kp'}\delta_{\rho\xi}\right)\times[1+Z^{\xi}(k)^{\dagger}Z^{\xi}(k-1)]^{-1}_{h'h}\\&\times\left(\delta_{jh}\delta_{\rho\xi}+\sum_{p=1}^{M-N_\xi}Z_{ph}^{\xi*}(k)\delta_{jp}\delta_{\rho\xi}\right)\times\left(\delta_{lh'''}\delta_{\sigma\xi'}+\sum_{p'''}^{M-N_{\xi'}}Z_{p'''h'''}^{\xi'}(k-1)\delta_{lp'''}\delta_{\sigma\xi'}\right)\\&\times[1+Z^{\xi'}(k)^{\dagger}Z^{\xi'}(k-1)]^{-1}_{h'''h''}\left(\delta_{ih''}\delta_{\sigma\xi'}+\sum_{p''=1}^{M-N_{\xi'}}Z_{p''h''}^{\xi'*}(k)\delta_{ip''}\delta_{\sigma\xi'}\right),\end{aligned} \tag{1.31}$$

and

$$\Gamma_{ijkl}^{\sigma\rho\rho\sigma}=V_{ijkl}^{\sigma\rho\rho\sigma}-V_{ijlk}^{\sigma\sigma\sigma\sigma}\delta_{\sigma\rho} \tag{1.32}$$

1.2.5 Ensemble average

The ensemble average of any operator O can be calculated

$$\langle\langle O\rangle\rangle=\frac{\mathrm{Tr}[Oe^{-\beta H}]}{\mathrm{Tr}[e^{-\beta H}]}=\frac{\int\Pi_{k=1}^{n}d\mu(Z(k))\langle Z(k)|Z(k-1)\rangle e^{-\tau\Sigma_{k=1}^{n}H(Z^*(k),Z(k-1)}(1/n)\Sigma_{l=1}^{n}\langle Z(l)|O|Z(l-1)\rangle}{\int\Pi_{k=1}^{n}d\mu(Z(k))\langle Z(k)|Z(k-1)\rangle e^{-\tau\Sigma_{k=1}^{n}H(Z^*(k),Z(k-1))}} \tag{1.33}$$

In this paper, particularly, we numerically calculate the ensemble average of the total energy <<*H*>>. By the definition, we have

$$\langle\langle H\rangle\rangle = \frac{\mathrm{Tr}[He^{-\beta H}]}{\mathrm{Tr}[e^{-\beta H}]} = -\frac{\partial}{\partial\beta}\log \Xi \tag{1.34}$$

It is impossible to directly numerically calculate the ensemble average of physical properties in Eq. (1.33) with the matrix elements of the Hamiltonian in Eq. (1.29) because of a huge amount of integral variables is generated. Therefore, the above integral is approximated to other numerical method such as the Monte Carlo method.

1.2.6 Monte Carlo procedure

The numerical calculation of the ensemble average of the physical property is progressed by a Monte Carlo method. We need the matrix elements, $h_{ij}{}^{\sigma}$ and $V_{ijkl}{}^{\sigma\rho\rho\sigma}$, between orbitals in each term of Eqs. (1.27) and (1.28). Because our initial coherent state is constructed by the restricted Hartree-Fock (RHF) orbitals or the unrestricted-based natural orbital (UNO), matrix elements based on the HF orbitals must be generated by Gaussian 94 program package[79]. The molecular integrals based on a basis set are obtained by means of HONDO95 program package[80]. We convert them into the molecular integrals based on the HF orbitals which are orthogonal. Finally, using the above molecular integrals, the number of the division n for the partition function and a temperature, the ensemble average of the physical property are calculated by means of a Metropolis algorithm. The random number with a density of a probability is generated by the rejection method. The density $p(Z^{\rho\dagger}, Z^{\rho})$ of the probability is written as

$$p(Z^{\rho\dagger}, Z^{\rho}) = \prod_{\rho=\alpha,\beta} |\det(1 + Z^{\rho\dagger} Z^{\rho})|^{N_\rho} \tag{1.35}$$

In order to avoid the negative sign problem, a reweighting method is attempted. In the conventional Monte Carlo method, the virtual Boltzmann factors are the absolute value of the original system

$$B(k,k-1) = |\langle Z(k)|e^{-\tau H}|Z(k-1)\rangle| \tag{1.36}$$

where $B(k, k\text{-}1)$ indicates a weighted function and is positive. The convergence of the calculations is so slow that we hardly get accurate results by small calculations. We have already presented the reweighting method of the midpoint procedure (MPP) method[81]. The MPP method is the following. We propose the midpoint function as a new reweighting function

$$B(k,k-1)=\langle Z(k)|e^{-(\tau/2)H}|m\rangle\langle m|e^{-(\tau/2)H}|Z(k-1)\rangle \tag{1.37}$$

where

$$|m\rangle=\frac{|Z(k-1)\rangle+|Z(k)\rangle}{\sqrt{2+\langle Z(k-1)|Z(k)\rangle+\langle Z(k)|Z(k-1)\rangle}} \tag{1.38}$$

The MPP method means that a path from $|Z(k\text{-}1)\rangle$ to $|Z(k)\rangle$ travels through the midpoint between two points at the midtime of $(k\text{-}1)\tau+(\tau/2)$.

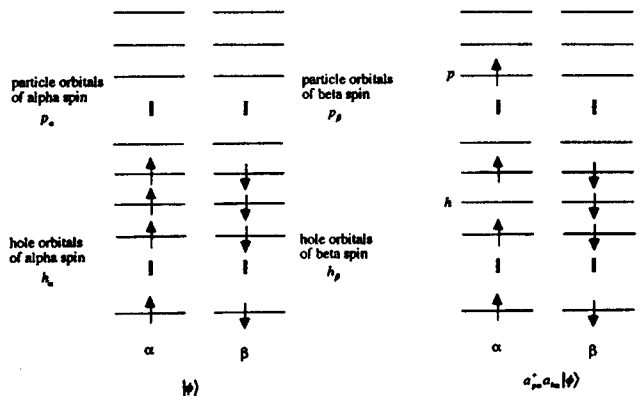

Figure 1.2 Graphical image of the Thouless parameterization.

Section 1.3

Numerical calculations of magnetization by the path integral method

1.3.1 Employed models

In order to examine the availability of our theoretical formulation and calculation scheme, path integral MC calculations have been carried out for various molecular systems[82]. Here, we study the magnetic behavior with our method for the qualitative prediction

We treated a system which consists of both methyl radical and hydrogen atom. **Figure 1.1**B illustrates the model system under consideration. The axis of magnetic field was set as z-axis. The through space length between these two radicals was indicated as R/Å and our calculations were progressed at fixed 2.0Å at first. And we also intend to apply it to a hole doped system, i.e., the Cu^{2+} (d^9) system in comparison with the Ti^{3+} (d^1) system. The magnetic coupling induced by those d-orbitals may extend to the magnetic behaviors for the dπ-pπ organic-metal conjugated system which relates to superconductor or hyper-polarizability, etc. The copper ion - hydrogen atom (Cu^{2+} - H•) system as shown in **Fig. 1.1**D is the simplest one that contains d^9 - s orbitals coupling. The bond length between these two radicals was fixed at 2.0Å and the axis of the magnetic field was set z-axis.

In our treatment temperature effects are obtained by calculating the partition function. Here, Hamiltonian consists of the *ab initio* Hamiltonian and the Zeeman Hamiltonian. According to the path integral method the term can be divided into N parts, that is the division number is N. A path integral representation is derived by inserting the closure relations. Partition functions are calculated in each Monte Carlo steps by the Metropolis method[83]. Random numbers generated with maximum length linearly recurring sequence. In order to avoid the negative sign problem a reweighting method is attempted.

Finally, the ensemble average of the total energy and the magnetization etc. are obtained by the above procedure as related to Eq. (1.33).

$$\langle M_z \rangle = \frac{Tr\left[e^{-\beta H} M_z\right]}{Tr\left[e^{-\beta H}\right]} \tag{1.39}$$

1.3.2 CH_3 radical system

Calculation about only SOMO-SOMO MC-AS

Here, the magnetic interaction between radical pairs was considered under the limitation of Monte Carlo Active Space (AS), that is, (α-hole, α-particle, β-hole, β-particle space)=(1, 1, 1, 1). Such limitation is found to be correspond to the necessity of only SOMO-SOMO direct interaction. At first, we investigated the dependences of the ensemble average of the total energy and the magnetization on the division number for the partition function. These calculations were carried out under conditions that temperature T is 1K and external magnetic field H is 0 or 1 a.u. (1 a.u. = 2.3506×10^5T). **Figures 1.3**-A and B show these results, respectively.

As increasing the division number, it is noteworthy that the total energy become more stable because of including more electronic correlations. However, we could not find remarkable improvements in the region which is larger than N=4000. The more huge number of divisions are desired in order to include more correlations, though it is very time consuming as increasing the number.

In order to contrast these above results, ab initio MO calculations were carried out by ab initio HF, post-HF and UNO CAS calculations. Here, we also employed the 4-31G basis sets. The energy of low spin state with RHF(based on UNO) was -39.978868020861 a.u. On the other hand, Coupled-Cluster method (RCCSD(T)) which the most involved electron correlations in these methods gave -40.143976717 a.u. The calculated J_{ab} values by APUHF, APUCC(T) and UNO CASCI{2,2} method were -7262.88, -11766.7 and -7969.66 cm^{-1}, respectively.

Expanding MC-AS

In the above we performed the calculations based on the path integral method about only the limited AS (1, 1, 1, 1). Here let us investigate the dependence on the AS. Judging from UNO analysis, it is found that the suitable MC-AS are (2, 2, 2, 2), (4, 4, 4, 4) and (5, 12, 5, 12). The latest AS is correspond to involving all orbitals. As the program coded by

our group can calculate in also any Monte Calro Active Spaces, calculations with these ASs were also performed. **Figures 1.4**-A, B and C depict the total energies and the magnetizations for each AS at same conditions which temperature T is 1K, the division number N is 1000 and the external magnetic field H is 1 a.u.

From these figures, it is noteworthy that curvature of the total energies vs the division number have same tendency, that is, as increasing the division number, the total energy will decrease up to the exact total energy obtained from the calculation by ab initio Full-CI method at the temperature of 0 K. The dependency on the ASs is found that the few damping of the total energy could not be taken in the case of the wider ASs. In such the case, huge number of steps is required because of many integral variables. Thus, it is important to consider the valance of the AS and N. On the other hand, it is expected that more significant results involved all contributions may be given in such the case, since more indirect correlations can be involved.

Unfortunately, we could not investigate the detailed contributions from magnetic interactions for the lack of sufficient available CPU time. We are carrying out the more accurate calculations for this purpose now. However, we can conclude that the only SOMO-SOMO interaction i.e. AS (1, 1, 1, 1) plays the dominant role to magnetic behaviors between methyl-hydrogen radicals as first step of approximation. Therefore, we employed this simplest and narrowest AS in following sections.

Dependences on magnetic field

As the discussed previous sections, availability of the our scheme for studies about the total energy and the magnetization were ensured. Here, let us study the dependence on the external magnetic fields. In relation to such a strong magnetic field, recently it is proposed that more interesting sciences which cannot be expected under traditional week magnetic field. Many empirical and theoretical studies are anticipated by a lot of scientists. The total energy and the magnetization for each external magnetic field from 0 to 1 a.u. are depicted in **Fig. 1.5**A. These calculation was performed under a condition that N=1000 and T=1K, though much larger N was desired as discussed the previous sections.

From this figure, it is found that the magnetization curvature increases drastically at H= 0.3 ~ 0.5 a.u. region. In order to analyze the result, let us investigate the behavior of triple and singlet state under various external magnetic fields. In **Fig. 1.5**B, the energy splitting diagram is illustrated. From this figure the relation between magnitude of external magnetic field and triple-singlet energy gap is drawn and this figure help to describe the behaviors under various magnetic fields. The result indicates that spin crossover is occurred in this region and the transition with the spin flop from singlet state to triple state.

Dependences on temperature

Here, we progressed the calculation at nearly spin crossover region (H = 0.3 a.u). **Figure 1.6** shows the results in various temperatures. The temperature will be equivalent to the energy gap between singlet state and triplet state, as illustrated in **Fig. 1.5**B. In this calculation, it seems that the critical temperature can be detected and spread widely. On the other hand, in a region of the higher temperature of 4000K, the two states are mixed each other with excessive heat energy and the magnetization is vanished.

Dependences on the distance between radical pairs

In the above sections, the fixed inter radical distance (R=2.0Å) was employed and our treatment was applied for the strong interaction system such as large J_{ab} values. In such system HOMO-LUMO gap is much larger because of direct interaction between SOMOs of each radicals. Here, we carried out calculations based on path integral method at a few distance R = 1.0, 2.0, 3.0 and 4.0Å in order to clarify its feature about various interaction from large gap limits to nearly degenerate limits. **Figure 1.7** depicts the calculated results.

From the this figure the magnetizations between at 1.0 and 2.0 a.u. etc. have distinct difference. These results are found to be consistent with our idea, that is, the spin crossover is occurred as relation to the S-T gap shown in **Fig. 1.5**B.

1.3.3 $Cu^{2+}(d^9)$ system

An *ab initio* RHF-MO orbital was employed as the initial coherent state in order to conserve orbital symmetry. The minimum (6D) basis set was used for qualitative discussion. The (1,1,1,1) space is used as the MC-AS. Thus it contains only SOMO-SOMO interaction, i.e., it takes σ, σ^* bonds into account. Graphical representation of these bonds is illustrated in **Fig. 1.1**D. And it is found that the shape of σ^* type anti-bond composed with d-s orbital differs from one composed with s-s or p-s orbital. Not only z component d_{zz} but also (x, y) components of d_{zz}, i.e., (d_{xx} and d_{yy}), take part in the anti-bonding MO.

We discuss the dependency on the external magnetic field, which is varied from 0.0 to 0.7 a.u. under conditions (N = 750 and T=1K). Here, according to the path integral method the exponential term in a partition function can be divided into N factors, that is, the division number is N. These results are illustrated in **Fig. 1.8**A. In this figure we showed the average and maximum values of the calculated magnetization. It is found that the curvature of the magnetization increases drastically at the regions of H = 0.2 ~ 0.5 a.u. The result

indicates that the spin crossover occur in this region. Thus, the transition with the spin flop from singlet state to triple state appears.

Secondarily, MC-AS is extended to (5,1,5,1) in order to include not only SOMOs but also other d-type orbitals. **Figure 1.1**D also shows these orbitals. The same calculations were carried out under conditions (N = 1500 and T=1K), and the numerical results are depicted in **Fig. 1.8**B. Though these values are smaller than those for MC-AS=(1,1,1,1), it is found that the magnetization appears at the regions of H = 0.2 ~ 0.6. Thus, the SOMOs mainly contribute to the magnetic behavior.

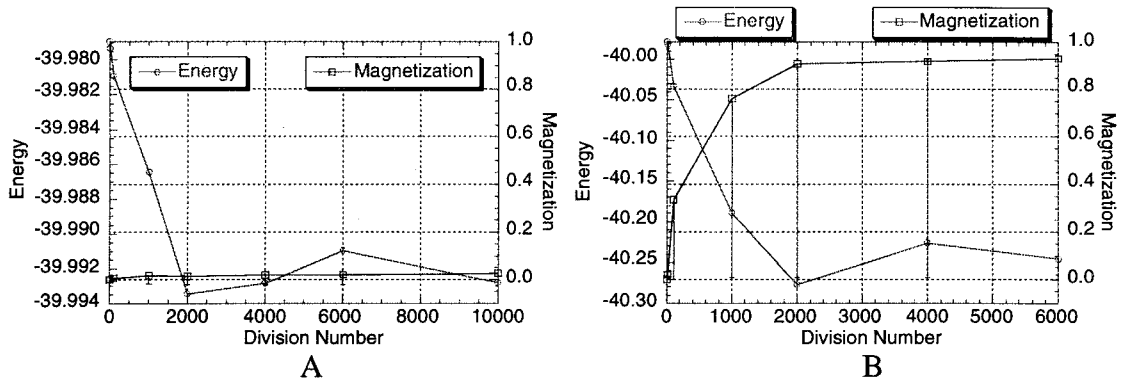

Figure 1.3 Total energy for the number of division at T=1K. Here, A and B indicate results at H=0 and 1 a.u., respectively.

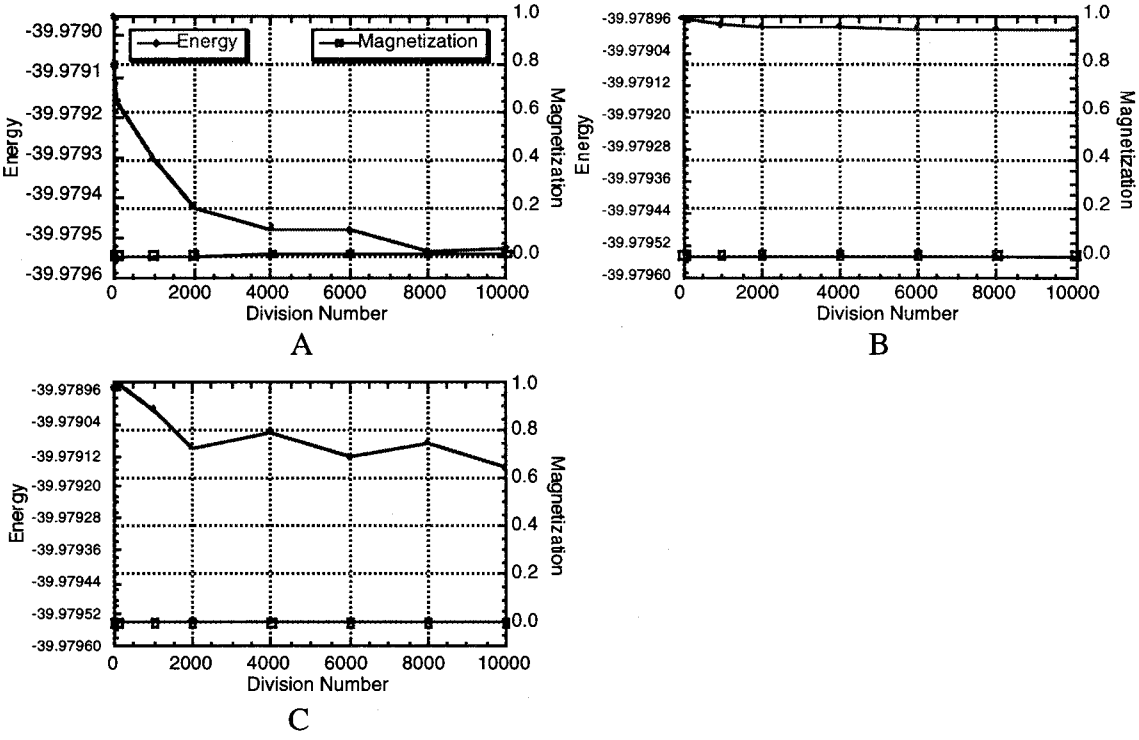

Figure 1.4 Total energy for the number of division at T=1K. Here, A, B and C indicate results at AC(2, 2, 2, 2), (4, 4, 4, 4) and (5, 12, 5, 12), respectively.

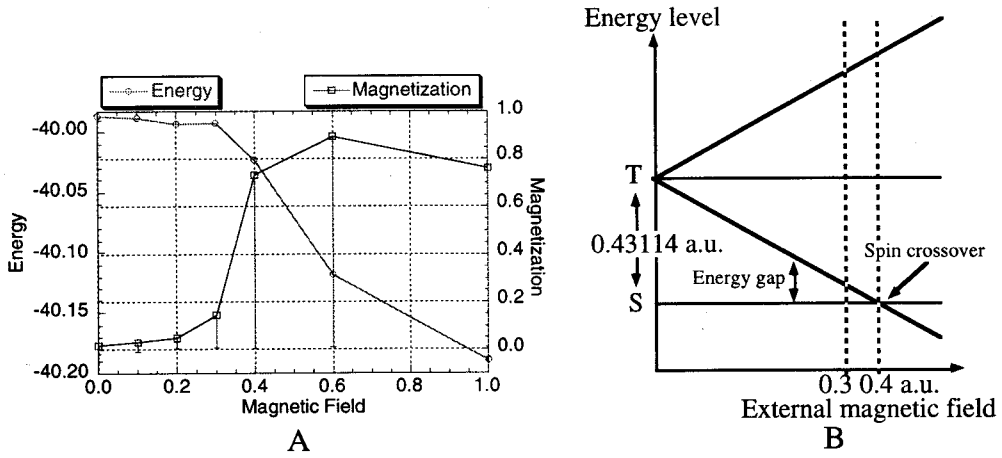

Figure 1.5 (A) Magnetization for various external magnetic field at T=1K.
(B) Energy splitting diagram impressed magnetic field

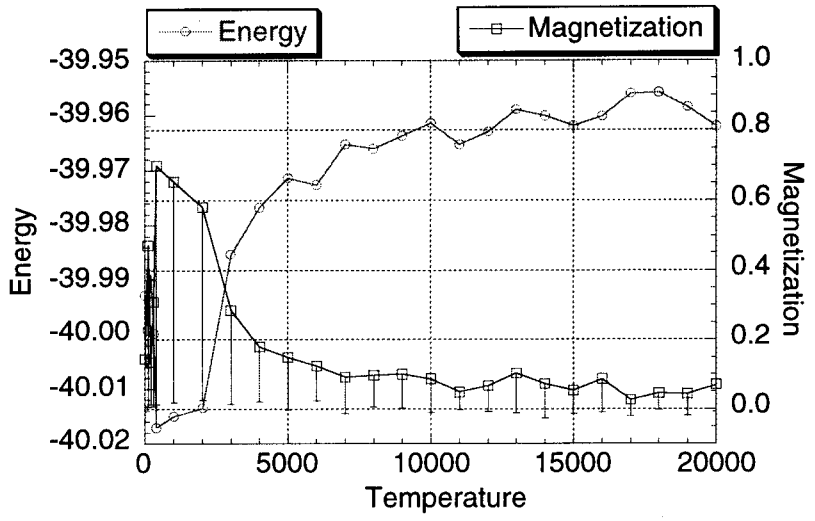

Figure 1.6 Magnetization for various temperature at H=0.3 a.u.

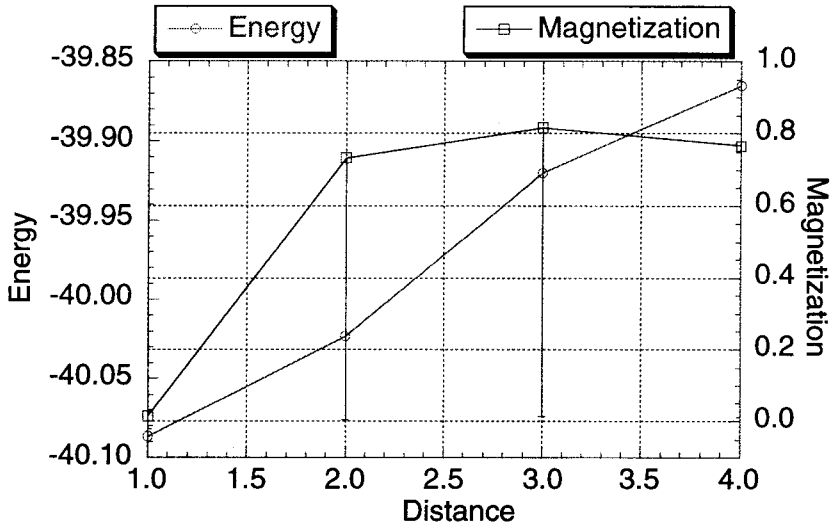

Figure 1.7 Magnetization for various inter-radical distance R /Å at T=1 K and H=1 a.u.

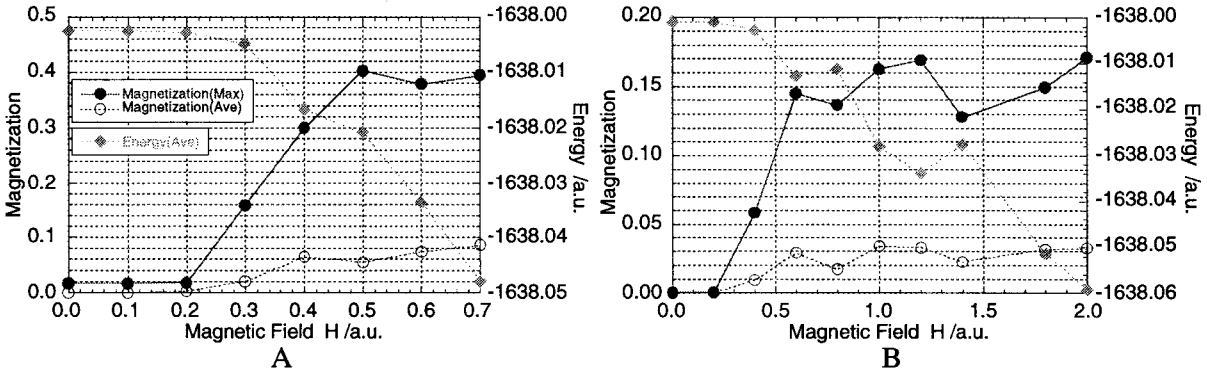

Figure 1.8 Magnetization given by path integral method for MC-AS = (1,1,1,1) (A) and (5,1,5,1) (B)

Section 1.4

Conclusion and future discussions

A path integral formulation by the generalized coherent states of the Thouless parameterization is presented to apply to molecular systems. Explicit expressions of the ensemble average of the physical property including the spin space is also derived. In order to compute the ensemble average, a novel calculating scheme is shown. The Monte Carlo method by the Metropolis algorithm is used. The method will be extended to avoid these problems by using an analogs to the complete active space (CAS) method and so on.

The author gives a computational scheme to calculate the ensemble average of the magnetization. The discussions in relation to the total energy and the number of the division for the partition function or the temperature are carried out. It is noteworthy that the path integral method could be developed and applied to the calculations of the magnetic properties in real molecular system. The author shows the magnetization value of the antiferromagnetic materials in strong magnetic field. Unfortunately, the numerical accuracy might not be sufficient because we could not take a huge number of divisions due to limited CPU time at the present time. However, even now we expect that this method had been effective to calculate the magnetic properties in qualitative discussions of temperature effects.

References

Part I

[1] M. Kinoshita, P. Turek, M. Tamura, K. Nozawa, D. Shiomi, Y. Nakazawa, M. Ishikawa, M. Takahashi, K. Awaga, T. Inabe and Y. Maruyama, Chem. Letters 1225 (1991).

[2] M. Tamura, Y. Nakazawa, D. Shiomi, K. Nozawa, Y. Hosokoshi, M. Ishikawa, M. Takahashi, and M. Kinoshita, Chem. Phys. Lett., 1991, 186, 401.

[3] Y. Nakazawa, M. Tamura, N. Shirakawa, D. Shiomi, M. Takahashi, M. Kinoshita, and M. Ishikawa, Phys. Rev., B46, 8906 (1992).

[4] K. Awaga and Y. Maruyama, J. Chem. Phys., 91, 2743 (1989).

[5] K. Awga, T. Inabe, U. Nagashima, and Y. Maruyama, J. Chem. Soc., Chem. Commun., 1617 (1989); 520 (1990).

[6] A, Zheludef, E. Ressouche, J. Schweizer, P. Turek, M. Wan and H. Wang, Solid State Commun., 90, 233 (1994).

[7] K. Inoue and H. Iwamura, Chem. Phys. Lett., 207, 551 (1993).

[8] K. Awaga, T. Inabe and Y. Maruyama, Chem. Phys. Lett., 190, 349 (1992)

[9] K. Awaga, T. Inabe, T. Nakamura, M. Matsumoto and Y. Maruyama, Synth. Met., 56, 3311 (1993).

[10] K. Awaga, T. Okuno, A. Yamaguchi, M. Hasegawa, T. Inabe, Y. Maruyama and N. Wada, Phys. Rev., B49, 3975 (1994).

[11] Y. Pei, O. Kahn, M. A. Aebersold, L. Ouahab, F. Le Berre, L. Pardi and J. L. Tholence, Adv. Mater., 6, 681 (1994).

[12] T. Sugimoto, M. Tsujii, T. Suga, N. Hosoito, M. Ishikawa and N. Takeda, Mol. Cryst. Liq. Cryst., 272, 183 (1995).

[13] T. Sugawara, M. M. Matsushita, A. Izuoka, N. Wada, N. Takeda and M. Ishikawa, J. Chem. Soc., Chem. Commun., 1723 (1994).

[14] R. Chiarelli, M. A. Novak, A. Rassat and J. L. Tholence, Nature, 363, 147 (1993).

[15] R. Chiarelli, A. Rassat and P. Rey, J. Chem. Soc., Chem. Commun., 1081 (1992).

[16] R. Chiarelli, A. Rassat, Y. Dromzee, Y. Jeannin, M. A. Novac and J. L. Tholence, Physica Scripta., T49, 706 (1993).

[17] Yves Dromzee, Robert Chiarelli, Serge Gambarelli and Andre Rassat, Acta Cryst., C52, 474 (1996).

[18] K. Togashi, R. Imachi, K. Tomioka, H. Tsuboi, T. Ishida, T. Nogami, N. Takeda and M. Ishikawa, Bull. Chem. Soc. Jpn., 69, 2821 (1996).

[19] T. Nogami, T. Ishida, M. Yasui, F. Iwasaki, N. Takeda, M. Ishikawa, T. Kawakami and K. Yamaguchi, Bull. Chem. Soc. Jpn., 69, 1841 (1996).

[20] A. Kajiwara, H. Sugimoto and M. Kamachi, Bull. Chem. Soc. Jpn., 67, 2377 (1994).

[21] K. Tomioka, S. I. Mitsubori, T. Ishida, T. Nogami and H. Iwamura, Chem. Lett., 1239 (1993).

[22] K. Tomioka, T. Ishida, T. Nogami and H. Iwamura, Chem. Lett., 625 (1993).

[23] T. Nogami, K. Tomioka, T. Ishida, H. Yoshikawa, M. Yasui, F. Iwasaki, H. Iwamura, N. Takeda and M. Ishikawa, Chem. Lett., 29 (1994).

[24] H. M. McConnell, J. Chem. Phys., 39, 1910 (1963).

[25] H. M.McConnell, Proc. R. A. Welch Found. Chem. Res., 11, 144 (1967).

[26] R. Breslow, Pure Apll. Chem., 54, 927 (1982).

[27] R. Breslow, B. Jaun, R. Q. Kluttz and C. Z. Xia, Tetrahedron, 38, 863 (1982).

[28] K. Awaga, T. Sugano, and M. Kinoshita, Chem. Phys. Lett., 141, 540 (1987).

[29] R. G. Parr and W. Yang, Density functional theory ofatoms and molecules (Oxford Univ. Press, Oxford, 1989).

[30] D. M. Dreizler and E. K. U. Gross, Density functional theory. An approach to the quantum many body problem (Springer, Berlin, 1990).

[31] T. Ziegler, Chem. Rev., 91, 651 (1991).

[32] J. A. Pople, P. M. W. Gill and B. G. Johnson, Chem. Phys. Letters, 199, 557 (1992).

[33] J. Andzelm and E. Wimmer, J. Chem. Phys., 96, 1280 (1992).

[34] B. G. Johnson, C. A. Gonzales, P. M. W. Gill and J. A. Pople, J. Chem. Phys., 98, 5612 (1993).

[35] J. C. Slater, Quantum theory of molecules and solids, Vol. 4. The self-consistent field for molecules and solids (McGraw-Hill, New York, 1974).

[36] A. D. Becke, Phys. Rev., A38, 3098 (1988).

[37] S. H. Vosko, L. Wilk and M. Nusair, Can. J. Phys., 58, 1200 (1980).

[38] J. P. Perdew and A. Zunger, Phys. Rev., B23, 5048 (1981).

[39] J. P. Perdew, Phys. Rev., B33, 8822 (1986).

[40] C. Lee, W. Yang and R. G. Parr, Phys. Rev., B37, 785 (1988).

[41] T. Kawamoto and N. Suzuki, Journal of Phy. Soc. Jpn., 63, 3158 (1994).

[42] J. Kanamiri, J. Phys. Chem. Solids, 10, 87 (1959).

[43] J. B. Goodenough, J. Phys. Chem. Solids, 6, 287 (1958).

[44] K. Yamaguchi, Y. Yoshioka and T. Fueno, Chem. Phys., 20, 171 (1977).

[45] Y. Yoshioka, K. Yamaguchi and T. Fueno, Theoret. Chim. Acta, 45, 1 (1977).

[46] S. Yamanaka, T. Kawakami, T. Noro and K. Yamaguchi, J. Mol. Structure (Theochem), 310, 185 (1994).

[47] K. Yamaguchi and T. Fueno, Chem. Phys. Lett., 159, 465 (1989).

[48] M. Okumura, K. Takada, J. Maki, T. Noro, W. Mori and K. Yamaguchi, Mol. Cryst. Liq. Cryst., 233, 41 (1993).

[49] M. Okumura, K. Yamaguchi, M. Nakano and W. Mori, Chem. Phys. Letters 207, 1 (1993).

[50] M. Okumura, W. Mori and K. Yamaguchi, Chem. Phys. Letters 219, 36 (1994).

[51] K. Yamaguchi, M. Okumura, J. Maki, T. Noro, H. Namimoto, M. Nakano, T. Fueno and K. Nakasuji, Chem. Phys. Lett., 190, 353 (1992).

[52] S. Yamanaka, T. Kawakami, H. Nagao and K. Yamaguchi, Chem. Phys. Lett., 231, 25 (1994).

[53] K. Yamaguchi, M. Okumura, W. Mori, J. Maki, K. Takada, T. Noro and K. Tanaka, Chem. Phys. Lett., 210, 201 (1993).

[54] S. Yamanaka, M. Okumura, K. Yamaguchi and K. Hirao, Chem. Phys. Lett., 225, 213 (1994).

[55] S. Yamanaka, T. Kawakami, S. Yamada, H. Nagao, M. Nakano and K. Yamaguchi, Chem. Phys. Letters, 240, 268 (1995).

[56] K. Yamaguchi, Int. J. Quant. Chem., S14, 269 (1980).

[57] S. Yamanaka, M. Okumura, M. Nakano and K. Yamaguchi, J. Mol. Struct. (Theochem), 310, 205 (1994).

[58] M. Nakano, I. Sigemoto, S. Yamada and K. Yamaguchi, J. Chem. Phys., 103, 2657 (1995).

[59] D. Gatteschi and K. Yamaguchi, "From Molecular Assemblies to the Devices" (E. Coronado Eds., Kluwer Pub.,1996) p561.

[60] M. Okumura, K. Yamaguchi and K. Awaga, Chem. Phys. Letters 228 (1994) 575.

[61] K. Takeda, K. Konishi, M. Tamura and M. Kinoshita, Phys. Rev., B53, 3374 (1996).

[62] M. Mito, T. Kawae, M. Takumi, K. Nagata, M. Tamura, M. Kinoshita and K. Takeda, Phys. Rev., B56, R14255 (1997).

Part II

[63] R. P. Feynman, Rev. Mod. Phys., 20, 367 (1948).

[64] R. P. Feynman, Phys. Rev., 76, 769 (1949).

[65] R. P. Feynman, Phys. Rev., 80, 40 (1950).

[66] J. P. Blaizot and H. Orland, Phys. Rev., 24, 1740 (1981).

[67] R. P. Feynman and A. R. Hibbs, Quantum Mechanics and Path Integrals(McGraw-Hill, New York, 1965).

[68] L. H. Ryder, Quantum Field Theory (Cambridge University Press, London, 1984).

[69] J. W. Negele and H. Orland, Quantum Many-Particle Systems (Addison-Wesley, Reading, 1988).

[70] J.-P. Blaizot and G. Ripka, Quantum Theory of Finite Systems (Massachusetts Institute of Technology, Massachusetts, 1986).

[71] H. Nagao, K. Nishikawa, and S. Aono, Chem. Phys. Lett. 190, 97 (1992).

[72] H. Nagao, K. Nishikawa and S. Aono, Chem. Phys. Lett. 215, 5 (1993).

[73] H. Kawabe, K. Nishikawa and S. Aono, Int. J. Quantum Chem., 51, 265 (1994).

[74] M. Suzuki, Prog. Theor. Phys., 56, 1454 (1976).

[75] M. Suzuki, Commun. Math. Phys., 51, 183 (1976).

[76] H. F. Trotter, Proc. Am. Math., 10, 545 (1959).

[77] F. W. Wiegel, Phys. Rev., C 16, 2 (1975).

[78] Quantum Monte Carlo Method in Condensed Matter Physics, edited by M. Suzuki (World Scientific, Singapore, 1993).

[79] M. J. Frisch, G. W. Trucks, H. B. Schlegel, P. M. W. Gill, B. G. Johnson, M. A. Robb, J. R. Cheeseman, T. A. Keith, G. A. Petersson, J. A. Mont-gomery, K. Raghavachari, M. A. Al-Laham, V. G. Zakrzewski, J. V. Oritiz, J. B. Foresman, J. Cioslowski, B. B. Stefanov, A. Nanayakkara, M. Challacombe, C. Y. Peng, P. Y. Ayala, W. Chen, M. W. Wong, J. L. Andres, E. S. Replogle, R. Gomperts, R. L. Martin, D. J. Fox, J. S. Binkley, D. J. Defrees, J. Baker, J. P. Stewart, M. Head-Gordon, C. Gonzalez, and J. A. Pople, GAUSSIAN 94, Gaussian, Inc., Pittsburgh, PA, 1995.

[80] M. Dupuis, A. Marquez, and E. R. Davidson, HONDO 95.3 from CHEM Station (IBM Corporation, Neighborhood Road, Kingston, New York, 12401, 1995).

[81] H. Kawabe, H. Nagao, and K. Nishikawa, Int. J. Quantum. Chem., 60, 1223 (1996).

[82] H. Nagao, H. Kawabe, T. Kawakami, M. Okumura, W. Mori, K. Nishikawa and K. Yamaguchi, Mol. Cryst. Liq. Cryst., 286, 171 (1996).

[83] N. Metropolis, A. Rosenbluth, M. Rosenbluth, A. Teller and E. Teller, J. Chem. Phys., 21, 1087 (1953).

List of Publications

Papers

[1] Effective exchange integrals for open-shell species by density functional methods
S. Yamanaka, T. Kawakami, H. Nagao, K. Yamaguchi,
Chem Phys Letters, **231**, 25-33 (1994).

[2] CASSCF and CASPT2 calculations of hole-doped polycarbenes. Possibilities of organic ferromagnetic conductors and metals
S. Yamanaka, T. Kawakami, M. Okumura, K. Yamaguchi,
Chem Phys Letters, **233**, 257-265 (1995).

[3] No-overlap and orientation principle for ferromagnetic interactions between nitroxide groups
T. Kawakami, S. Yamanaka, W. Mori, K. Yamaguchi, A. Kajiwara and M. Kamachi,
Chem Phys Letters, **235**, 414-421 (1995).

[4] Theoretical studies of spin density populations on nitroxide and nitronylnitroxide derivatives
S. Yamanaka, T. Kawakami, S. Yamada, H. Nagao, M. Nakano, K. Yamaguchi,
Chem Phys Letters, **240**, 268-277 (1995).

[5] Theoretical studies of spin populations on nitronyl nitroxide, phenyl nitronyl nitroxide and *p*-NPNN
S. Yamanaka, T. Kawakami, H. Nagao, K. Yamaguchi,
Mol. Cryst. Liq. Cryst., **271**, 19-28 (1995).

[6] Theoretical approaches to molecular magnetism II: No-overlap and orientation principles for ferromagnetic interactions
T. Kawakami, S. Yamanaka, H. Nagao, W. Mori, M. Kamachi, K. Yamaguchi,
Mol. Cryst. Liq. Cryst., **272**, 117-129 (1995).

[7] Theoretical studies of effective exchange interactions between nitroxides via hydrogen atoms
T. Kawakami, S. Takeda, W. Mori and K. Yamaguchi,
Chem Phys Letters, **261**, 129-137 (1996).

[8] Theoretical calculation of effective exchange integrals for one- and two-dimensional poly(phenylenemethylene) systems. Possibilities of organic ferro- and ferri-magnetic solids
D. Yamaki, S. Yamada, G. Maruta, T. Kawakami, W. Mori and K. Yamaguchi,
Mol. Cryst. Liq. Cryst., **279**, 9-18 (1996).

[9] Theoretical studies of the ferromagnetic intermolecular interaction of *p*-carboxylate phenyl nitronyl nitroxide

T. Kawakami, A. Oda, W. Mori, K. Yamaguchi, K. Inoue and H. Iwamura,
Mol. Cryst. Liq. Cryst., **279**, 29-38 (1996).

[10] Calculation of magnetization by path integral method I
H. Nagao, H. Kawabe, T. Kawakami, M. Okumura, W. Mori, K. Nishikawa and K. Yamaguchi,
Mol. Cryst. Liq. Cryst., **286**, 171-176 (1996).

[11] Calculation of magnetization by path integral method II
T. Kawakami, H. Nagao, K. Ueda, W. Mori and K. Yamaguchi,
Mol. Cryst. Liq. Cryst., **286**, 177-184 (1996).

[12] Proposed Mechanism of Ferromagnetic Interaction of Organic Ferromagnets: 4-(Arylmethyleneamino)-2,2,6,6-tetramethylpiperidin-1-oxyls and Related Compounds
T. Nogami, T. Ishida, M. Yasui, F. Iwasaki, N. Takeda, M. Ishikawa, T. Kawakami and K. Yamaguchi,
Bull. Chem. Soc. Jpn., **69**, 1841-1848 (1996).

[13] Magnetic Interaction via β-Hydrogen Atoms in TEMPO Derivatives
T. Kawakami, A. Oda, S. Takeda, W. Mori, T. Ishida, M. Yasui, F. Iwasaki, T. Nogami and K. Yamaguchi,
Mol. Cryst. Liq. Cryst., **306**, 141-150 (1997).

[14] Theoretical Studies on Magnetic interactions in 2', 5' -Dihydroxyphenyl Nitronyl Nitroxide Crystal
A. Oda, T. Kawakami, S. Takeda, W. Mori, M. M. Matsushita, A. Izuoka, T. Sugawara and K. Yamaguchi,
Mol. Cryst. Liq. Cryst., **306**, 151-160 (1997).

[15] Solid state 1H-MAS-NMR and Spin Densities on Protons of the Organic Ferromagnetic TEMPO Derivatives
G. Maruta, S. Takeda, T. Kawakami, W. Mori, K. Yamaguchi, R. Imachi, T. Ishida and T. Nogami,
Mol. Cryst. Liq. Cryst., **306**, 307-314 (1997).

[16] Theoretical Studies on Magnetic Interactions in *p*-Cyanophenyl Nitronyl Nitroxide Crystal
A. Oda, T. Kawakami, S. Takeda, W. Mori, Y. Hosokoshi, M. Tamura, M. Kinoshita and K. Yamaguchi,
Mol. Cryst. Liq. Cryst., **306**, 331-338 (1997).

[17] Calculation of magnetization by path integral method
T. Kawakami, H. Nagao, W. Mori and K. Yamaguchi,
Synthetic metals, **85**, 1753-1754 (1997).

[18] Path integral method by means of generalized coherent states and its numerical approach to molecular systems. I. Ensemble average of total energy
H. Nagao, Y. Shigeta, H. Kawabe, T. Kawakami, K. Nishikawa, K. Yamaguchi,
J. Chem. Phys., **107**, 6283-6289 (1997).

[19] Theoretical study of electronic structures of one-dimensional magnetic clusters composed of doublet lithium and copper atoms
T. Kawakami, S. Yamanaka, Y. Takano, Y. Yoshioka, K. Yamaguchi,
Journal of Molecular Structure: THEOCHEM, **451**, 89-107 (1998).

[20] Exchange Interactions in Mesoscopic Magnetic Clusters. *Ab Initio* Size-Consistent Calculations of Effective Exchange Interactions in Mesoscopic Magnetic Clusters Composed of Triplet Methylenes and Quartet Nitrogen Atoms
T. Kawakami, S. Yamanaka, Y. Takano, Y. Yoshioka, K. Yamaguchi,
Bull. Chem. Soc. Jpn., **71**, 2097-2108 (1998).

[21] A theoretical explanation of the pressure effects on intermolecular interactions of β-phase of para nitrophenyl nitroxide
M. Okumura, M. Mitoh, K. Takeda, T. Kawakami, K. Yamaguchi,
submitted.

[22] Exchange Interactions in the Genuine Organic Ferromagnet Accompanying Pressure Induced Ferro- to Antiferromagnetic Transition
K. Takeda, M. Mito, T. Kawae, H. Deguchi, S. Takagi, M. Okumura, T. Kawakami, K. Yamaguchi, M. Kinoshita,
submitted.

[23] Theoretical Studies of Intra- and Inter- magnetic Interactions in TMAO (1, 3, 5, 7 - tetramethyl - 2, 6 - diazaadamantane N, N' - dioxyl)
T. Kawakami, A. Oda, S. Takeda, W Mori and K. Yamaguchi,
Mol. Cryst. Liq. Cryst., in press.

[24] Theoretical Studies of the Pressure Effects for β-Phase of *p*-NPNN
M. Okumura, T. Kawakami, A. Oda, K. Yamaguchi, M. Mito and K. Takeda,
Mol. Cryst. Liq. Cryst., in press.

[25] Theoretical Studies of Magnetic Interactions in 3', 5'-Dihydroxyphenyl Nitronyl Nitroxide Crystal
A. Oda, T. Kawakami, G. Maruta, S. Takeda, W. Mori, K. Yamaguchi, M. M. Matsushita, A. Izuoka and T. Sugawara,
Mol. Cryst. Liq. Cryst., in press.

Books

[26] 「分子磁性」スピン整列規則の理論と計算
山口兆・川上貴資・山木大輔
学会出版センター (伊藤公一編) p13-27 (1996).

[27] "MOLECULE-BASED MAGNETIC MATERIALS Theory, Techniques, and Applications" Theoretical Approaches to Molecular Magnetism
T. Kawakami, S. Yamanaka, D. Yamaki, W. Mori, and K. Yamaguchi,
ACS (Edited by Mark M. Turnbull, Toyonari Sugimoto, and Laurence K. Thompson)
ACS Symposium Series 644, Chapter 3 p30-43 (1997).

[28] "Molecular Magnetism - New Magnetic Materials" Theoretical Models for Molecular Magnetizm and Molecular Spinics
K. Yamaguchi, T. Kawakami, D. Yamaki, Y. Yoshioka,
講談社サイエンティフィク (伊藤公一・木下實編), in press.

[29] "Magnetic Properties of Organic Materials" Theory of Molecular Magnetism
K. Yamaguchi, T. Kawakami, A. Oda and Y. Yoshioka,
Marcel Dekker, Inc. (Edited by Prof. Paul M. Lahti), in press.

Others

[30] Ab Initio Molecular Orbital Studies of Singlet Oxygen Reactions of Olefins, Enol Ethers, and Enamines
Y. Yoshioka, S. Yamada, T. Kawakami, M, Nishino, K. Yamaguchi, and I. Saito,
Bull. Chem. Soc. Jpn., **69**, 2683-2699 (1996).

[31] Theoretical and Experimental Studies of a Charge-Transfer Mechanism for Biomimetic Oxygenations of Phenol and Indol Derivatives
Y. Yoshioka, S. Yamanaka, S. Yamada, T. Kawakami, M. Nishino, K. Yamaguchi and A. Nishinaga,
Bull. Chem. Soc. Jpn., **69**, 2701-2722 (1996).